From the Department of Molecular Medicine and Surgery
Karolinska Institutet, Stockholm, Sweden

DEVELOPMENT OF PROBES FOR MOLECULAR IMAGING

Evaluation in models of inflammation and atherosclerosis

Mona Ahmed

Karolinska Institutet

Stockholm 2019

Published by Karolinska Institutet
Printed by E-print AB 2019

ISBN 978-91-7831-340-2

Development of probes for molecular imaging

Evaluation in models of inflammation and atherosclerosis

THESIS FOR DOCTORAL DEGREE (Ph.D.)

By

Mona Ahmed

Principal Supervisor:
Kenneth Caidahl, MD, PhD, Professor
Karolinska Institutet
Department of Molecular Medicine and Surgery
Unit of Clinical Physiology

Co-supervisor(s):
Björn Gustafsson, MScEng, PhD
Karolinska Institutet
Department of Molecular Medicine and Surgery
Unit of Clinical Physiology

Ulf Hedin, MD, PhD, Professor
Karolinska Institutet
Department of Molecular Medicine and Surgery
Unit of Vascular Surgery

Silvia Aldi, MSc, PhD
Karolinska Institutet
Department of Department of Medical
Biochemistry and Biophysics,
Section for Medical Inflammation Research

Opponent:
Ebo de Muinck, MD, PhD, Professor
Linköping University
Department of Medical and Health Sciences
Division of Cardiovascular Medicine

Examination Board:
Helene Zachrisson, MD, PhD, Associate Professor
Linköping University
Department of Medical and Health Sciences
Division of Cardiovascular Medicine

Anders Sundin, MD, PhD, Professor
Uppsala University
Department of Surgical Sciences
Division of Radiology

Myriam Aouadi, PhD
Karolinska Institutet
Department of Medicine Huddinge
Division of Integrated Cardio Metabolic Centre

In memory of my Father

"I was taught that the way of progress was neither swift nor easy."

— Marie Curie, Physicist, Chemist, and winner of the 1903 Nobel Prize in Physics and the 1911 Nobel Prize in Chemistry

POPULÄRVETENSKAPLIG SAMMANFATTNING

Hjärt-kärlsjukdomar är bland de vanligaste och dödligaste sjukdomarna i världen. En av de viktigaste bakomliggande orsakerna till hjärt-kärlsjukdomar är åderförkalkning där blodkärlens väggar blir inflammerade och så kallade plack byggs upp av bl.a. kolesterolpartiklar från blodet. Plack utvecklas långsamt i artärerna och blir med tiden större och riskerar att täppa till kärlens blodflöde, vilket kan ge upphov till bland annat kärlkramp. Dessutom kan vissa plack innehålla mycket inflammatoriska celler vilket gör dem instabila med risk för att brista. Om placket brister bildas en blodpropp i hjärtats kranskärl eller i halskärlen som ger blodflöde till hjärnan, och symptom på hjärtinfarkt respektive stroke kan då uppträda.

Forskningen syftar till att utveckla nya kontrastmedel för icke-invasiv avbildning av inflammation i sjukdomsprocesser, speciellt åderförkalkning och instabila inflammerade plack. Förhoppningen och strävan är att ett nytt skonsamt undersökningsalternativ som möjliggör tidigare diagnos av dessa tillstånd kan identifiera de patienter som behöver en invasiv eller specifik sorts behandling.

Idén är att kontrastmedel eller molekylära prober, som består av stora molekyler eller mycket små partiklar, ska vara målsökande och hitta till specifika inflammatoriska cellmarkörer som finns på eller i instabila plack. För att uppnå en specifik målsökning krävs det att man känner till vilka markörer som är specifika för just de celler som är aktiva i en sjukdom och att man har strategier för att möjliggöra målsökning av dessa markörer. En sådan målsökning möjliggörs genom att man modifierar kontrastmedlets yta med exempelvis antikroppar mot den identifierade cellmarkören eller andra förändringar som gör att cellen känner igen kontrastmedlet. Ett fungerande kontrastmedel eller molekylär prob måste dessutom ha egenskaper som ger, eller förbättrar bilder som tas med en eller flera olika avbildningstekniker. Molekylen eller partikeln måste då bära på funktionella enheter som har minst en av dessa egenskaper.

Totalt undersökte vi sju olika typer av molekylära prober i denna avhandling. I delarbete I och II bestod dessa av gasbubblor, av biokompatibelt material med olika funktionella egenskaper i skalet för bland annat ultraljud, nuklearmedicinsk och magnetisk resonansavbildning. I delarbete III-IV användes humant serum albumin som bärarmolekyl som modifierades för målsökning och för att ge upphov till signal med nuklearmedicinska tekniker. I delarbete II-IV modifierades dessa prober med antikroppar eller kemiska strukturer för målsökande avbildning av inflammation. De molekylära probernas egenskaper, upptagsmekanismer och tillämpbarhet för avbildning undersöktes i cell- och djurstudier.

Forskningen som utförts inom ramen för denna avhandling är ett multidisciplinärt samarbete som involverar olika typer av naturvetenskapliga forskare. Avsikten var att kartlägga celler och specifika markörer involverade i åderförkalkning och att utveckla kontrastmedel som studeras i cell- och djurstudier för målsökning och avbildning med olika bildtekniker så som ultraljud, skiktröntgen, magnetkamera eller nuklearmedicinska tekniker. Målet för framtiden är att kunna bidra till den medicinvetenskapliga utvecklingen genom att detektera farlig åderförkalkning som kan motivera särskild behandling, vilket i slutändan gagnar patienten.

ABSTRACT

The imaging field is rapidly evolving and in the last two decades there have been tremendous developments in the field of multimodal imaging. Multimodal molecular imaging approaches that utilize ultrasound/magnetic resonance imaging (US/MRI), single-photon emission computed tomography/computed tomography (SPECT/CT), or positron emission tomography/MRI (PET/MRI) may provide additional detailed information at the cellular and molecular level to help identify patients with vulnerable plaques that are at risk of rupture. The search for specific biomarkers in combination with specific and optimized molecular probes may help to prevent adverse events such as myocardial infarctions or strokes. Current clinical contrast agents do not provide information on the inflammatory components of atherosclerotic plaques; thus, more specific molecular probes are needed. This thesis focuses on probe development for different molecular imaging techniques using multimodal and targeting approaches.

Several types of molecular probe were evaluated: bimodal and multimodal microbubbles, as well as chemically modified human serum albumin (HSA)-based probes (aconitylated (Aco) and maleylated (Mal)) for targeting markers of inflammation; adhesion molecules on endothelial cells or macrophages, and scavenger receptor A1 (SR-A1) on macrophages. Evaluation of these molecular probes was facilitated by their physical properties enabling assessment with fluorescence microscopy, flow cytometry, and nuclear imaging properties for *in vivo* molecular imaging with SPECT/CT and PET/MRI.

We found that functionalizing molecular probes with targeting moieties greatly improved the targeting specificity and avidity to the target compared to non-targeted molecular probes. Furthermore, these molecular probes were successfully radiolabeled with a detectable *in vivo* signal by ^{99m}Tc-anti-ICAM-1- MBs imaging of inflammation with SPETC/CT, and atherosclerosis by ^{89}Zr-Mal-HSA with PET/MRI. *Ex vivo* evaluation of HSA-based probes showed significant accumulation in atherosclerotic lesions of *Apoe*$^{-/-}$ mice, as quantified by gamma counter and phosphor imaging autoradiography, compared to wild type (WT) mice.

In conclusion, adhesion molecule targeting and scavenger receptor targeting with functionally modified probes in this thesis showed potential for the imaging of inflammation and atherosclerosis. Of the evaluated probes, modified HSA-based probes seem to have the greatest potential for clinical application in molecular imaging of atherosclerosis.

LIST OF SCIENTIFIC PAPERS

I. **Ahmed M,** Cerroni B, Razuvaev A, Härmark J, Paradossi G, Caidahl K, Gustafsson B. Cellular Uptake of Plain and SPION-Modified Microbubbles for Potential Use in Molecular Imaging. *Cell Mol Bioeng*. 2017, 10(6): 537-548.

II. **Ahmed M,** Gustafsson B, Aldi S, Dusart P, Egri G, Butler LM, Bone D, Dähne L, Hedin U, Caidahl K. Molecular Imaging of a New Multimodal Microbubble for Adhesion Molecule Targeting. *Cell Mol Bioeng*. 2019, 12(1): 15-32. *https://doi.org/10.1007/s12195-018-00562-z*

III. **Ahmed M,** Baumgartner R, Aldi S, Dusart P, Hedin U, Gustafsson B, Caidahl K. Human serum albumin-based probes for molecular targeting of macrophage scavenger receptors. *Resubmitted after revision. Int J Nanomed 2019.*

IV. **Ahmed M,** Tegnebratt T, Tran T, Damberg P, Gisterå A, Tarnawski L, Hedin U, Eriksson P, Holmin S, Gustafsson B, Caidahl K. Evaluation of a ^{89}Zr-labelled probe for molecular imaging and targeting of macrophage scavenger receptors in a mouse model of atherosclerosis. *In manuscript*.

TABLE OF CONTENTS

LIST OF ABBREVIATIONS

^{18}F	fluorine-18
^{18}F-FDG	fluorine-18 labeled fluorodeoxyglucose
2D	2-dimensional
3D	3-dimensional
^{89}Zr	zirconium-89
^{89}Zr-Mal-HSA	maleylated human serum albumin labeled with zirconium
ABCA1	ATP-binding cassette transporter A1
ABCG1	ATP-binding cassette transporter G1
ACAS	asymptomatic carotid atherosclerosis study
acLDL	acetylated LDL
Aco	aconityl
Aco-HSA-DFO	aconityl modulated HSA with DFO
AFM	atomic force microscopy
ALTOs	arterial tertiary lymphoid organs
apo	apolipoprotein
ApoA1	apolipoprotein A1
ApoB-48	apolipoprotein B-48
ApoC	apolipoprotein C
ApoE	apolipoprotein E
Apoe$^{-/-}$	knock-out of apolipoprotein E gene
ATP	adenosine triphosphate
B-mode	brightness mode
CAMs	cell adhesion molecules
CANTOS	canakinumab anti-inflammatory thrombosis outcomes study
CCL2	C-C motif chemokine ligand 2 (MCP-1)
CCL5	C-C motif chemokine ligand 5 (RANTES)
CD	Cluster of Differentiation
$CD14^{high}$	pro-inflammatory type of monocytes in humans
$CD16^{neg}$	patrolling type of monocytes in humans
CD62E	E-selectin
CD62P	P-selectin
CETP	cholesteryl ester transfer protein
CEUS	contrast-enhanced ultrasound
CLSM	confocal laser scanning microscopy
CMs	chylomicrons
CNR	contrast-to-noise ratio
cRGD	cyclic RGD recognized by $\alpha_v\beta_3$ integrin receptor
CRP	C-reactive protein
CT	computed tomography
CTA	computed tomography angiography
CVD	cardiovascular disease

DAMPs	danger-associated molecular patterns
DAPI	4',6-Diamidino-2-Phenylindole, Dihydrochloride
DFO	deferoxamine
DOTA	tetraazacyclododecane tetraacetic acid
DOTATATE	covalently bonded DOTA bifunctional chelator
ECG	electrocardiography
ECM	extracellular matrix
ECs	endothelial cells
ECST	European carotid surgery trial
ESC	European society of cardiology
ESVS	European society of vascular surgery
FcRn	neonatal Fc receptor
FDG	2-deoxy-2-fluoro-D-glucose
FEMPA	N-{2-[2-fluoroethoxy]-5-methoxybenzyl}-N-[2-(4-methoxyphenoxy)pyridin-3-yl]acetamide
FITC	fluorescein isothiocyanate
FMO	fluorescence minus one
FMT	fluorescent molecular tomography
FSE	fast spin echo
Gd	gadolinium
GP	glycoprotein
GSM	grayscale median
HCtSMCs	human carotid smooth muscle cells
HDL	high density lipoproteins
HMG-CoA	3-hydroxy-3-methylglutaryl CoA
HSA	human serum albumin
HUVECs	human umbilical vein endothelial cells
ICAM-1	intracellular adhesion molecule 1
IDL	intermediate density lipoprotein
IFN-γ	interferon gamma
IL-13	interleukin 13
IL-1β	interleukin-1β
IL-4	interleukin 4
IL-6	interleukin 6
iNOS	inducible nitric oxide synthases
IRW	Inveon^{TM} Research Workplace
iTLC	thin-layer chromatography
IVUS	intravascular ultrasound
KLF4	Kruppel-like factor 4
KO	knock-out
LAMP2	Lysosome-associated membrane protein 2 (CD107b)
LDL	low-density lipoprotein
LDLR	LDL receptor
Ldlr$^{-/-}$	knock-out of LDL receptor gene
LPS	lipopolysaccharide
LRNC	lipid-rich necrotic core

ly6C^{hi}	pro-inflammatory type of monocytes in mice
Ly6C^{low}	patrolling type of monocytes in mice
M1 and M2	polarized macrophage types
Mal	maleyl/maleylated
Mal-BSA	maleylated bovine serum albumin
Mal-HSA	maleylated human serum albumin
Mal-HSA-DFO	maleyl modulated HSA with DFO
MCP-1	monocyte chemoattractant protein-1 (CCL2)
M-CSF	macrophage colony-stimulating factor
MDA	malondialdehyde
MDA-LDL	malondialdehyde- LDL
mFcRn	mouse FcRn
MHC	major histocompatibility complex
MMPs	matrix metalloproteases
MoAoECs	mouse aortic endothelial cells
MR	mannose receptor
MRA	magnetic resonance angiography
MRI	magnetic resonance imaging
MSR1	macrophage scavenger receptor 1
Myh11	myosin heavy chain 11
NASCET	North American symptomatic carotid endarterectomy trial
NF- κB	nuclear factor kappa B
NLRP3	NACHT, LRR, and PYD domains-containing protein 3
NO	nitric oxide
NOTA	triazacyclononane triacetic acid
OSEs	oxidation-specific epitopes
oxLDL	oxidized low density lipoprotein
oxPL	oxidized phospholipids
PAI	photoacoustic imaging
PCI	percutaneous coronary intervention
PCSK9	proprotein convertase subtilisin/kexin type 9
PE-CAM-1	platelet-endothelial cell adhesion molecule-1
PEG	polyethylene glycol
PET	positron emission tomography
PI-ARG	phosphor imaging autoradiography
PVA	polyvinyl alcohol
RANTES	regulated upon activation, normal T cell expressed, and secreted (CCL5)
RAW264.7	macrophage; Abelson murine leukemia virus transformed
RF	radiofrequency
RGD	Arg-Gly-Asp
ROI	region of interest
ROS	reactive oxygen species
SMCs	smooth muscle cells

SNR	signal-to-noise ratio
SPECT	single-photon emission computed tomography
SPION	supraparamagnetic iron oxide nanoparticles
SR	scavenger receptor
SR-A1	scavenger receptor A1
SR-B1	scavenger receptor B1
SUV	standardized uptake value
SUV_{max}	maximum standardized uptake value
TBR	target-to-background ratio
TBR_{max}	maximum target-to-background ratio
TEM	transmission electron microscopy
TGF-β	transforming growth factor beta
TGs	triglycerides
Th1	T helper cell type 1
Th17	T helper cell type 17
Th2	T helper cell type 2
THP-1	human monocytic leukemia-derived cell line
Treg	regulatory (suppressor) T-cells
TSPO	translocator protein
US	ultrasound
USPIO	ultra-small paramagnetic particles of iron oxide
VCAM-1	vascular cell-adhesion molecule 1
VH	virtual histology
WHHL	Watanabe heritable hyperlipidemic (rabbit)
WT	wild type (mouse)
VLDL	very-low-density lipoprotein
VOI	volume of interest
VSMCs	vascular smooth muscle cells

1 RATIONALE

At present, despite significant diagnostic and therapeutic improvements, cardiovascular diseases (CVDs) account for the majority of deaths worldwide. Accurate diagnosis is important in giving the patient the right treatment at the right time. The challenging questions for cardiologists and vascular surgeons remain: How can one discover *patients at risk* of future symptomatic events from atherosclerotic lesions? Which patients should we screen, treat, and operate on? Today we are able to identify culprit lesions in the coronary arteries via gold standard angiography in symptomatic patients, but what about the subclinical disease burden and the "asymptomatic patients" with currently non-obstructive but potentially dangerous atherosclerosis? We know that some of these harbor features that will eventually cause the plaque to rupture, but there are insufficient diagnostic tools. In order to answer these questions, it is not uncommon for a patient to undergo several diagnostic examinations.

In clinical practice, the lumenography approach using invasive angiography is still the backbone of imaging. However, the information provided is limited and insufficient to predict the likelihood of future thromboembolic events. The research field of *molecular imaging* has focused on developing noninvasive methods to improve the visualization of vulnerable plaque. A lot of research has also been dedicated to finding specific biomarkers to predict future events by screening patients or subjects in the general population. When combined with today's rapid advances in the molecular imaging field using more specific molecular imaging probes, this might allow us to detect and visualize rupture-prone plaques.

Nuclear imaging techniques in combination with anatomical imaging, such as computed tomography (CT) or magnetic resonance imaging (MRI), have emerged as promising tools due to their benefits in localizing targets with high sensitivity and molecular precision (Brinjikji et al. 2016; Tarkin et al. 2016). The most studied targets in atherosclerosis include microcalcification, neovascularization, macrophages, and adhesion molecules expressed on activated endothelium (Quillard et al. 2012; Sriranjan et al. 2016; Tarkin et al. 2016). The most commonly utilized radiotracer in molecular imaging is fluorine-18 fluorodeoxyglucose (^{18}F-FDG) (Rudd et al. 2008; Rudd et al. 2009). However, the tracer has low specificity, which limits its use, and more *specific probes* for the imaging of inflammation in atherosclerosis are needed. Developing effective probes for this purpose is often difficult and is an area of intense research. Extensive *in vitro* and *in vivo* preclinical evaluation is needed before application to humans. This thesis focuses on the probe development and preclinical evaluation of probe-cell interactions in endothelial cells and macrophages as well as the feasibility of *in vivo* atherosclerotic plaque detection for application in molecular imaging of inflammation.

2 REVIEW OF LITERATURE

2.1 Cardiovascular Diseases

CVDs are the leading cause of global fatalities. Over 80% of all CVD deaths are due to myocardial infarctions and strokes (World Health Organization 2017). Myocardial infarction and ischemic stroke occur as a result of blockage of the blood vessels, giving rise to symptoms such as chest pain or neurological deficits. Established risk factors based on the Framingham heart study include unhealthy diet, tobacco use, inadequate physical activity, and inherited genetic factors. These factors may in turn lead to high blood glucose level (diabetes), hyperlipidemia, hypertension, and obesity, and increase the risk of cardiovascular events (Benjamin et al. 2018; Mahmood et al. 2014). The underlying cause in most cases is atherosclerosis, which is compartmentalized into coronary artery disease, carotid artery disease, and peripheral artery disease. Patients with atherosclerotic lesions may be classified as symptomatic or asymptomatic (Naghavi et al. 2003). Although so-called silent myocardial infarctions exist (Barbier et al. 2006), events are usually symptomatic. With carotid stenosis, indications of plaque vulnerability are more pronounced among symptomatic patients (Matic et al. 2018). Stenosis in the carotid or coronary arteries can be evaluated by computed tomography (CT) and, in the former case, also by ultrasound. However, both myocardial infarctions and strokes can occur as a result of atherosclerotic plaque rupture and subsequent thrombosis without a prior advanced arterial obstruction (Naghavi et al. 2003). Characterization of plaque vulnerability, or the vulnerable patient, is therefore important for the possibility of optimizing treatment and preventive measures in atherosclerosis on an individualized basis.

Clinical management focuses on preventive strategies (primary, secondary, and tertiary), diagnostic strategies (screening, acute exams, and follow-ups), and medical treatment and interventions. To help guide clinicians, the European Society of Cardiology (ESC) ((ESC) 2018) and the European Society of Vascular Surgery (ESVS) (Naylor et al. 2018; Powers et al. 2018) have established guidelines and clinical algorithms by which patients' conditions should be managed to prevent the first onset or recurrence of events and reduce mortality. Identification of patients at risk of cardiovascular events is crucial. Related research, focusing on basic scientific and diagnostic improvements—such as this thesis—is necessary to transfer the knowledge derived from preclinical research into clinical applications that benefit the patient.

2.2 Atherosclerosis

2.2.1 The History of Atherosclerosis

Leonardo Da Vinci was among the first to describe atherosclerosis (Davies et al. 1996). In the mid-eighteenth century one of the first cases of plaque rupture was reported: the Danish artist Bertil Thorvaldsen suffered a sudden cardiac arrest in the middle of a concert and the subsequent autopsy attributed coronary plaque rupture as the cause of death. At the end of the eighteenth century, two theories arose describing the pathophysiology of atherosclerosis: the *thrombogenic theory* proposed by Carl von Rokitansky and the *inflammatory theory* with in-depth histological characterization of atherosclerotic lesions proposed by Rudolf Virchow. Virchow proposed a link between the thrombogenicity of the blood, the diseased vessel wall, and the resulting hemodynamics, which collectively caused thrombosis. These factors are termed *Virchow's triad*. Virchow's hypothesis of local intimal injury formed the basis of the *response to injury hypothesis* formulated by Ross and Glomset in the 1970s, describing smooth muscle cell proliferation as a response to injury (Ross et al. 1976a; Ross et al. 1976b). The release by endothelial cells of an endothelium relaxing factor, later identified as nitric oxide (NO) and crucial for vascular function, was proposed by Robert Furchgott, who shared the Nobel Prize in physiology or medicine with Ferid Murad and Louis Ignarro in 1998 (Rubin 2019). Furthermore, in the 1990s, two other hypotheses were presented: one describing lipid retention as the major cause of atherogenesis (Watanabe et al. 1985; Williams et al. 1995) and the other describing inflammatory processes as the driving cause (Hansson et al. 2002). Intense research within the field, spearheaded by Libby's, Hansson's, and Fogelman's groups, have led to an understanding of some of the underlying inflammatory mechanisms of atherosclerosis, involving cells from both the innate and adaptive immune systems, chemical factors, and local or systemic inflammation (Slijkhuis et al. 2009). Extensive research has also focused on the detection of inflammatory biomarkers as a sign of unstable disease (Matic et al. 2018; Ridker et al. 2009).

C-reactive protein (CRP) in blood, measured by high sensitivity assays, has been linked to increased risk of cardiovascular disease (Ridker et al. 2009; Slijkhuis et al. 2009), although other factors such as infectious diseases may also increase CRP. However, Narula et al. showed that local factors such as inflammation in individual atherosclerotic plaques are associated with a higher risk of rupture and might be better predictors for risk stratifications (Narula et al. 2008; Narula et al. 2007). Some of the underlying mechanisms of plaque rupture have been identified and include inflammation, protease activity, apoptosis, and prothrombotic factors, for example tissue factors (Geovanini et al. 2018). Despite many theories being developed in past years, the

precise mechanisms responsible for plaque rupture are unknown and not easily predicted; hence the importance of improved diagnostic tools.

2.2.2 Pathogenesis of Atherosclerosis

Atherogenesis is the process of forming plaques in the intimal layer of arteries. Atherosclerosis is a disease in which the inside of an artery narrows due to the buildup of plaque. Today, the general concept of atherosclerosis as a chronic inflammatory disease is well established. The inflammatory processes in the arteries develop over decades and involve endothelial dysfunction and abnormal accumulation of lipids. The lesion progression may be histologically classified into different phases (Stary grade I-VI) and different types of plaque—stable and unstable or vulnerable—which also facilitate the understanding of disease progression (Stary et al. 1995; Stary et al. 1994).

2.2.2.1 Endothelial Function and Dysfunction in Atherosclerosis

Normal arteries have designated layers. Starting from the lumen, the endothelium is a monolayer of endothelial cells (ECs) that lines the inner wall of the vasculature and, together with subendothelial connective tissue, compromises the tunica intima. The next layer is built up with connective tissue and several layers of smooth muscle cells (SMCs), responsible for vascular elasticity, and is called the tunica media. The outermost layer, called tunica externa or the adventitia, consists of connective tissue, small blood vessels, lymphatic vessels, nerves, and surrounding perivascular fat.

ECs are key players in acute and chronic inflammatory reactions within the arterial wall (Gimbrone et al. 2016). In a healthy state, the endothelium maintains homeostasis by controlling vascular tone and vascular permeability. The endothelium has the ability to produce substances that affect both vasoconstriction and vasodilation (Furchgott et al. 1980). ECs are affected by the tangential force of the flowing blood on the vascular bed, (i.e. the shear stress). In laminar flow, the shear stress is high, promoting EC survival, alignment in the direction of flow, and upregulation of atheroprotective transcription factors such as Kruppel-like factor 4 (KLF4) (Zhou et al. 2012) or production of vasodilators and anticoagulant factors. In turbulent flow with low shear stress, often seen in inner curvature and bifurcations, plaques are more likely to develop due to endothelial cell dysfunction (Chiu et al. 2011; Hsieh et al. 2014). This process is associated with impaired production of the vasodilator nitric oxide (NO). The decrease in NO will in turn lead to increased vascular permeability and vascular tone. At the

sites of low shear stress, gene expression alterations via nuclear factor kappa B (NF-κB) pathways activate the endothelium and upregulate adhesion molecules, pro-inflammatory chemokines, and cytokines that will attract leucocytes (Nakashima et al. 1998). Adhesion molecules are expressed early in atherosclerosis (Cybulsky et al. 2001; Davies et al. 1993; O'Brien et al. 1993). The process of transendothelial migration of leucocytes into the intima is assisted by the expression of endothelial ligands. The immune cells recognize the ligands by their surface antigens. The process starts with leucocyte rolling and binding to E-selectin and P-selectin on the endothelium. Firm adhesion of the leucocyte is mediated by the vascular cell-adhesion molecule 1 (VCAM-1) and intracellular adhesion molecule 1 (ICAM-1). Next, the leucocyte transmigrates by crawling—either paracellularly, between endothelial connections, or transcellularly—across the EC, into the subendothelial space (Leon et al. 2008; Schnoor 2015). Adhesion molecules are one of the most studied targets for molecular imaging of inflammation in atherosclerosis (Behm et al. 2008; Gargiulo et al. 2016; Kaufmann et al. 2007a; Klibanov et al. 2006; Villanueva et al. 1998).

2.2.2.2 Lipid Metabolism

Lipids are the collective term for fatty acids, triglycerides (TGs), and certain components of the membrane such as phospholipids and cholesterol.

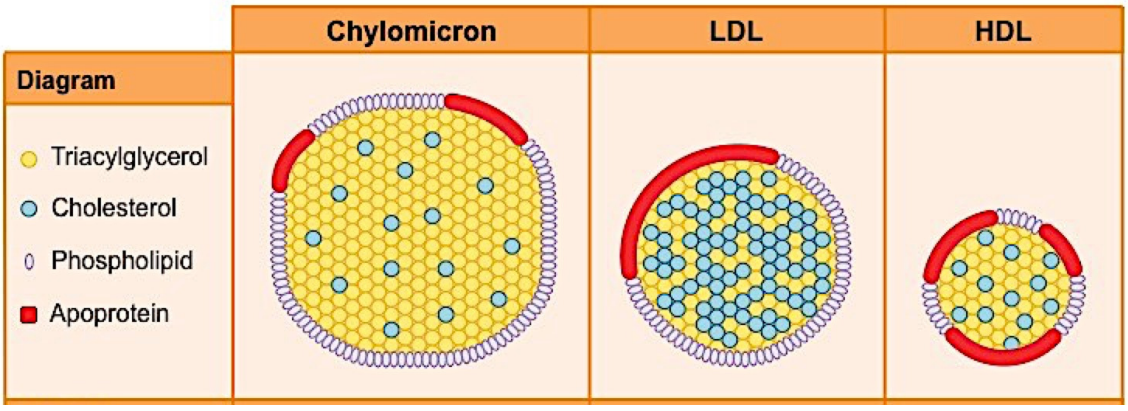

Figure 2.1: Examples of the different lipoproteins and their lipid and protein content. Refer to text for detailed explanation. Picture reference from Cornell B, 2016. Lipoproteins. Available at: http://ib.bioninja.com.au [Accessed 28 January 2019].

Blood lipids are derived from endogenous biosynthesis and dietary intake lipids. Lipids are hydrophobic and therefore carried in association with proteins called apolipoproteins (apo), the combination being referred to as lipoproteins. Lipoproteins are hydrophilic structures of phospholipid shells and may comprise several apolipoproteins. They carry a "cargo" of triglycerides, free cholesterol, and cholesteryl esters. Lipoproteins are classified, based on their

size and density, as chylomicrons (CMs): very low, intermediate, and low- or high-density lipoproteins (VLDL, IDL, LDL or HDL respectively), **Figure 2.1**. CMs are produced in the intestine from dietary lipids, consist mainly of TGs, and contain apolipoprotein B48, C and E (ApoB-48, ApoC, ApoE).

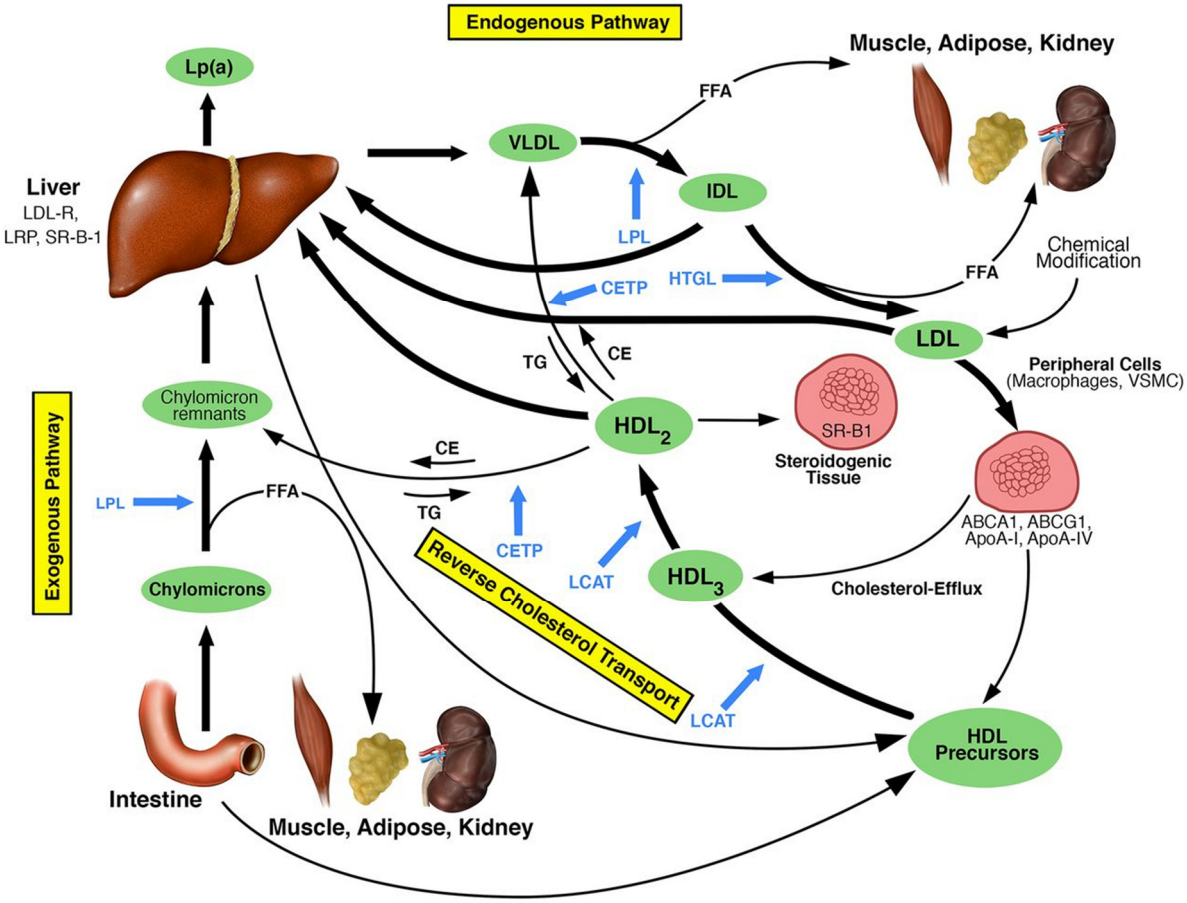

Figure 2.2: Schematic illustration of the major normal lipoprotein metabolic pathways. Blue arrows refer to points of action of the respective enzymes in blue. ABCA1, ATP-binding cassette transporter A1; ABCG1, ATP-binding cassette transporter G1; ApoA-I, apolipoprotein A-I; ApoA-IV, apolipoprotein A-IV; CE, cholesterol ester; CETP, cholesteryl ester transfer protein; FFA, free fatty acid; HTGL, hepatic triglyceride lipase; IDL, intermediate-density lipoprotein; LCAT, lecithin–cholesterol acyltransferase; LDL-R, LDL receptor; LPL, lipoprotein lipase; LRP, LDL-R–related protein; SR-B1, scavenger receptor B1; TG, triglyceride; VLDL, very low-density lipoprotein; VSMC, vascular smooth muscle cells. Reproduced from (Kronenberg 2018), with permission from the American Society of Nephrology.

CMs are transported via the lymphatic system to the blood circulation where they become remnant CMs after the removal of TGs. This is accomplished by the enzyme lipoprotein lipase releasing free fatty acid to the adipose tissue and muscles together with glycerol for glucose synthesis in the liver. CM remnants are then transported back to the liver. VLDL is largely produced in the liver and contains mainly TGs and apolipoprotein B100 (ApoB100), but it also acquires ApoC and ApoE. After the release of TGs it becomes IDL. LDL is derived from VLDL in the bloodstream and contains mainly cholesterol and ApoB100

as its major structural protein. The LDL receptor (LDLR) mediates the uptake of LDL from the bloodstream into hepatic cells and the cells of the peripheral tissue. Once LDL is bound to LDLR, the complex is endocytosed, free cholesterol is released into the cell, and LDLR recycled back to the cell surface. LDL is considered to be pro-atherogenic and is often referred to as the "bad cholesterol" in everyday speech since it transports hepatic lipids to the peripheral tissue (including atherosclerotic plaques) and is the main carrier of cholesterol in humans. On the other hand, HDL—referred to as the "good cholesterol"—is believed to be atheroprotective, transporting cholesterol from the peripheral tissue to the liver, and has Apolipoprotein A1 (ApoA1) as the major structural lipoprotein (Baynes 2018; Feingold 2018).

The HDL particles may to some extent protect the artery from cholesterol overload by facilitating cholesterol efflux from the lipid loaded cells in the vessel wall—a process known as reverse cholesterol transport, promoting plaque reduction. Reverse cholesterol transport on macrophages is mediated via four efflux pathways. The two passive diffusion pathways are via aqueous diffusion and via facilitated diffusion (SR-B1-mediated pathways). The two active processes involve members of the ATP-binding cassette (ABC) family of transmembrane transporters, namely ATP-binding cassette transporter A1 (ABCA1) and ATP-binding cassette transporter G1 (ABCG1) on macrophages. Free excess cholesterol is also transported to ApoA1 and ApoA1V on HDL particles. The HDL particles can transform into larger particles (HDL_3 and HDL_2) by acquisition of additional cholesteryl esters, triglycerides and apolipoproteins. Large HDL particles bind to SR-B1 in liver and steroidogenic tissues and release their cargo to the cells. HDL can also interact with the cholesteryl ester transfer protein (CETP) that facilitates an exchange of cholesteryl esters (CEs) and TGs between LDL particles (Kronenberg 2018; Phillips 2014), **Figure 2.2**. Excess intracellular cholesterol can also be effluxed to ApoE-containing lipoproteins, produced mainly by hepatocytes and macrophages, for transportation to the liver (Getz et al. 2009; Seo et al. 2015).

Hyperlipidemia is one of the risk factors of CVD and a cornerstone of medical treatment is the use of lipid lowering drugs such as HMG-CoA reductase inhibitors, popularly known as "statins", which block cholesterol synthesis in the liver. The lipid-lowering effect from statins is not only due to reduced biosynthesis, but also to the concomitant upregulation of LDLR in the liver (Ridker et al. 2009; Tang et al. 2009a; Tawakol et al. 2013; Wu et al. 2007). A new class of lipid-lowering drugs, the proprotein convertase subtilisin/kexin type 9 (PCSK9)-inhibitors, can be applied to reduce the lysosomal degradation of LDLR via PCSK9, further increasing LDL clearance. This drug has been approved for the treatment of patients with familiar hypercholesterolemia (Ahn et al. 2015).

2.2.2.3 Lipid Dysregulation and Formation of Foam Cells (Stary grade I-II)

LDL particles from the bloodstream can infiltrate the vessel wall and become modified. The initiation of atherosclerosis involves accumulation of lipids in the intimal layer, triggering an inflammatory response by secretion of cytokines by leukocytes and upregulation of adhesion molecules on ECs. Circulating monocytes in the bloodstream will respond to the expression of adhesion molecules on the EC surface and migrate into the intima of the arterial wall, where they become macrophages (Libby 2002; Stary et al. 1994). Accumulation of LDL particles in the arterial wall leads to modifications, such as oxidation, and the modified particles will be taken up by macrophages transitioning them into foam cells (Stary grade I), a hallmark of early atherosclerosis. Foam cells are defined as cells with numerous lipid droplets. The uptake of modified LDL by macrophages and foam cells can occur via scavenger receptors (SRs) (Kunjathoor et al. 2002). Further information about SRs and the role of macrophages is described in section 2.3.2.

An imbalance of cholesterol uptake and efflux can cause the free non-esterified cholesterol in plaque to form cholesterol crystals that serve as pro-inflammatory stimuli. When the lesion accumulates foam cells and lipid-laden SMCs, it will give rise to fatty streaks (Stary grade II) (Chellan et al. 2016; Stary et al. 1994). Oxidized low-density lipoprotein (oxLDL) and oxidized phospholipids (oxPL) have been associated with high cardiovascular risk (Byun et al. 2017; Tsimikas et al. 2012; van der Valk et al. 2016). During oxidation of LDL, the by-products of lipid peroxidation generate many pro-inflammatory chemical modifications of both the lipid and protein moieties, collectively termed oxidation-specific epitopes (OSEs). Examples of OSEs are oxPL and malondialdehyde (MDA) epitopes, both of which are well defined chemically and immunologically. They represent danger-associated molecular patterns (DAMPs) and induce a pro-inflammatory response (Binder et al. 2016; Miller et al. 2011).

2.2.2.4 Lesion Progression and Plaque Vulnerability

As lesion development progresses, macrophages, foam cells, and lipid-laden SMCs continue to gather and larger deposits of lipids accumulate inside the plaque (Stary grade III). Dense accumulation of extracellular lipid promotes lipid core formation and inflammatory cell infiltration (Stary grade IV). The pro-inflammatory milieu triggers SMC proliferation and migration with an increased extracellular matrix (ECM) and a covering layer of connective tissue called the fibrous cap. The lesion may undergo positive remodeling in an attempt to resolve inflammation without luminal narrowing. As the lesion increases in size, an increase in fibrosis and intimal thickening is observed. The so called fibroatheroma, classified by Virmani

et al. (Virmani et al. 2000), consist of the classical lipid core and fibrous cap (Stary grade V). At this stage of atheroma, lesions are usually still asymptomatic.

The naturally phagocytic macrophages will not only endocytose lipids, but also cell debris from dying cells undergoing programmed cell death—so-called apoptosis. Apoptotic material and cellular debris make up the necrotic core of the lesion. The process whereby phagocytic cells remove necrotic or apoptotic cells is called efferocytosis (Moore et al. 2011). In the cascade of pro- and anti-inflammatory signaling, non-resolving inflammation will eventually trigger a destruction of the intima. As the lesion progresses, with luminal narrowing and lesions becoming more advanced, proteolytic degradation of ECM by matrix metalloproteases (MMPs) results in thinning of the fibrous cap and gives rise to *thin cap fibroatheroma*, defined as less than 65 µm thickness (Narula et al. 2013; Virmani 2003). Other features, such as cholesterol crystals and intraplaque hemorrhage, may also be visible. At this stage of the disease, the lesions are more disorganized and symptoms are likely to appear. Deposits of calcium ranging from microcalcification to larger calcified nodules and whole plaque calcifications may be observed. Calcification is usually a feature of more stable plaques, but can cause plaque instability if it occurs in small nodules—a feature associated with increased risk of cardiovascular events (Ruiz et al. 2015; Sage et al. 2010). The calcified nodules can be imaged by ultrasound, giving rise to a "spotty" appearance (Ehara et al. 2004).

As the lesion grows, the disease burden increases and some of the areas inside the plaque will become hypoxic and trigger the formation of new blood vessels (a process known as neovascularization). This process is a target for molecular imaging. At this point, the plaque harbors features of high vulnerability with an increased risk of plaque rupture or erosion. The rupture of the plaque normally occurs at the edges of the lesion; the so-called shoulder regions, with great mechanical stress. In plaque erosion, the endothelial layer is absent, revealing thrombogenic material such as tissue factor and collagen and triggering a coagulation cascade, with platelet aggregation and thrombosis (Virmani et al. 2002). Thrombus formation (Stary grade VI) does not necessarily lead to an acute blockage of the vascular lumen and might, instead, partially dissolve. The ruptured plaque will then heal and often cause an increase in lesion size (Libby et al. 2005; Sanan et al. 1998; Virmani et al. 2000). However, if the stenosis is significant, either because of an obstructive lesion or a thrombosis blocking the blood flow in a coronary or carotid artery following rupture or erosion, this could lead to decreased perfusion in the heart or brain tissue and result in ischemic myocardial infarction or ischemic stroke.

2.2.3 Inflammation in Atherosclerosis

Although this thesis focuses on targeting activated endothelial cells and SRs on macrophages, it is important to understand the complex interplay between the cells in the atherosclerotic plaque. Inflammatory cells and their mediators are key players in atherosclerosis and involve cells from both the adaptive and innate immune systems. The immune cells will react to molecular structures, triggering an inflammatory cascade. In atherosclerosis, these altered structures include modified LDL (e.g. oxLDL), cholesterol crystals, degraded material, and debris from ECM (Geovanini et al. 2018; Libby 2002). A schematic drawing of the atherosclerotic plaque components and the inflammatory mediators is shown in **Figure 2.3**.

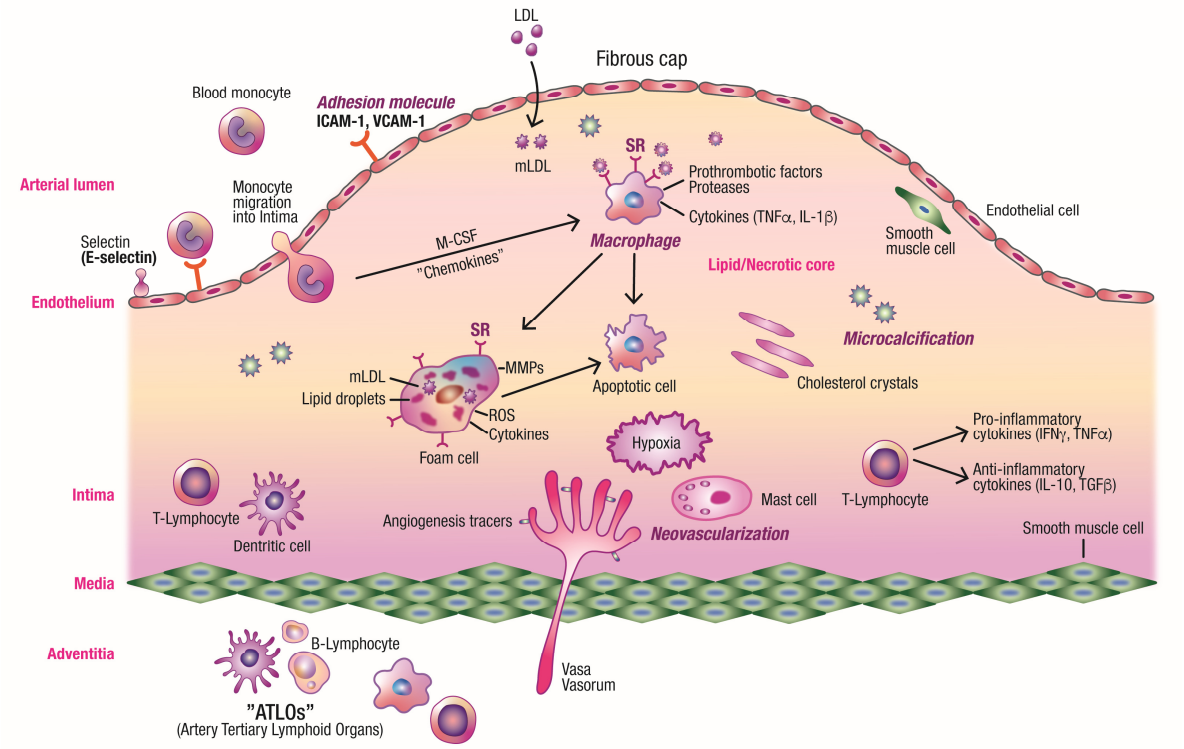

Figure 2.3: Illustration of the effector cells in atherosclerosis and the most common molecular imaging targets of atherosclerotic plaques (*adhesion molecules, macrophages, neovascularization and microcalcification*). Circulating inflammatory cells are recruited to the plaque by cytokines, chemokines, and the expression of adhesion molecules on the endothelial cell surface. In the intima, the monocytes differentiate into macrophages and ingest modified LDL (mLDL). Macrophages transform into foam cells with lipid droplet accumulation and some cells will undergo apoptosis, eventually leading to the formation of a lipid/necrotic core. Vascular smooth muscle cells constitute the media and contribute to fibrous cap formation. Other present cells are: T-lymphocytes, dendritic cells, and mast cells. Some of these cells are localized in the adventitia together with B-lymphocytes (ATLOs).

Factors affecting the trafficking of immune cells in the atherosclerotic plaque may be divided into pro-inflammatory and anti-inflammatory factors. Such signaling molecules are called cytokines or chemokines, a subclass of cytokines. These are produced by cells within the plaque. The typical cytokines affecting plaque progression and, hence, regarded as pro-inflammatory, include interferon gamma (IFN-γ) and tumor necrosis factor alpha (TNF-α), and interleukins such as IL-1β and IL-6, while the atheroprotective, anti-inflammatory cytokines include transforming growth factor beta (TGF-β), IL-4 and IL-10. Important chemokines in atherogenesis, which function to attract monocytes to penetrate the intima, include monocyte chemoattractant protein-1 (MCP-1/CCL2). The chemokine that attracts T-cells to plaque is regulated on activation, normal T cell expressed, and secreted (RANTES/CCL5). Hence, cytokines function to direct extravasation, polarization, and differentiation of cells. Chemokines attract and recruit cells to enter the tissue via a process known as chemotaxis (Hansson et al. 2006). TGF-β functions to stimulate extracellular collagen maturation, stabilizing the plaque and positively regulating the synthesis of collagen by SMCs (Amento et al. 1991). IFN-γ, on the other hand, destabilizes the plaque by inhibiting SMC differentiation, proliferation, and collagen production and maturation. A link between the cholesterol metabolism and innate immunity is the NLRP3 inflammasome, activated by cholesterol crystals in foam cells, that leads to the secretion of IL-1β (Duewell et al. 2010). IL-1β stimulates the production of IL-6 in SMCs and macrophages (Loppnow et al. 1990), which in turn signal the liver to produce CRP (Hansson 2005). Recently, monoclonal antibodies that specifically target IL-1β (Canakinumab) have been developed. The clinical trial CANTOS showed that explicitly targeting inflammation can reduce clinical cardiovascular events (Ridker et al. 2017).

2.2.3.1 Monocytes and Macrophages in Atherosclerosis

Origin: Myeloid progenitor cells in the bone marrow give rise to monocytes, macrophages, dendritic cells, neutrophils and mast cells, among others. Recent studies on linage tracing of cells in atherosclerotic plaques have shown that lesional cells expressing macrophage markers can also originate from vessel wall-derived cells, such as transdifferentiated vascular SMCs (Bennett et al. 2016), although their properties and fate are still largely undefined. Hence, not all macrophages are necessarily myoleoid progenitors derived from circulating monocytes. In many organs, adult tissue macrophages originate during embryonic development and not from circulating monocytes. They are proliferative cells maintained by self-renewal and are located in many different organs of the body, functioning as a first line of defense in response to pathogens and microbial infections. Tissue resident macrophages are found in the brain, lungs,

liver (Kupffer cells), spleen, adipose tissue, and in the peritoneum (Hashimoto et al. 2013; Hoeffel et al. 2015; Yona et al. 2013). Mouse peritoneal macrophages are among the best-studied macrophage populations in terms of cell biology, development, and inflammatory responses (Cassado Ados et al. 2015).

Recruitment of circulating monocytes: Monocytes circulate in the bloodstream and are drawn to migrate into intima upon chemokine secretion and endothelial cell activation. Monocytes are a heterogeneous population, giving rise to different polarized macrophages in the tissue upon cytokine stimulation and other stimuli. In mice, monocytes may be divided into pro-inflammatory $Ly6C^{hi}$ and patrolling $Ly6C^{low}$ monocytes. In humans the corresponding subsets are $CD14^{high}/CD16^{neg}$ (Moore et al. 2011; Woollard et al. 2010).

Macrophages: $Ly6C^{hi}$ monocytes transmigrate into the subendothelial space and differentiate into inflammatory macrophages. These naturally phagocytic cells of the innate immune system play a central role in the initiation, progression, and resolution of atherosclerosis (Moore et al. 2018). One can view this as a vicious cycle of events leading to a chronic inflammatory state.

Macrophage proliferation: In an initial state, proliferating macrophages act to control the disease and ingest retained and modified lipoproteins via phagocytosis, pinocytosis, or receptor-mediated pathways such as SRs and toll-like receptors (TLRs) (Tabas et al. 2015). Eventually the macrophages will be transformed into foam cells. Cholesterol efflux to HDL from the macrophages is facilitated by ABCA1 and SR-B1 to HDL for transportation to the liver (Phillips 2014; Webb et al. 1998).

Macrophage retention: If the amount of lipoproteins and cholesterol engulfed by the macrophages exceeds the capacity of reverse cholesterol transport, accumulation will occur within the macrophages. Accumulating lipid-laden macrophages in atherosclerotic plaques have a diminished migratory capacity, which contributes to failure to resolve inflammation and thus leads to advanced and complex plaques.

Macrophage death and failed resolution: An overload of free cholesterol leads to endoplasmatic reticulum stress and pro-inflammatory signaling, causing the macrophage to eventually undergo apoptosis or necrosis, with the latter exposing intracellular material. The apoptotic/necrotic cells and cellular debris can be cleared by neighboring macrophages. However, if there is an imbalance in the dying-cell clearance capacity of the macrophages—so-called impaired efferocytosis—this will add up to a lipid rich necrotic core that aggravates inflammation and gives rise to a persistent immune cell infiltration. Hence, advanced atherosclerotic lesions result from the defect resolution of inflammation. Secretion of reactive oxygen species (ROS) increases oxidative stress, and secretion of proteases such as MMPs

leads to ECM degradation and weakening of the fibrous cap. Macrophages may also secrete prothrombotic factors, promoting thrombus formation (Moore et al. 2018; Moore et al. 2011).

***Polarization of macrophages*:** The polarization of macrophages is based on environmental signals such as cytokines, macrophage colony-stimulating factor (M-CSF), and interleukins. Macrophages can switch from different polarized states depending on external signals. This will cause changes in gene transcription and, hence, the expression of different surface molecules. Importantly, macrophages in human atherosclerotic lesions consist of a spectrum of intermediate phenotypes. However, traditionally macrophages are divided into the classically-activated pro-inflammatory M1 macrophages and the alternatively-activated anti-inflammatory M2 macrophages. The polarization into M1 macrophages is driven by cytokines such as TNF-α and IFN-γ as well as by bacterial lipopolysaccharide (LPS) and, in atherosclerosis, also by oxLDL and cholesterol crystals as triggers of cytokine secretion. M1 polarized macrophages in the plaques are a source of pro-inflammatory cytokines such as IL-1β, IL-6, IL-12, and TNF-α in addition to a broad range of MMPs. They also express chemokine receptor ligands, produce reactive oxygen species (ROS), and activate inducible nitric oxide synthase (iNOS), an enzyme catalyzing the production of NO from L-arginine. NO is an important modulator of vascular tone and insulin secretion and participates in anti-bacterial defense via oxidative processes. Taken together, these promote further recruitment of leucocytes; hence, M1 macrophages are considered to promote atherosclerotic development.

M2 polarization is induced by IL-4 and IL-13, and these macrophages are able to secrete fibronectin and TGF-β and express mannose receptor (MR). These macrophages are considered to have a resolving function that promotes plaque regression (Colin et al. 2014; Moore et al. 2013; Moore et al. 2011; Peled et al. 2014). M2 macrophages may be further subclassified into M2a, M2b, and M2c (Bobryshev et al. 2016). M1 and M2 macrophages have been extensively studied in atherosclerosis and have been histologically localized in the fibrous cap, and M1 has also been identified in the shoulder regions of the plaque (Stoger et al. 2012). However, M1 and M2 macrophages do not cover the full spectrum of macrophage polarization and other subsets of polarized macrophages have been identified in atherosclerotic plaques, as reviewed by Bobryshev and Martinez (Bobryshev et al. 2016; Martinez et al. 2014).

2.2.3.2 Other Inflammatory Cells in Atherosclerosis

Different cells from the innate immune system, such as neutrophils, mast cells, and natural killer cells, may play important roles at different stages of the disease development, but these cells constitute minor populations in the plaque compared to macrophages. Macrophages are also regarded as the main effector cell type in the plaque.

***Mast cells*:** Mast cells are commonly found at sites of plaque rupture and release MMPs, which degrade the ECM and promote plaque instability (Kovanen et al. 1995). These cells may be found near plaque neovessels and may play a role in neovessel formation and intraplaque hemorrhage by increasing leakage from neovessels (Bot et al. 2015).

***Neutrophils*:** Neutrophils are mainly involved in the early phases of atherosclerosis and are one of the first inflammatory cell types to enter the tissue in response to inflammatory stimuli. Neutrophils have been associated with plaque progression due to the secretion of proteases and ROS adding to the oxidative stress in the lesion (Naruko et al. 2002; Weber et al. 2008).

***Dendritic cells*:** Dendritic cells are antigen-presenting cells that are important for adaptive immunity, derived from blood monocytes or lymphoid precursors, and found in atherosclerotic lesions, as well as adjacent to lymph nodes and tertiary lymphoid tissues in the adventitia. The arterial tertiary lymphoid organs (ALTOs) serve as an interaction site for B cells, T cells, and dendritic cells. In atherosclerosis dendritic cells act as mediators between innate and adaptive immunity, presenting internalized antigens such as oxLDL on class II major histocompatibility complex (MHC) to T cells (Zernecke 2015).

***Lymphocytes*:** Lymphocytes, derived from common lymphoid progenitor cells, are cells of the adaptive immune system including both T- and B-lymphocytes. Activated T cells, especially CD4+ T cells (Treg and Th), are a significant population in atherosclerotic plaque. CD4+ cells are the main effector cells in the adaptive immune system in atherosclerotic plaque (Zhou et al. 1996). Pro-inflammatory Th1 cells can secrete IFN-γ, promoting monocyte infiltration and macrophage activation (Buono et al. 2003; Zhou et al. 2006). Th2 cells are less frequently found in atherosclerotic plaque and are considered to be of minor importance for atherogenesis. Other minor populations of T cells in the atherosclerotic plaque are proatherogenic Th17 and antiatherogenic Treg cells, the latter secreting anti-inflammatory cytokines such as IL-10 and TGF-β (Gotsman et al. 2008; Ketelhuth et al. 2016). B cells, however, are rarely found in atherosclerotic plaques, but can be found in the adventitia below the intimal lesion. Circulating antibodies have been detected that target frequently-observed antigenic derivatives from atherosclerotic plaques. Many studies have focused on B cell

epitopes present in modified LDL. The presence of antibody producing B cells and the potential beneficial effect of various antibodies have led to the idea that vaccination against modified LDL might be possible. Initial studies have focused on oxLDL or malondialdehyde-modified epitopes in LDL, although vaccination with native LDL also shows a significant protective effect in animal studies (Hansson et al. 2011; Nilsson et al. 2012; Shevach 2009).

2.2.3.3 Vascular SMCs in Atherosclerosis

Vascular SMCs (VSMCs) constitute one of the major cell types found in the atherosclerotic lesion. In normal arteries, SMCs in the media maintain muscle tone. During atherogenesis these cells undergo phenotypic changes and lose their homeostatic function. In early atherogenesis, VSMCs are activated by the presence of modified LDL in the intima. Previous studies have described these phenotypic changes in VSMCs as a change from a synthetic state—expressing classical markers such as smooth muscle alpha actin (Acta2), calponin, and smooth muscle myosin heavy chain (Myh11)—to a proliferating and migrating phenotype, downregulating genes and hence losing the expression of classical VSMC markers (Alexander et al. 2012). More recent studies using lineage tracing of VSMCs have shown that these cells undergo phenotypic switching, acquiring a more macrophage-like phenotype inside the plaque. This transdifferentiation of vascular SMCs has been recognized *in vitro* and in animal models; however, further validation in human samples is needed. Moreover, the proliferation of VSMCs in early atherogenesis seems to have a reparative role in atherosclerosis because of the production of ECM and formation of fibrous caps. The role of VSMCs' migration in human atherosclerosis is not fully understood due to a lack of specific markers in this process. However, the inflammatory milieu in plaques will also result in lipid-laden VSMCs that further increase MMP secretion and cytokine production, eventually forcing the VSMCs to become senescent, unable to divide, and undergo cell death, adding to the disease burden (Bennett et al. 2016).

2.2.4 Animal Models Utilized in the Imaging of Atherosclerosis

Animal models for studying atherosclerosis include mice, rabbits, pigs, and non-human primates, although the latter two have become less frequently used (Getz et al. 2012). Ideally, animal models of atherosclerosis should have similar lipoprotein profiles and lesional formation as humans. Lesion development should contain all stages of disease including plaque rupture and thrombosis. The Watanabe heritable hyperlipidemic (WHHL) rabbits, which were

developed by Dr. Yoshio Watanabe at Kobe University in Japan (Watanabe 1980), have contributed to ground-breaking discoveries in understanding the impact of lipoproteins on atherosclerosis. These pioneering studies using rabbits established the basis for the modern theory of atherosclerosis: the "lipid hypothesis" and the role of lipids as proatherogenic in addition to the "inflammatory hypothesis" and the role of inflammatory cells such as macrophages and T lymphocytes as the key cellular components for the initiation and progression of atherosclerosis (Geovanini et al. 2018; Hansson 2005; Moore et al. 2011). Other transgenic and gene knock-out (KO) models have also been used in rabbits. However, since the beginning of 1990s when the development of genetically modified KO models in mice took off, there has been a reduced trend in using rabbit KO models (Fan et al. 2015).

Ever since the mouse KO model was introduced, it has been widely utilized in atherosclerosis, mainly because of their similarity to the human genome and the convenient possibility of genetic manipulations for studying disease mechanisms. Another advantage is that the progression of the disease is rather rapid in these animals. In WT mice, the majority of the cholesterol is in the form of HDL (~ 85%) whereas for humans the majority is in the form of LDL (~ 65-85%). WT mice do not naturally develop atherosclerosis; therefore, they must be manipulated to better mimic a human lipoprotein profile and a significant hypercholesterolemia is needed to induce atherosclerosis in these models. High-fat and cholesterol enriched diets are therefore utilized. The most common mouse models in atherosclerosis are ApoE deficient (*Apoe*$^{-/-}$) and LDLR deficient (*Ldlr*$^{-/-}$) mice (Getz et al. 2012). The major limitations of atherosclerotic mouse models are differences in the lipoprotein metabolism compared to humans and the fact that they do not spontaneously develop plaque ruptures, the unstable plaque characteristics seen in human lesions. To better mimic plaque vulnerability in mouse models of atherosclerosis and observe plaque rupture, cuffing or ligation of the artery has been used (Sasaki et al. 2006). Furthermore, the locations of lesions are not identical to the arterial sites of lesions in humans. In mice, lesions are often restricted to the upper part of the aorta; the aortic root, and the aortic arch, and the carotid arteries, whereas lesion in the abdominal aorta is not as dominant as it is in humans. In the traditional KO mouse models coronary lesions are limited or absent (Kapourchali et al. 2014). In combined KO models, such as the combination of ApoE and SR-B1 deficiencies, lesions of the coronary artery can develop (Braun et al. 2002). Cross breeding of human apoB100 transgenic mice with LDL receptor-deficient mice will also aggravate lesion formation (Sanan et al. 1998). Other combinations with either *Apoe*$^{-/-}$ or *Ldlr*$^{-/-}$ backgrounds have also been utilized (Kapourchali et al. 2014). The atherosclerotic mouse model included in this thesis is the *Apoe*$^{-/-}$ mouse. The most common animal models of atherosclerosis are summarized in **Table 2.1**.

Table 2.1: Animal models of atherosclerosis and their characteristics.

Animal model	Characteristics of atherosclerosis	Lesion formation (stages and locations)	Comparison to humans	Reference
Mice				
***Apoe*$^{-/-}$**	Develops spontaneous atherosclerosis, which is accelerated by feeding with fat- and cholesterol-enriched diets. Elevated levels of circulating cholesterol-rich VLDL particles.	Stages of lesion formed (I-V). Aortic root, aorta (carotid artery, older mice).	Lipoprotein profile, site and type of lesions differs.	(Zhang et al. 1992)
***Ldlr*$^{-/-}$**	Dietary cholesterol necessary for developing hypercholesterolemia and atherosclerosis. Associated with elevated levels of circulating cholesterol-rich LDL and VLDL particles.	Stages of lesion formed (I-IV). Aortic root, aorta.	Lipoprotein profile, site and type of lesions differs.	(Sanan et al. 1998)
Rabbits				
Watanabe Heritable Hyper-lipidemic	Naturally deficient in LDL receptors resembling human familial hypercholesterolemia. (High VLDL/LDLs and extremely low HDLs).	Fatty streaks to advanced lesions. Starts in the aortic arch and thoracic aorta and finally develops in the abdominal aorta. Also develops coronary atherosclerosis and spontaneous myocardial infarction.	Lipoprotein profile similar to humans. Similar to advanced lesions in humans.	(Watanabe 1980)
Cholesterol fed rabbits (New Zealand white, and Japanese white)	Resembling human familial hypercholesterolemia. (High VLDL/LDLs and extremely low HDLs).	Starts in the aortic arch and thoracic aorta and finally develops in the abdominal aorta. Also develop coronary lesions.	Lipoprotein profile similar to humans. Lesion site differs.	(Fan et al. 2015)

2.3 Molecular Imaging Targets of Inflammation in Atherosclerosis

Many different molecular probes have been developed for this purpose. The target should be valid and relevant to the disease process. It should also be expressed to a measureable extent compared to the healthy state or possess clearly altered metabolic activity compared to the healthy state. Adhesion molecules and macrophages are amongst the most studied targets for molecular imaging of inflammation in atherosclerosis.

2.3.1 Adhesion Molecules

Cell adhesion molecules (CAMs) are a subset of cell adhesion proteins located on the cell surface. CAMs are involved in binding with other cells, such as the recruitment of leucocytes into the subendothelial space, or binding with the ECM. These molecules are transmembrane receptors that comprise an extracellular, a transmembrane, and an intracellular domain. There are four major superfamilies or groups of CAMs including: the integrin family, the immunoglobulin superfamily, selectins, and cadherins. The most widely studied immunoglobulin superfamily for molecular imaging targeting includes ICAM-1, VCAM-1, and the platelet-endothelial cell adhesion molecule-1 (PE-CAM-1), while the most studied in the selectin family are E-selectin (CD62E) and P-selectin (CD62P) (Elangbam et al. 1997). The expression of adhesion molecules such as E-selectin, ICAM-1, and VCAM-1 is induced on the surface of the activated endothelial cells lining lipid rich atherosclerotic plaques (Cybulsky et al. 2001; Davies et al. 1993; O'Brien et al. 1993). Over-expression of ICAM-1 has been demonstrated, not only on the endothelial cells, but also on VSMCs and macrophages of human atherosclerotic plaques (Poston et al. 1992; Wood et al. 1993). Davies et al. found that VCAM-1 appears focally on endothelial cells covering fibrous or lipid-rich plaques and in intraplaque neovessels (Davies et al. 1993). VCAM-1 binds the very late antigen-4 (VLA 4) on the surface of leucocytes. Preclinical studies have shown that blocking or knocking out this receptor significantly inhibits leucocyte recruitment (Koni et al. 2001). VCAM-1 does not seem to be significantly expressed on the endothelium in non-affected areas and therefore might serve as an interesting diagnostic target to specifically detect inflammatory atherosclerotic lesions (Nakashima et al. 1998; Park et al. 2013). Probes for molecular imaging of adhesion molecules have been developed for contrast enhanced ultrasound (CEUS) (Behm et al. 2008; Bettinger et al. 2012; Kaufmann et al. 2007a; Klibanov et al. 2006; Villanueva 2008; Villanueva et al. 1998), MRI (Li et al. 2014), and nuclear imaging techniques (Broisat et al. 2014; Nahrendorf et al. 2009; Nakamura et al. 2013).

2.3.2 Scavenger Receptors

Scavenger receptors (SRs) are a group of membrane glycoproteins, first identified in macrophages and described by Brown and Goldstein in 1979 (Brown et al. 1979; Goldstein et al. 1979) and further characterized by Platt, Greaves and Gordon (Greaves et al. 2009; Platt et al. 2001; Platt et al. 2002). The SR-A1 receptor was the first to be discovered because of its

ability to mediate the formation of foam cells. Subsequently, many other SRs have been discovered.

> *Scavenger receptors are defined as cell surface receptors able to bind multiple ligands and promote the removal of non self or altered self targets. They often function by mechanisms that include endocytosis, phagocytosis, adhesion, and signaling that ultimately lead to the elimination of degraded or harmful substances (Prabhudas et al. 2014).*

Since their first discovery 40 years ago, a broad number of different ligands have been identified including pathogens; lipopolysaccharide, Gram positive and Gram negative bacteria; modified proteins such as acetylated LDL (acLDL), malondialdehyde-LDL (MDA-LDL), oxLDL, maleylated (Mal) LDL or albumin, and native protein; ApoA-1, ApoE, lipids, and polysaccharides; dextran sulphate and fucoidan; as well as nucleic acids (Ben et al. 2015). According to their architecture, they are categorized into eight different classes, termed SR-A to SR-H, reviewed by Prabhudas et al. (Prabhudas et al. 2014). Additionally, two other classes, SR-I and SR-J have been described but not included in the general SR nomenclature (Zani et al. 2015). The classes are subdivided further into "types" based on additional variations in their sequences due to alternative splicing. In some of the SR classes, multiple names have been assigned to the same receptor subtype. This is the case for the SR class A1, SR-A1 (also known as macrophage SR1; MSR1, SCARA1, CD204) and the proposed consensus definition of SR nomenclature is presented by Dr. Prabhudas et al., a collaboration of 15 researchers from five different countries. The most common SRs involved in the uptake of modified LDL particles are the ones from Class A, B, and E. These are listed in **Table 2.2**.

2.3.2.1 The Role of SR-A1 in Atherosclerosis

SR-A1 is expressed by macrophages and found in macrophage-rich areas of both human and mouse atherosclerosis. However, expression in normal VSMC and EC is low (Gough et al. 1999; Matsumoto et al. 1990; Naito et al. 1992; Nakata et al. 1999). Expression of SR-A1 is seen in mature macrophages of the mononuclear phagocyte system (a.k.a. the reticuloendothelial system), such as liver sinusoidal endothelial cells (LSECs) and Kupffer cells, alveolar macrophages, or splenic and lymph node macrophages (Hughes et al. 1995). The role of SR-A1 in CVD and atherosclerosis is still a matter of debate due to contradictory *in vivo* results. Between 1997 and 2005, many studies conducted in SR-A1 deficient (SR-A1$^{-/-}$) mice with either *Apoe*$^{-/-}$or *Ldlr*$^{-/-}$ backgrounds, showed decreased lesion size upon deletion of the gene. Hence, these studies indicated a pro-atherogenic role for SR-A1 (Ben et al. 2015; Kunjathoor et al. 2002; Sugano et al. 2001; Suzuki et al. 1997; Zhao et al. 2005).

Table 2.2: Scavenger receptor nomenclature and LDL uptake.

New nomenclature	Currently known as	Encoded by (gene)	Modified LDL uptake
Class A			
SR-A1	SR-A1, SCARA1	MSR1 gene	AcLDL, oxLDL, Mal-LDL
SR-A1.1	SR-AII	A splice variant of MSR1 gene	AcLDL, oxLDL, Mal-LDL
SR-A1.2	SR-AIII	A splice variant of MSR1 gene	
SR-A6	SCARA2	MARCO	AcLDL
Class B			
SR-B1	SR-BI	SCARB1	AcLDL, oxLDL, native LDL, native HDL
SR-B1.1	SR-BII	A splice variant of SCARB1 gene	
SR-B2	SCARB3	CD36	AcLDL, oxLDL
Class E			
SR-E1	LOX1	ORL1	oxLDL

Table data from references: (Greaves et al. 2009; Prabhudas et al. 2014)

Observations that challenge this conclusion (Ben et al. 2015; Kuchibhotla et al. 2008; Moore et al. 2005) did not show any significant alteration in plaque size by SR-A1 compared to CD36 deficiency or when examined in double KO mice models, although some results showed a reduction in lesion necrosis, inflammation, and macrophage apoptosis (Manning-Tobin et al. 2009). Differences in the *in vivo* observations of the role of SR-A1 in atherosclerosis may be due to differences, such as age and diet, in atherosclerotic mouse models. However more recent findings have shown that SR-A1 may function via anti-inflammatory responses by, for example, promoting an M2 macrophage phenotype in adipose tissue in mice (Zhu et al. 2014). Furthermore, Robbins et al. (2013) showed that the accumulating macrophage foam cells in the established atherosclerotic lesions primarily originated from a SR-A1-mediated proliferative response (Robbins et al. 2013). Previously, it was believed that macrophages did not proliferate in the atherosclerotic lesion and that the only sources of new macrophages originated from migrating blood monocytes. However, Robbins et al. showed that lesional macrophages do proliferate and SR-A1 may therefore contribute to atherogenesis, primarily by mediating macrophage proliferation. A large number of macrophages in atherosclerotic lesions is an indicator of unstable and rupture-prone phenotypes (Jaffer et al. 2006; Narula et al. 2008; Virmani et al. 2002). Nevertheless, SR-A1 is an interesting target for detecting macrophage-rich inflammatory atherosclerotic plaques with molecular imaging. Promising findings within

the field of probe development for molecular imaging was demonstrated *in vitro* by Lipinski et al. (Lipinski et al. 2006) utilizing gadolinium-containing immunomicelle probes for possible MRI application as well as *in vivo* by utilizing SR-A1–targeted iron oxide nanoparticles for MRI detection of atherosclerotic lesions (Amirbekian et al. 2007; Segers et al. 2013).

2.3.3 Other Markers

Other potential molecular targets for molecular imaging are markers of apoptosis, angiogenesis, or atherothrombosis. The most extensively studied marker for angiogenesis is the $\alpha_v\beta_3$ integrin, a cell surface glycoprotein receptor expressed by macrophages, medial and some intimal SMCs, and endothelial cells. Expression of $\alpha_v\beta_3$ is found in the shoulder region of advanced plaques and in the necrotic core of human atherosclerotic lesions (Antonov et al. 2004; Byzova et al. 1998; Gargiulo et al. 2016). Thrombotic markers such as glycoprotein (GP) IIb/IIIa complex is expressed on the surface of activated platelets. The GP IIb/IIIa receptor is a potential marker for the imaging of aggregated platelets in atherosclerotic plaques. Peptides containing the Arg-Gly-Asp (RGD) sequence are highly adhesive for GP IIb/IIIa, and the cyclic (c) RGD has 30-fold greater affinity for the GP IIb/IIIa complex than the linear form. cRGD is also recognized by the $\alpha_v\beta_3$ integrin receptor (Gargiulo et al. 2016; Schottelius et al. 2009). Therefore cRGD has been utilized for targeting purposes by coupling to microbubbles (MBs) (Guo et al. 2015; Metzger et al. 2015) in addition to contrast agents used for MRI (Burtea et al. 2008) and radioisotopes in nuclear imaging (Burtea et al. 2008).

2.4 Imaging of Atherosclerosis

Before elaborating on the imaging of atherosclerosis, some important terminology needs to be defined, **Table 2.3**.

Table 2.3: Imaging terminology.

Nomenclature	Definition
Molecular imaging	*In vivo* visualization, characterization, and measurement of biological processes at the molecular and cellular levels.
Molecular imaging probes	Agents used to visualize, characterize, and quantify biological processes in living systems. It can be referred to by many other terms, such as ligand, tracer and contrast agent.
Contrast agents (CAs)	Substances used to increase the contrast of structures or fluids within the body in medical imaging. CAs absorb or alter external electromagnetism or US and are different from radiopharmaceuticals, which emit radiation themselves.
Superparamagnetic iron oxide nanoparticles (SPIONs)	SPIONs are synthesized from iron oxide with ferromagnetic properties. The two main forms are magnetite (Fe_3O_4) and its oxidized form maghemite (γ-Fe_2O_3). When the ferromagnetic particles' size is decreased, they obtain superparamagnetic properties. Diameter range of nanoparticles between 10 and 100 nm can be used in medical imaging: standard SPIO (SSPIO), 50-150 nm; and ultra-small SPION (USPIO) <50 nm).
Radionuclide (Synonym: Radioisotope)	An atom with excess nuclear energy making it unstable. This energy can be emitted in different ways by a process known as radioactive decay of an atomic nucleus.
Radioactive decay	Radionuclides can decay, giving rise to different types of radiation: alpha, beta, or gamma radiation (or "rays"). One radionuclide can decay giving rise to only one or several types of radiation. Out of the three types of radiation, gamma rays are the most penetrating form of radiation.
Radiotracer (Synonym: Radioligand)	A molecular probe labeled with a radionuclide.
Metal chelators	Molecules with inherent functionality to capture and bind specific metal ions such as DFO, NOTA, or DOTA.
Spatial resolution	Spatial resolution determines how sharp the image will be and is defined by the voxel size or the size or number of pixels in one image. In radiology: the ability of the imaging modality to resolve or differentiate between two objects in space. In fluorescence microscopy: the minimum separation between two points that results in a certain level of contrast between them.
Temporal resolution	Refers to the precision of a measurement with respect to time.
Voxel	A three dimensional pixel.

Table data from reference (Chen et al. 2011; Chen et al. 2010; Chen et al. 2017; Gropler et al. 2007). DFO = deferoxamine, NOTA = triazacyclononane triacetic acid, DOTA = tetraazacyclododecane tetraacetic acid.

2.4.1 Angiography

Conventional angiography was considered to be the standard method for evaluating carotid stenosis. Moreover, the trials published in the 1990s (North American Symptomatic Carotid Endarterectomy Trial [NASCET], the European Carotid Surgery Trial [ECST], and the Asymptomatic Carotid Atherosclerosis Study [ACAS]) were based on this method. However, since the introduction and development of Doppler ultrasound, CT angiography (CTA), and MR angiography (MRA), conventional angiography has become less popular for carotid stenosis diagnostic purposes, essentially being reserved for endovascular treatment (Benjamin et al. 2018; Brinjikji et al. 2016; Saba et al. 2010).

For diagnosis of coronary artery disease, *invasive angiography* is still considered to be the gold standard technique. This technique is based on the radio-opacity of intra-arterially injected iodinated contrast agents visualized by x-ray. A pre-shaped catheter is introduced percutaneously via the peripheral arteries in the groin (femoral artery) or in the wrist (radial artery) to intubate the coronary ostia and inject the contrast agent under x-ray fluoroscopy. The advantages of angiography are high diagnostic accuracy afforded by superior spatial (0.1–0.2 mm) and temporal (10 ms) resolution, which is unmatched by noninvasive techniques (Tarkin et al. 2016). Therefore, invasive angiography remains the best anatomic reference test to determine the severity of coronary luminal obstruction and guide clinical management, particularly for revascularization decisions. However, its limitation is the overall low diagnostic yield, restricted to luminal imaging of the degree of vessel stenosis but providing no information about vessel components or the functional effects of the stenosis (Patel et al. 2010). Angiography is primarily applied in high-risk symptomatic patients and often accompanied by opening of the coronary vessel by percutaneous coronary intervention (PCI). Modern clinical intravascular coronary imaging techniques include optical coherent tomography and intravascular ultrasound (IVUS). IVUS utilizes an intravascular ultrasound catheter and provides more details than conventional angiography or ultrasound alone. Grayscale IVUS has a limited ability to differentiate individual plaque components but, if combined with virtual histology (VH)-IVUS, enables detection of the necrotic core, dense calcium, fibrous, and fibrofatty plaque with reasonable accuracy (Nair et al. 2007). Reliable and reproducible detection of the thin fibrous cap is limited, with insufficient spatial resolution and artifacts due to a low signal-to-noise ratio (SNR). Optical coherent tomography utilizes near-infrared light with high spatial resolution, providing accurate measurement of fibrous cap thickness with strong correlation to histology (Kume et al. 2006). However, tissue penetration is limited to 3

mm, making it hard to image the whole plaque (Gargiulo et al.; Tarkin et al. 2016). Some of the noninvasive imaging modalities are listed in **Table 2.4**.

2.4.2 Ultrasound

An ultrasound transducer contains piezoelectric crystals, which both transmit and receive the ultrasound signal or sound wave. Various transducers with different frequencies and shapes are suitable for specific parts of the body depending on the body surface and depth of penetration needed to visualize the organ or structures. Some sound waves will be absorbed by the tissue or reflected in other directions and scattered. The reduction in amplitude of the ultrasound beam as a function of distance through the tissue is called attenuation, which will affect the resulting image. The transducer receives the echoes and sends them to a computer, which uses them to create an image or sonogram. Ultrasound B-mode (2D) imaging is well-established as a method for visualizing atherosclerosis of the larger arteries, such as carotids, yielding anatomical information on plaques that obstruct the lumen of the blood vessel. B-mode ultrasound images are also used to assess the echogenicity of plaques, which is proportional to the density of the tissue and its capacity to reflect ultrasound (Gropler et al. 2007). Calcifications are strongly reflective and may create a shadow. *Plaque echolucency,* indicating softer, more lipid rich tissue, is a marker of plaque vulnerability (Huibers et al. 2016). This feature is seen in up to 50% of recently symptomatic plaques compared with less than 5% of asymptomatic plaques (Huibers et al. 2016). A study by Ballotta et al. (2014) showed that the risk of stroke among patients with echolucent plaques is up to 13% regardless of the degree of stenosis, which is a higher risk compared to the risk of stroke in patients with high grade stenosis (Ballotta et al. 2014).

Thus, measuring the echogenicity of plaques can provide information on whether a plaque is “hard” (i.e. fibrotic and calcified [appearing bright and echodense]), or contains a darker “soft” core and is assumed to have a high lipid content and little fibrosis (appearing echolucent, i.e. black). Since soft plaques are dark, they may be difficult to delineate or even to discover in the B-mode image if they have a similar reflectivity as blood. An important use of B-mode with color, Doppler (so called Duplex scanning) is used to visualize the blood stream and thereby reveal or exclude soft plaque. The composition of plaques, which is likely to influence their vulnerability, can be visually interpreted by, for example, applying the Gray-Weale score (Ballotta et al. 2014). Vulnerability may also be related to the overall echogenicity and measured as grayscale median (GSM). Duplex ultrasound (2D-Doppler) allows measurement of blood flow velocity and hemodynamic properties for estimation of the severity

of carotid stenosis: an accessible imaging technique commonly used in patients with recent strokes or as a part of risk assessment scanning (Alonso et al. 2015; Brinjikji et al. 2016).

2.4.3 Magnetic Resonance Imaging

MRI is a noninvasive imaging modality based on the magnetic properties of hydrogen atoms. The spin vector of the hydrogen atom in a sample is randomly oriented until it is placed in an external magnetic field. To give a simplified description, an MR scanner consists of a large electromagnet with a static magnetic field in which the patient lies. The resulting magnetization of all protons inside the body aligns with the magnetic field. To generate images, spatially varying magnetic fields, (i.e. magnetic field gradients) are used to make the resonance occur at different frequencies. Very powerful magnets of 1.5 Tesla or more are needed for good sensitivity. The corresponding frequencies for hydrogen nuclei are in the range of radio-waves; that is, 63 MHz at 1.5 Tesla. A radio wave antenna (coil) is used to send out signals to the body and to receive signals back. These signals are then computed into images, **Figure 2.5**. During the image acquisition process, a radiofrequency (RF) excitation pulse is applied to excite the spins. After the given pulse, the spins will in time return to the orientations of the magnetic field, and the relaxation time can be calculated. By varying the timing of the RF-pulses, using more complex sequences of RF-pulses, and switching gradients, the contrast between different tissue types can be optimized. However, the lengthy acquisition time of MRI limits the temporal and spatial resolution (Gropler et al. 2007).

2.4.3.1 MRI in Atherosclerosis

The periodic motion of the heart, the pulsatile blood flow, and the motion of the lungs should be considered when imaging the heart and nearby vessels. By synchronizing the acquisition of the data with the heartbeat, images from different phases of the cardiac cycle can be acquired. Electrocardiography (ECG)-triggering can adjust for cardiac movement to provide anatomical imaging of vessels in or near the heart. Magnetic resonance angiography (MRA) refers to the visualization of flow within vessels and can be performed with or without contrast enhancement. In vascular imaging with MRI, both the luminal information and imaging of the vessel wall is possible. MRA without intravenous administration of contrast utilizes the phenomenon of the flow-related enhancement of spins entering into the image slice, and these spins give rise to a stronger signal (brighter appearance) than the surrounding stationary spins in the tissue. There are a wide variety of pulse sequences available for plaque characterization with MRI and ultimately they result in different image appearances. Examples of such are fast

spin echo (FSE) and gradient echo. It is also possible to obtain black blood images, acquired using so-called spin-echo, which results in images with high contrast between the dark lumen and the vessel wall. MRI is the most well-established imaging modality for plaque characterization. It can be used with high reliability to detect intraplaque hemorrhage, lipid rich-necrotic cores (LRNC), and thin fibrous caps (Brinjikji et al. 2016; Koppal et al. 2017; Tarkin et al. 2016). However, visualization of the carotid arteries is more feasible with MRI than of the coronary arteries due to rapid movement of the heart and low temporal resolution. MRI can also be combined with other techniques such as PET, which can identify inflamed tissue as well as the metabolic state and myocardial ischemia (Tarkin et al. 2016).

2.4.4 Computed Tomography Angiography

CTA is preferred over MRI for anatomical coronary imaging, primarily because motion artifacts arise during the prolonged acquisition time with MRI, resulting in inferior temporal resolution. Imaging artifacts with CT may arise from calcification in the coronaries with CT, possibly causing difficulty in determining the vascular lumen dimension. CTA can also be applied for anatomical carotid imaging and has proved useful for detection of macro calcification. CTA is based on rotating an x-ray source and detector in addition to iodinated contrast agents for the visualization of vessels. Data from several projections is reconstructed into images of multiple planes. CT, preferably without contrast, can be used to differentiate soft and calcified lesions to assess the calcium burden in the vessel (calcium score) in selected patients with a low to moderate probability of CVD. Determination of the calcium score is useful as a negative predictive value, since absence of calcium in the coronary arteries indicates a low risk of cardiovascular events (Miller et al. 2008; Shaw et al. 2012; Tarkin et al. 2016).

Table 2.4: Noninvasive imaging modalities.

Noninvasive imaging modalities	Spatial resolution (mm)	Detection limit (probe)	Contrast agent or tracer	Advantages	Limitations
Ultrasound	Depends on axial and lateral resolution (transducer frequency) 0.3 - 0.1 (3 - 10 MHz) 0.03 (30 MHz) 0.04 - 0.1 (SA-US) 0.15 - 1 (C-US)	Not well characterized yet	Microbubbles	Real-time Low cost High temporal resolution (s) Portable No ionizing radiation	Operator-dependent Poor SNR
Magnetic resonance	0.01- 0.1 (SA-MRI) 0.5 -1.5 (C-MRI)	10^{-3} - 10^{-5} mM to µM	Gd-based contrast agents Nanoparticles; USPIO, SPIO	High spatial resolution and soft tissue contrast Functional parameters No ionizing radiation High SNR	Toxic effect of SPIONs or Gd High cost Long scans, and data post-processing time
X-ray computed tomography	0.02 - 0.3 (µCT) 0.5 - 2 (C-CT)	10^{-2} - 10^{-3} (potentially 10^{-9} - 10^{-10} with NP) mM to nM	Iodinated molecules (particles) Gold nanorods	Fast acquisition time High temporal resolution (s - min) Provides molecular and structural information	Ionizing radiation Low soft tissue contrast Medium cost
Nuclear imaging	1 - 2 (µPET) 3 - 5 (C-PET) 0.5-2 (µSPECT) 7-15 (C-SPECT)	PET: 10^{-11} - 10^{-12} pM SPECT: 10^{-10} - 10^{-11} nM to pM	Positron or gamma ray emitting radionuclides	Molecular and functional parameters High sensitivity	Ionizing radiation Poor spatial resolution (mm) High-medium cost
Photo-acoustic imaging	< 0.1	< 10^{-12} pM	NIR Fluorophores	High sensitivity No ionizing radiation High depth of penetration (<5cm) Low cost	Data post-processing and acquisition procedures are still being optimized

Table reference from (Brinjikji et al. 2016; Chen et al. 2011; Gargiulo et al. 2016; Tarkin et al. 2016). SA = small-animal, C = clinical, Gd = Gadolinium, SPIO = Superparamagnetic Iron Oxide, USPIO = ultrasmall SPIO, SPIONs = SPIO nanoparticles, SNR = signal-to-noise ratio.

2.5 Molecular Imaging of Atherosclerosis

Evidently we cannot rely on the level of stenosis for assessment of plaque vulnerability, since plaque vulnerability may be present without a significant degree of luminal stenosis. Features of plaque vulnerability include inflammation manifested, for example, as macrophage infiltration, a thin fibrous cap, a large necrotic core, hemorrhage, microcalcification, or neovascularization (Alonso et al. 2015; Hansson et al. 2015; Naghavi et al. 2003). Some of these features can be imaged with molecular imaging and targeted probes. These molecular imaging techniques include contrast-enhanced ultrasound (CEUS), MRI, CT, positron emission tomography (PET), single-photon emission computed tomography (SPECT), fluorescent molecular tomography (FMT), and photoacoustic imaging (PAI) (Brinjikji et al. 2016; Tarkin et al. 2014). These imaging modalities provide information beyond plaque structure, **Figure 2.4**.

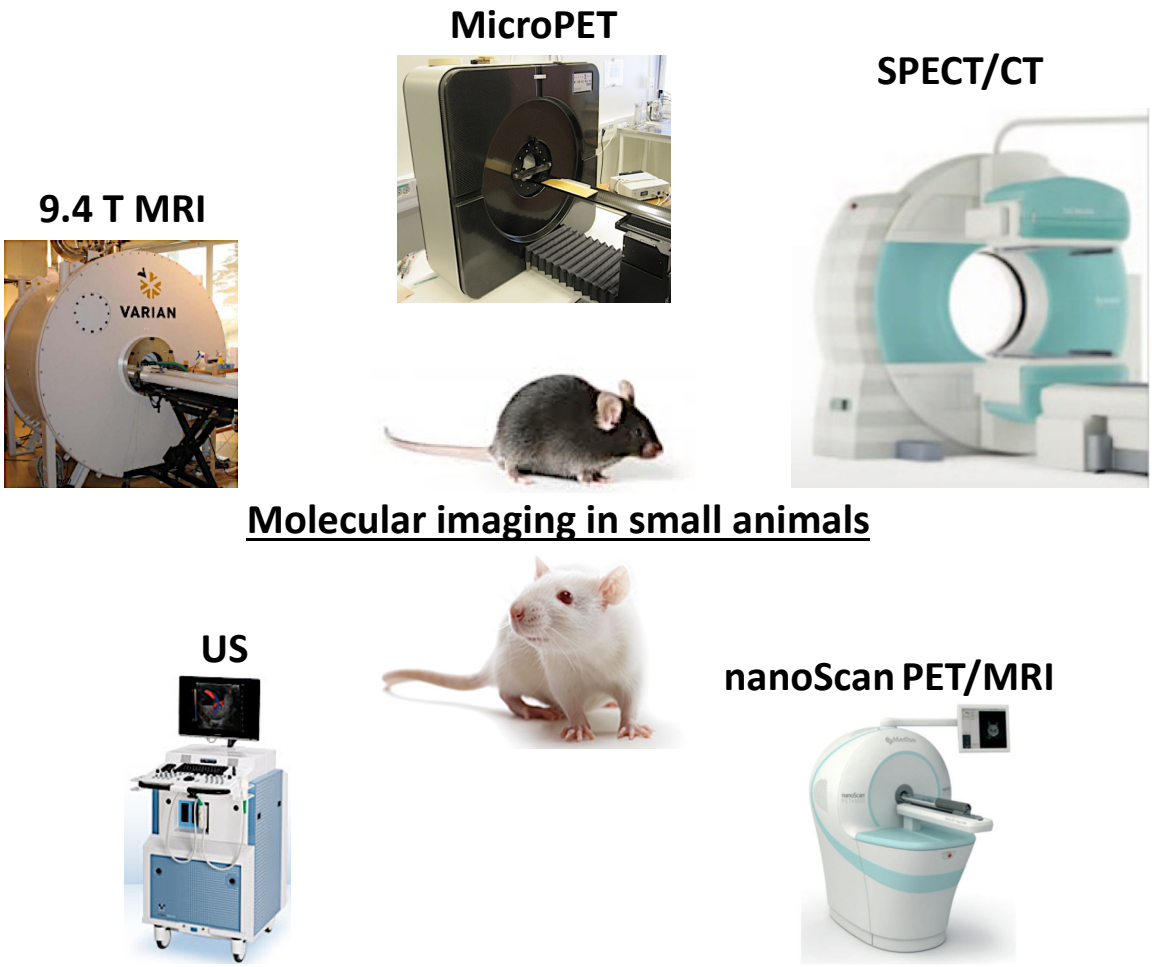

Figure 2.4: Both hybrid systems and single modal imaging modalities are available for small-animal molecular imaging, and some are illustrated here, as well as SPECT/CT for human use.

2.5.1 Contrast Enhanced US

Ultrasound characterization of atherosclerotic plaques may be improved by using intravenously administrated contrast agents: so-called CEUS. Typically, these contrast agents consist of gas filled MBs of lipid or biocompatible polymers such as polyvinyl alcohol. The sizes range from 1 to 5 μm in diameter. The MBs are used for characterizing the plaque surface and can be used to detect surface irregularities due to plaque erosion. The MBs do not diffuse into the surrounding tissue and are used for intravascular assessment of vessel lumen and neovascularity within the atherosclerotic carotid plaque (Bettinger et al. 2012; Kaufmann 2009; Klibanov 2013; Paradossi 2010).

When acoustic waves encounter MBs, the MBs are compressed by positive pressure and expanded by negative pressure. As a result, an asymmetric oscillation of MBs occurs, called *non-linear oscillation*, producing asymmetric echoes. These echoes are different from the tissue, producing mainly linear reflected ultrasound, but also second harmonic oscillations to a certain extent, which is important for so called tissue harmonic imaging and has revolutionized image quality with ultrasound scanning (Caidahl et al. 1998). The asymmetric echo harmonics are utilized to differentiate the ultrasound signal originating from the contrast agent from that originating from the tissue. The CEUS technique cancels the linear ultrasound from tissues and utilizes the non-linear ones from the MBs to highlight contrast in the images. When combined with B-mode ultrasonography, CEUS provides further details of plaque characterization. More than 90% of echolucent plaques demonstrate contrast enhancement (Clevert et al. 2011; Huang et al. 2008). CEUS is prone to an artifact known as pseudo-enhancement, leading to over-interpretation of vessel wall enhancement. Retention of MBs on the plaque surface has been shown to correlate with plaque disruption and inflammation since macrophages are known to phagocytose this contrast agent (Lindner et al. 2000). MBs can be conjugated further, directly or by an avidin/streptavidin biotinylation method, with targeting ligands such as antibodies or peptides, rendering them more specific for the targeting of specific biomarkers on the endothelium or activated platelets (Bettinger et al. 2012; Green 1963; Klibanov et al. 2006; Palmowski et al. 2008).

2.5.2 Contrast Enhanced MRI

MR angiography with contrast enhancement utilizes intravenously administrated contrast agents, of which gadolinium is the most commonly used. Molecular imaging with MRI is performed with two major types of contrast agents: 1) paramagnetic gadolinium-based (signal

enhancement) or contrast agent with superparamagnetic properties; 2) iron oxide-based nanoparticles (signal reduction), such as superparamagnetic iron oxide nanoparticles (SPIONs) or ultra-small superparamagnetic nanoparticles of iron oxide (USPIO) for visualization of plaque characteristics. Gadolinium-labeled RGD probes for MRI have been used for targeting of angiogenesis and have been shown to correlate with evidence of plaque angiogenesis (Hatsukami et al. 2000). The surface of the SPIONs are often coated with biocompatible molecules such as polymers: poly (vinyl alcohol) (PVA), polyethylene glycol (PEG), dextran, dendrimers, or proteins such as albumin (Chiellini et al. 2003; Mahmoudi et al. 2011; Singh et al. 2010) to improve biocompatibility and biodistribution, which also allows for targeted modifications. USPIO have been used for the visualization of inflammation (Tang et al. 2006; Tang et al. 2009b). However, for targeting angiogenesis and inflammation, using a nuclear medicine technique would provide greater sensitivity than MR imaging does.

2.5.3 Nuclear Imaging

2.5.3.1 SPECT

SPECT is a sensitive noninvasive imaging method based on gamma-ray emitting radionuclides, such as ^{99m}Tc, ^{111}In, or ^{123}I, which are intravenously injected into the patient. There is also a possibility for further modification with ligand coupling for specific targeting of different tissues inside the body. A SPECT system is based on a gamma camera: a device designed to externally image radionuclide distribution in an object. Such a system consists of one or more detectors that can be rotated around the object. Although the images recorded are two-dimensional (2D), when a number of images (projections) are acquired by rotating the detector around the object, a set of slices representing the three-dimensional (3D) volume can be reconstructed. However, information is degraded due the attenuation (absorption) of gamma rays in the object. When images are co-registered with those from a conventional CT scanner, a correction can be made for the attenuation and the radionuclide distribution can also be better coupled to anatomical structures. The spatial resolution of clinical SPECT is around 10-16 mm and is hence less ideal for the imaging of small structures. SPECT is applied in myocardial perfusion and brain imaging, but can also be used in tumor imaging, infection (leukocyte) imaging, thyroid imaging, or bone scintigraphy where a 3D-representation can be helpful (Gargiulo et al. 2016; Gropler et al. 2007; Tarkin et al. 2014). Several SPECT tracers have also been evaluated for inflammation imaging (Yang et al. 2018), for example, ^{99m}Tc-cAb-VCAM-1 (Broisat et al. 2014), and some are listed in **Table 2.6**.

2.5.3.2 PET

PET is a very sensitive method, often combined with CT and, more recently, with MRI for anatomical imaging. Compared to clinical SPECT, the spatial resolution is superior in clinical PET (3-5 mm) and therefore also better for imaging of atherosclerotic plaques. PET, similarly to SPECT, uses radionuclides, but instead of gamma-ray emitting radionuclides, the PET technology is based on positron (β+) emitting radionuclides. A positron is defined as the antiparticle or antimatter counterpart to an electron, and has a positive electric charge (+1) and the same mass as an electron.

A brief mention of PET technology and technical challenges: During radioactive decay of the radionuclide, a positron is emitted and moves through the tissue until it encounters an electron. The distance is referred to as positron range and varies with positron energy. The encounter of an electron with its antiparticle, the positron, leads to annihilation, in which they vanish, with the formation of two antiparallel 511 kiloelectron volt (keV) gamma rays (photons), equaling the rest energy. These photons travel through the tissue before they reach the PET detector. The PET camera, consisting of a ring-like detector system, is able to detect these photons on opposite sides, **Figure 2.5**. The data is transformed into 3D images via computational reconstruction algorithms. The absorption and scatter (deflected energy) caused by the photon-tissue interaction is defined as the attenuation. Attenuation corrections in PET can improve image quality and provide more accurate quantifications of PET data (Conti et al. 2016; Gropler et al. 2007).

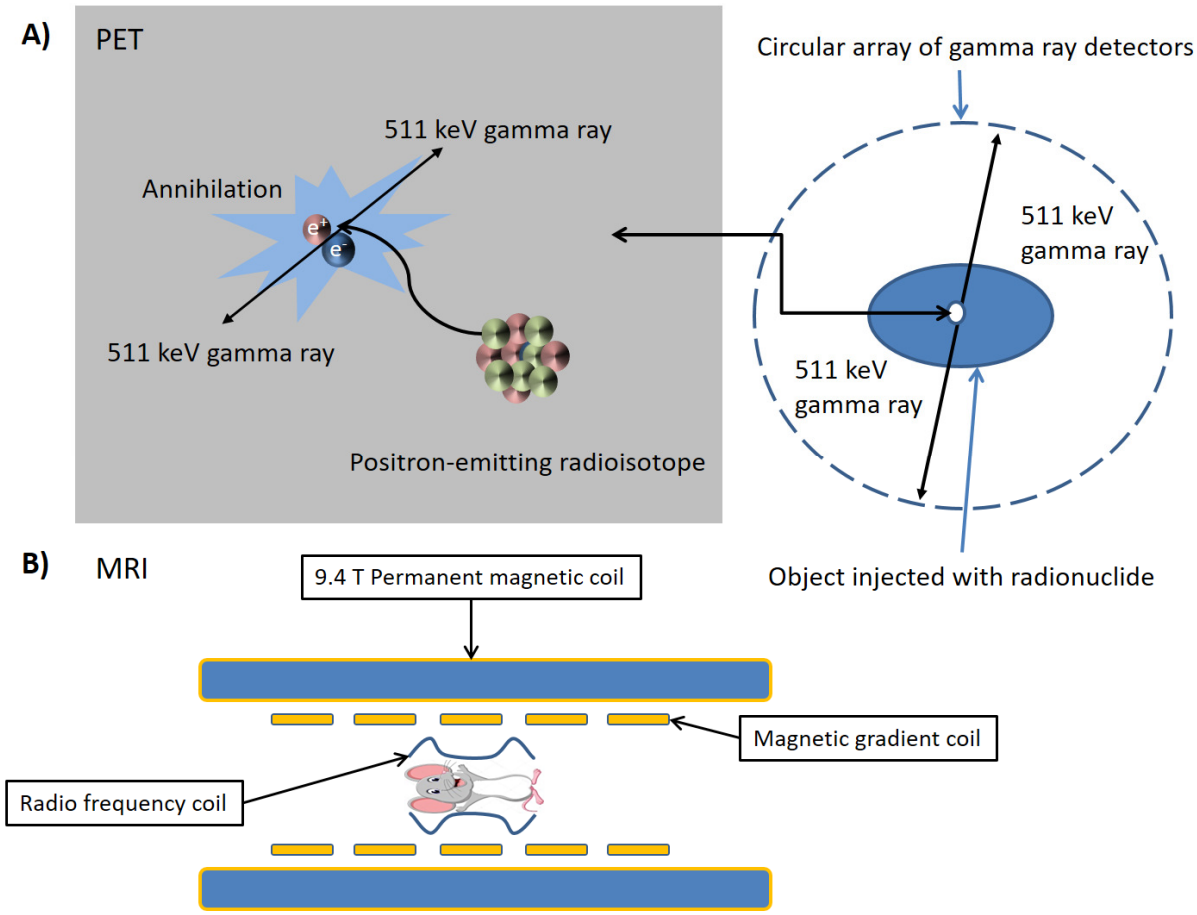

Figure 2.5: Schematic representation of the PET and MRI procedures. (A) Schematic showing the basic principle of PET imaging, adapted with permission, from the work of Dr. Mike Jackson, Small Animal and Materials Imaging Core Facility, Max Rady College of Medicine, Rady Faculty of Health Sciences, University of Manitoba. The principle is explained in detail in the text (B) Schematic drawing of an MRI scanner with its main components highlighted.

Radionuclides differ in half-life and positron range. The energy of the proton will determine the range. The positron range will in turn affect the overall spatial resolution. Typical short-range (<1 mm) positron emitters include ^{11}C, ^{18}F, ^{64}Cu, and ^{89}Zr, and long-range (>1 mm) positron emitters include ^{15}O, ^{68}Ga, and ^{82}Rb. Furthermore, these radionuclides can be divided into pure positron emitters and prompt gamma positron emitters. Gamma radiation emitted in decay cascades with the positron emission producing spurious coincidences, which blur the PET image and produce quantification errors, as in ^{82}Rb applications. Common radioisotopes for PET and SPECT are listed in **Table 2.5**. When choosing which radionuclide to use one should consider the half-life of the radioisotope. In general, short-range positron emitters are better suited for the imaging of small structures, since they travel a shorter distance in tissue before encountering an electron. The PET radioisotopes with long positron range imply a blurring of the radioisotope source distribution and a consequent loss of spatial resolution (Conti et al. 2016). In addition, some radioisotopes have an alternative high-energy β– decay

that could be used for radiotherapy. The radionuclide can be coupled to a "probe" or "ligand" of choice and the combination is called a radiotracer or radioligand. Radioisotopes with a short half-life are convenient for compounds that reach their target very quickly, like ^{15}O in brain studies or ^{18}F-fluorodeoxyglucose (^{18}F-FGD) used in several applications in oncology (Yang et al. 2018), while long lived isotopes are better suited when the target is reached more slowly: for example, in immuno-PET, radioisotopes such as ^{89}Zr-labeled (Dilworth et al. 2018; Fischer et al. 2013; Zhang et al. 2011) or ^{64}Cu ones can be labeled with monoclonal antibodies for imaging (Jauw et al. 2016; van Dongen et al. 2007).

Table 2.5: Examples of PET and SPECT radioisotopes and their properties.

Radioisotope	Half-life ($t_{1/2}$)	Decay mode (Branching β+ in %)	Emitted positron energy E_{max} (MeV)	Emitted positron energy E_{mean} (MeV)	Decay product
PET (pure positron emission)					
^{15}O	2 min	β+ (99.9)	1.732	0.735	^{15}N
^{11}C	20.4 min	β+ (99.8)	0.960	0.386	^{11}B
^{18}F *	110 min	β+ (96.9)	0.634	0.250	^{18}O
^{64}Cu	12.7 h	β+ (17.5)	0.653	0.278	^{64}Ni
^{89}Zr *	78.4 h	β+ (22.7)	0.902	0.396	^{89m}Y
PET (prompt gamma positron emission)					
^{82}Rb	1.3 min	β+ (81.8) (γ 15.1)	3.379 (E = 0.777 MeV)	1.535	^{82}Kr
^{68}Ga	67.8 min	β+ (87.7) (γ 3.2)	1.899 (E = 1.077 MeV)	0.836	^{68}Zn
SPECT					
^{99m}Tc *	6 h	γ	E = 0.142		^{99}Tc
^{123}I	13.2 h	γ	E = 0.159		^{123m}Te
^{111}In	67.2 h	γ	E = 0.245		^{111}Cd

Table references (Conti et al. 2016; Gropler et al. 2007). * Indicates the radioisotopes utilized in this thesis.

2.5.4 PET Imaging of Inflammation in Atherosclerosis

To date there is probably no better non-invasive imaging technique to identify molecular processes in the development of atherogenesis than PET. The use of PET tracers for imaging of atherosclerosis has become an important area of interest. There are many possible targets for the imaging of atherosclerosis and one of the most studied features of plaque vulnerability is inflammation, since it is related to a high risk of plaque rupture (Alonso et al. 2015; Hansson

et al. 2015; Tarkin et al. 2014; Wu et al. 2013). The most frequently utilized PET tracer, also outside the scope of atherosclerotic disease, is ^{18}F-FDG (Hyafil et al. 2018). FDG is a glucose analogue taken up in cells primarily via glucose transporters and further phosphorylated by hexokinase to FDG-6-phosphate. Unlike glucose, which is phosphorylated to glucose-6-phosphate, FDG-6-phosphate cannot be further metabolized and is therefore trapped in the cells. Therefore, uptake of ^{18}F-FDG is directly associated with glucose metabolism. Macrophages and myeloid cells have a high glucose metabolism. Studies have shown that polarization of macrophages to M1 phenotype increases ^{18}F-FDG uptake and consumption compared to M2 macrophages (Rodriguez-Prados et al. 2010; Tavakoli et al. 2013). Interestingly, macrophages seem to have an immunometabolic function in maintaining hemostasis in metabolic tissue, but also as a key driver of disease developments such as insulin resistance, which leads to diabetes type 2 (Mauer et al. 2010). The pro-inflammatory phenotype of macrophages relies on anaerobic glycolysis, which refers to the breakdown of glucose to puruvate and conversion to lactate and seems to promote insulin resistance, while the anti-inflammatory phenotype relies on aerobic metabolism and promotes insulin sensitivity. In obesity, the visceral adipose tissue accumulates macrophages of pro-inflammatory phenotype, increasing cytokine production and the inflammatory response (Verdeguer et al. 2017), which might cause off-target accumulation of ^{18}F-FDG in obese patients.

Despite the above-mentioned limitation, ^{18}F-FDG has been considered a surrogate marker of plaque inflammation. In a prospective study, Yun et al. were the first researchers to report on the association of ^{18}F-FDG uptake in vessels and cardiovascular risk (Yun et al. 2002). Rudd and colleagues were, however, the first to show uptake of ^{18}F-FDG in atherosclerotic lesions in a prospective study published in 2002 (Rudd et al. 2002). Since then, the imaging of atherosclerosis with ^{18}F-FDG has been utilized in both human and animal studies to image inflammation in atherosclerotic lesions (Rudd et al. 2007; Tarkin et al. 2014; Tawakol et al. 2005; Wells et al. 2017). Uptake of ^{18}F-FDG has been shown to correlate with lesion macrophages in atherosclerosis in animal models (Wenning et al. 2014; Zhang et al. 2006). Masteling et al. found that high ^{18}F-FDG activity in carotid plaques was localized to areas with macrophage infiltration (Masteling et al. 2011). In a clinical study with 21 patients undergoing carotid endarterectomies following ^{18}F-FDG-PET/CTA, the maximum standardized uptake value (SUVmax) was associated with increased concentration of CD68, a SR (class D) marker expressed on phagocytic cells, mainly macrophages (Menezes et al. 2011). A similar finding came from a small study by Tawakol et al., who found that CD68 staining was higher in high SUV plaques than in low SUV plaques (Tawakol et al. 2006). Other studies have found that FDG uptake is higher in lipid-rich plaques compared with collagen-rich

plaques (Silvera et al. 2009). At present, imaging of atherosclerotic plaques utilizing ^{18}F-FDG ranges from large scale clinical studies to simple proof of concept studies; for example, the effect of statins in lowering ^{18}F-FDG uptake (Tahara et al. 2006; Tawakol et al. 2013; Wu et al. 2007) to more thorough investigations, and evaluation in combination with new developments of anti-inflammatory therapies (Fayad et al. 2011; Gaztanaga et al. 2015) to gain more information about disease pathology. However, since FDG is taken up by cells that are metabolically active, it is not a specific marker of inflammation in atherosclerosis and not all studies are consistent: some have failed to show uptake of ^{18}F-FDG in atherosclerotic lesions (Laurberg et al. 2007) or correlation to macrophages (Myers et al. 2012). There are also variabilities depending on several factors such as metabolic state, or imaging time point post injection (Bucerius et al. 2014; Huet et al. 2015). High blood glucose levels (>7 mmol/l) can also diminish the ^{18}F-FDG uptake in vessels (Bucerius et al. 2014). Other limitations are high physiological uptake in the myocardium, limiting the visualization in coronary arteries, which to some extent might be possible to suppress by, for example, fasting or low-carbohydrate diets. Others have tried to suppress myocardial tracer uptake in preclinical settings by giving ketamine/xylazine anesthesia (Nahrendorf et al. 2008).

2.5.4.1 Other PET Tracers

The research field consists of investigators looking to develop new potential PET tracers and the majority has been restricted to testing in cell and animal models (Bucerius et al. 2019; Chen et al. 2010; Yang et al. 2018). Others have tried to target different features of the atherosclerotic plaque, aside from inflammation, such as hypoxia (Mateo et al. 2014), neoangiogenesis markers such as $\alpha_v\beta_3$ integrin (Beer et al. 2014; Laitinen et al. 2009b; Paeng et al. 2013), and microcalcification with sodium fluoride (^{18}F-NaF) (Joshi et al. 2014). Joshi et al. (2014), found that imaging with ^{18}F-NaF was more reliable than ^{18}F-FDG in identifying vulnerable coronary plaques. These authors also investigated uptake in carotid artery specimens and found that ^{18}F-NaF uptake occurred at the site of all carotid plaque ruptures and was strongly associated with active calcification, macrophage infiltration, apoptosis, and necrosis. In addition, other PET tracers, initially used in oncology (DeGrado et al. 2001; Norlen et al. 2018; Sundin 2012), were later applied to the vascular imaging of inflammation in atherosclerosis. This included less specific macrophage receptor targeting of, for example, translocator protein (TSPO), evaluated as a target for macrophage cholesterol efflux (Lecanu et al. 2013; Taylor et al. 2014). It has been studied in preclinical settings for aortic plaque imaging (Hellberg et al. 2017; Laitinen et al. 2009a) and in a clinical setting for carotid plaque imaging (Gaemperli et al. 2012). Other

radiotracers have been evaluated, such as the somatostatin receptor in which ^{68}Ga-DOTATATE was correlated with macrophage-rich areas in *Apoe*$^{-/-}$ mice (Li et al. 2013) and correlated with calcification and cardiovascular risk factors in retrospective clinical studies of cancer patients (Rominger et al. 2010). Targeting of choline metabolism in macrophages by utilizing choline analogues has shown accumulation in macrophage-rich atherosclerotic lesions in preclinical studies (Laitinen et al. 2009a; Matter et al. 2006) and in clinical studies (Bucerius et al. 2008).

2.5.4.2 ^{89}Zr-based PET Tracer for Imaging of Inflammation in Atherosclerosis

Besides the radionuclide ^{18}F, other radionuclides have been used to image atherosclerosis with PET, such as ^{68}Ga, ^{64}Cu, and ^{89}Zr. The application of more long-lived isotopes, such as the two latter, could enable extensive *ex vivo* evaluation in a preclinical setting compared to ^{18}F. ^{89}Zr has been mostly frequently utilized in immuno-PET in the field of oncology (Dilworth et al. 2018; Fischer et al. 2013; Jauw et al. 2016; Zhang et al. 2011), but there are some recently published studies in the field of atherosclerosis (Majmudar et al. 2013; Senders et al. 2018). Majmudar et al. (2013) reported promising results and the feasibility of *in vivo* atherosclerotic hybrid PET/MR imaging with an ^{89}Zr-labeled dextran coated nanoparticle as well as high uptake by monocytes and macrophages in excised atherosclerotic aortas from *Apoe*$^{-/-}$ mice. Senders et al. (2018) report a novel PET tracer for imaging atherothrombotic burden and plaque vulnerability with ^{89}Zr-LA25: a human antibody Fab fragment LA25 binding to advanced MDA epitopes, namely malondialdehyde-acetaldehyde (MAA) adducts: OSEs found in human atherothrombotic lesions. The authors concluded that ^{89}Zr-LA25 could be a promising PET tracer for coronary atherosclerosis imaging given its 2.5-fold higher aorta-to-myocardial uptake ratio in diseased animals than the currently approved ^{18}F-FDG. Other PET tracer candidates have also been described utilizing ^{89}Zr to monitor leucocyte trafficking in inflammation (Fairclough et al. 2016). Molecular probes for targeted imaging in atherosclerosis are summarized in **Table 2.6**.

Table 2.6: Molecular imaging probes for the imaging of atherosclerosis.

Biological events	Molecular target	Imaging modalities	Imaging Probes	Species/ vessel	References
Vascular inflammation, endothelial activation	VCAM-1, ICAM-1, P-Selectin, E-Selectin	CEUS, MRI, PET, SPECT	Targeted MBs, targeted USPIO, ^{18}F-, ^{68}Ga-, ^{99m}Tc-labeled-antibodies	Animals/ aorta	(Broisat et al. 2014; Kaufmann et al. 2007a; Kaufmann et al. 2007b; Li et al. 2014; Nahrendorf et al. 2009; Nakamura et al. 2013)
Vascular permeability	Albumin	MRI	Gadofosveset	Human/ multiple vascular beds	(Phinikaridou et al. 2013)
Macrophage receptors	Scavenger receptors (SR-A1, LOX-1)	MRI, SPECT, PET	Targeted USPIO, Gd- probes, ^{99m}Tc-labeled antibodies, Mal-HSA, ^{64}Cu/Gd/TAMRA-Mal-BSA	Animals/aorta	(Gustafsson et al. 2006; Jarrett et al. 2010; Jarrett et al. 2008; Li et al. 2010; Segers et al. 2013; Wen et al. 2014)
	Mannose receptor		^{68}Ga-NOTA-neomannosylated human serum albumin (MSA), ^{18}F-FDM		(Kim et al. 2016; Tahara et al. 2014)
	Translocator protein (TSPO)		^{11}C-PK11195, ^{18}F-FEMPA		(Hellberg et al. 2017; Laitinen et al. 2009a)
	Somatostatin receptor		^{68}Ga-DOTATATE		(Li et al. 2013)
Leukocyte trafficking	Leucocytes		^{89}Zr-Chitosan nanoparticles		(Fairclough et al. 2016)
Metabolic activity	Glucose metabolism	PET	^{18}F-FDG	Humans and animals/aorta, carotid, coronary	(Rudd et al. 2007; Rudd et al. 2002; Tarkin et al. 2014; Tawakol et al. 2006; Tawakol et al. 2005; Zhang et al. 2006)
	Phospholipid metabolism		^{18}F-FMCH/^{11}C-Choline	Animals and humans/aorta and carotid	(Bucerius et al. 2008; Kato et al. 2009; Laitinen et al. 2010; Matter et al. 2006)

Neoangiogenesis	$\alpha_v\beta_3$	MRI, SPECT, PET	Gd-labeled RGD probes, ^{18}F-labeled RGD , ^{68}Ga-labeled RGD	Animals and humans/aorta and carotid	(Beer et al. 2014; Burtea et al. 2008; Laitinen et al. 2009b; Paeng et al. 2013)
Hypoxia	Redox	PET	^{18}F-FMISO (and a few other tracers)	Animals/aorta	(Mateo et al. 2014)
Microcalcification	Bone mineralization	PET	^{18}F-NaF	Animal/ coronary	(McKenney-Drake et al. 2018)
Platelet adhesion, atherothrombosis	GPVI, GP IIb/IIIa	CEUS, PET	Targeted MBs, ^{64}Cu-labeled probes	Animals/aorta and carotid	(Bigalke et al. 2013; Guo et al. 2015; Metzger et al. 2015)
Atherothrombosis	Von Willebrand factor, Oxidation-specific epitopes (OSEs)	CEUS, PET/MRI	Targeted MBs, ^{89}Zr-LA25	Animals/aorta	(McCarty et al. 2010; Senders et al. 2018)

2.5.5 Multimodal Imaging

The combination of imaging modalities for diagnostic purposes can provide synergistic advantages over single modalities. The rapidly evolving imaging field has led to the development of hybrid imaging, referring to the integration of hardware from two (or more) imaging technologies to form a new, more powerful imaging modality. Some examples of hybrid imaging modalities are PET/CT, PET/MR, SPECT/CT, and US/MR (Hricak et al. 2010). The image acquisition can be obtained simultaneously with PET/MR, or sequentially, but performed without moving the patient from the bed. The combination of these techniques might allow improved characterization of the atherosclerotic plaque. Separately, each of these techniques is suitable for imaging of different features of the plaque; stenosis, fibrous cap, plaque composition (core), plaque volume with MRI, micro-calcification, inflammation, hypoxia, and angiogenesis with PET. Combining PET and MRI in hybrid imaging allows for outstanding visualization of the atherosclerotic plaque in combination with detection of inflammation. An advantage of hybrid imaging (e.g. PET/CT) is the possibility of obtaining attenuation correction of PET data using CT attenuation coefficients. CT scans are, however, associated with high radiation doses and combination with MR imaging would limit radiation to PET. Combining PET with MRI enables visualization of more plaque components than PET/CT (Ripa et al. 2016).

Hybrid imaging is different from fusion imaging. Fusion imaging refers to two separate hardware units where the images have been fused or overlaid by software rather than combined

hardware adjustments of positions. Hence the patient or experimental animal undergoes two separate scans, not necessarily within a short timeframe. Images from a PET scan can later be fused or overlaid with the ones acquired from MRI. Anatomical misalignment, caused by differences in patient positioning or respiration, can significantly influence image interpretation, resulting in false localization of the imaging probes in atherosclerotic lesions. Thus, good software systems for vascular imaging of inflammation are crucial in fusion imaging (Giovanella et al. 2010).

2.5.6 Multimodal Probes and Coupling to Biomacromolecules

The advances in hybrid imaging have created a need for multimodal molecular probes, involving a single probe with several incorporated physical features to enable imaging with different modalities. This is a rather novel interdisciplinary research field, which has been explored more often in the field of cancer research than for CVDs. Multimodal probes may be beneficial when studying the pathogenesis of diseases and different properties of imaging modalities may be utilized in a single setting (Bucerius et al. 2019; Yang et al. 2018).

Clinically utilized contrast agents or probes are single modal. More bimode molecular imaging probes have been developed for potential clinical use than multimodal probes: the first might be more relevant for clinical applications and the second allows for extensive pre-clinical evaluation on a research basis. Nahrendorf et al. described a novel trimodal nanoparticle consisting of an iron oxide core for MRI and an optically detectable near-infrared fluorochrome that is radiolabeled with ^{64}Cu for PET imaging and targeting of macrophage phagocytosis (Nahrendorf et al. 2008). In 2006, Gustafsson et al. reported a trimodal macromolecule carrier, maleylated bovine serum albumin (Mal-BSA), for the targeting of macrophages, coupled to Gd for a signal enhancement in MRI and radiolabeled with ^{64}Cu (Gustafsson et al. 2006). In 2010, Jarret et al. applied this probe in an *Apoe*$^{-/-}$ ligation mouse model in a proof of principle study (Jarrett et al. 2010). In addition, Jarrett and Gustafsson reported a similar probe, combining ^{64}Cu-labeled and magnetic nanoparticles for potential multimodal imaging applications (Gustafsson et al. 2006; Jarrett et al. 2010; Jarrett et al. 2008).

Conjugation to biomacromolecules has been utilized to increase the circulation half-life of diagnostic or therapeutic agents, one of the most common being albumin (Cao et al. 2015; Smith et al. 2001). The advantages are due in part to its size (which is above the renal threshold), solubility, and *in vivo* stability. Native albumin specifically interacts with the native Fc receptor in a pH-dependent fashion in the endosome and is responsible for recycling albumin back into circulation, hence contributing to the long circulatory albumin half-life of

19 days. The coupling with albumin can be performed *in vitro* by covalent binding or by *in vivo* non-covalent coupling (a reversible binding) in which the probe or drug binds albumin in the circulation after intravenous injection (Cao et al. 2015; Sleep et al. 2013). Gadofosveset is one example of an MRI contrast agent that reversibly binds to human serum albumin (HSA) *in vivo* after injection (Caravan et al. 2002).

In summary, the following goals should be achieved in vascular imaging with molecular probes:

- **High specificity to the target:** To have a specific tracer or probe with a long enough circulating half-life to reach the target site with high uptake in the lesion
- **High binding affinity with the target:** To obtain high uptake of the imaging probe in target tissue within a limited circulation timeframe requires that the imaging probe has binding properties with a fast on-rate (K_{on}) and slow off-rate (K_{off}).
- **Choice of the most appropriate radionuclide:** This means choosing the ideal radionuclide for the target you want to image and matching the half-life of the probe. Low positron energy and positron range are favorable physical properties for the imaging of small structures such as atheroslcerotic lesions.
- **High contrast ratio:** High signal-to-noise ratio (SNR) or contrast-to-noise ratio (CNR) as in addition to target-to-background ratio (TBR) to ensure appropriate interpretation of the physiological and pathological conditions of the diseases. Hence, the remaining radioactivity in the blood pool and the surrounding tissue should be low to minimize the background signal.
- **High stability *in vivo*:** Maintenance of the intact structure of an imaging probe is important for increasing the likelihood of the probe reaching the target. This is a major challenge because numerous enzymes or proteases that are present in serum or targeted tissue may degrade the imaging probe.
- **Low immunogenicity and toxicity:** To reduce side-effects.
- **Production and economic feasibility:** Important for large scale or clinical use.

3 AIMS

The overall aim of this thesis was to develop probes for the molecular imaging of inflammation and to evaluate the specificity of the probes under *in vitro* conditions and their applicability in *in vivo* models of inflammation and atherosclerosis.

The specific aims of each study were:

I. To evaluate the cellular interaction of polyvinyl alcohol (PVA)-based microbubbles (MBs) and the influence of nanoparticle location in the shell.

II. To investigate whether antibody conjugation of MBs could improve the targeting of inflammatory markers and to evaluate this by SPECT/CT fusion imaging in a rat inflammation model.

III. To develop modified human serum albumin (HSA)-based probes for molecular targeting of macrophage scavenger receptors, and to evaluate the specificity of the probes and their cellular uptake routes.

IV. To evaluate radiolabeled modified HSA probes and determine their feasibility with regard to targeting and visualizing inflammation in atherosclerotic plaques under *in vivo* and *ex vivo* conditions by molecular imaging in a mouse model of atherosclerosis.

4 METHODOLOGICAL CONSIDERATIONS

4.1 General Study Design

This thesis project constitutes two MB-based studies (**study I** and **II**) and two studies (**III** and **IV**) on modified HSA-based probes. In **study I**, the *in vitro* cellular interaction of non-targeted bi-modal MBs with or without superparamagnetic iron oxide nanoparticles (SPIONs) is evaluated, and in **study II**, more advanced multimodal MBs targeting adhesion molecules are evaluated. Further, in the second study, cellular interaction and specificity are investigated through *in vitro* experiments, and the *in vivo* feasibility is evaluated by SPECT/CT imaging in a rat model of peritonitis. In **study III**, the cellular uptake routes and specificity of HSA-based probes are evaluated under *in vitro* conditions. In **study IV**, these probes are evaluated for plaque uptake in an *Apoe*$^{-/-}$ mouse model of atherosclerosis with the help of fusion imaging with PET and MRI as well as extensive *ex vivo* evaluation of probe uptake in atherosclerotic plaques. The overall design of the four studies is presented in **Figure 4.1**.

	Molecular imaging probes		Probe characteristics	Experiments
MICROBUBBLES	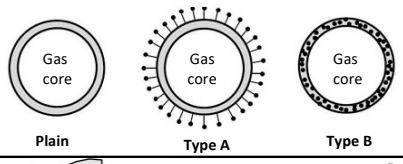	STUDY I	No specific interactions Potential bimodal-imaging - Ultrasound (MB) - MRI (SPIONs) - Fluorescence microscopy (FITC, Rhodamine)	**Study I** *In vitro* interactions with macrophages and endothelial cells
	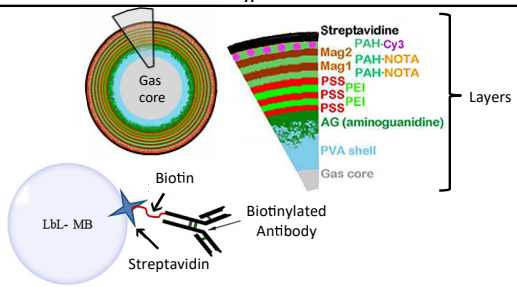	STUDY II	Targeting adhesion molecules with antibodies Potential multimodal imaging - Ultrasound (MB) - Nuclear imaging (NOTA) - MRI (SPIONs) - Fluorescence microscopy (Cy3)	**Study II** *In vitro* adhesion molecule targeting on endothelial cells and macrophages with fluorescence techniques *In vivo* hybrid imaging of inflammation with SPECT/CT in a rat model of peritonitis
HSA-BASED PROBES	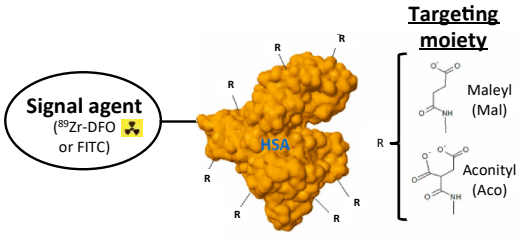	STUDY III + IV	Targeting scavenger receptor (SR-A1) on macrophages Imaging - Nuclear imaging (DFO) - Potential for MRI - Fluorescence (FITC)	**Study III** *In vitro* evaluation of cellular uptake routes and specificity. Evaluation of interaction with human macrophages, ECs and SMCs **Study IV** *In vivo* evaluation of plaque uptake in a mouse model of atherosclerosis with fusion imaging (PET/MRI). *Ex vivo* evaluation with gamma counter, PI-ARG and histological staining

Figure 4.1: Summary of the molecular imaging probes and the overall study design.

4.2 Probe Development and Evaluation

4.2.1 Microbubbles (Study I and II)

The MBs utilized in **study I** and **study II** were developed within the scope of the European Commission's 3MiCRON project. Briefly, these MBs were (on average) 3 μm in size, and they were based on a previously developed MB with biocompatible synthetic organic PVA material (Cavalieri et al. 2005; Cerroni et al. 2011; Paradossi 2010). The MBs were further functionalized, within the scope of the 3MiCRON project, for potential MRI by the conjugation of SPIONs on the outside of the MBs or by the incorporation of SPIONs in the shell. The different types of conjugations between SPIONs and MBs, as well as the physical, magnetic, and US imaging properties of these MBs were recently reported (Barrefelt et al. 2014; Brismar et al. 2012; Grishenkov et al. 2009).

In **study I**, the following different types of MBs were evaluated under *in vitro* conditions for cellular interaction with macrophages and endothelial cells: PVA only (plain), MBs with SPIONs on the outside (type A), and MBs with SPIONs incorporated in the shell (type B).

In **study II**, a similar but more advanced PVA-based MB, with several different layers with multimodal properties, was developed in the lab of Lars Dähne (Surflay Nanotec GmbH, Germany). Two layers of SPIONs were embedded between the shell layers for MRI; a metal chelating ligand (NOTA) layer was used for nuclear imaging; a fluorescent layer, for fluorescence microscopy evaluation; and an outmost layer of streptavidin, for conjugation with antibodies. These advanced MBs were evaluated for their *in vitro* targeting properties and interaction with macrophages and endothelial cells. The MBs were also evaluated for their physical and imaging properties. The physical properties were evaluated using transmission electron microscopy and atomic force microscopy, and the imaging properties were evaluated based on the US acoustic characteristics and nuclear imaging properties. Nuclear imaging was performed *in vivo* in a rat model of peritonitis. The SPECT and MRI properties of non-targeted MBs have been previously reported, and their biodistribution has been evaluated in rats (Barrefelt et al. 2013a; Barrefelt et al. 2013b).

4.2.2 Radiotracers (Study II and IV)

In **study II**, ^{99m}Tc-labeling was used for imaging with SPECT/CT. Technetium-99m pertechnetate ($^{99m}TcO_4^-$) was produced in a ^{99}Mo/^{99m}Tc-generator on site at the Department of Radiopharmacy, Karolinska University Hospital. The procedure for radiolabeling the MBs with ^{99m}Tc, with NOTA as the chelating ligand, is described in detail in **study II**. Immediately

after radiolabeling, the purification procedure was started with a series of washing steps. Labeling efficiency was validated by instant thin-layer chromatography, which yielded ≥95% ^{99m}Tc-labeling. The resulting ^{99m}Tc-anti-ICAM-1-labeled MBs were utilized for SPECT/CT imaging in vivo.

In **study III** and **IV**, the PET radionuclide ^{89}Zr was generated in a cyclotron, a particle accelerator, and delivered by Perkin Elmer (BV Cyclotron VU, Amsterdam, the Netherlands). The radiolabeling procedure for HSA-DFO, Mal-HSA-DFO, and Aco-HSA-DFO is described in detail in **study III** and **IV**. The agents were analyzed and purified using high-performance liquid chromatography. The fractions with the highest radio peak were collected and used in the experiments. The labeling yield and radiochemical purity of the ^{89}Zr-labeled tracers (^{89}Zr-HSA, ^{89}Zr-Mal-HSA, and ^{89}Zr-Aco-HSA) were determined by instant thin-layer chromatography. In **study IV**, clinically approved fluorine-18-labeled fluorodeoxyglucose (^{18}F-FDG) was produced on site (Department of Radiopharmacy, Karolinska University Hospital); it met all the criteria for human use and was applied without further purification. The properties of the molecular probes and their target molecules are summarized in **Figure 4.2**.

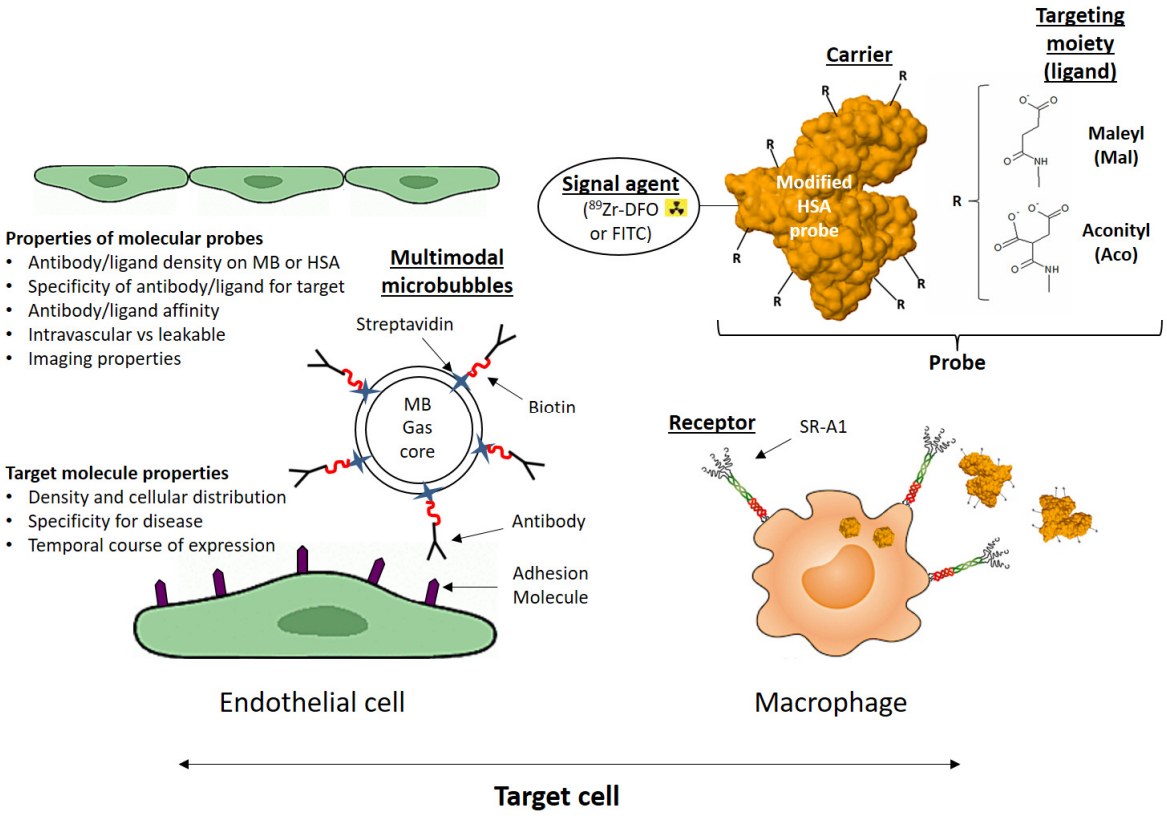

Figure 4.2: Molecular probes and their target molecules. Strategies for targeting by surface conjugation with specific ligands or antibodies able to bind disease related molecules.

4.2.3 Radiosafety

Nuclear imaging results in ionizing radiation exposure, and it is important for the investigator to be well protected and educated about the potential risk of repeated radiation exposure. Radiosafety is an important concept when it comes to working with and handling radioactive material. Radioactivity cannot be seen or be felt in smaller doses, so safety precautions are important for personnel as well as patients. The radiation dose depends on the type of radiation (α, β, or γ), duration of the exposure and the distance from the source, and whether the radiation shield was used. Both gamma emitters and positron emitters are used in this project. Gamma rays are the most penetrative form of radiation. However, the radiation can be shielded with lead, and safety precautions to minimize contamination and radiation dosimetry should always be applied. The goal is to minimize the radiation dose as much as possible to avoid hazardous side effects, as significant radiation exposure is associated with an increased risk of cancer. Although the risk from a single scan is low, there could be adverse cumulative effects of radiation exposure over a life time.

4.3 Experimental Cells

It is important to choose relevant cells for your disease model. Immortalized cell lines, which proliferate in an uninhibited manner, are usually more easy to culture but different from primary isolated cells, which normally only can be cultured until a certain passage before the classical markers are lost and their morphology starts to get altered. Expression of adhesion molecules by cells in a controlled 2D environment is very different from that in the complex 3D structures within the body where cells interact physically and chemically with each other and the ECM. This must be taken into consideration during the translation of *in vitro* findings into *in vivo* applications. It is possible that in *in vivo* settings, the same types of cells behave differently or show different expression patterns or morphology. For example, unlike *in vitro* cultured endothelial cells, *in vivo* endothelial cells are in contact with the basement membrane and are constantly exposed to blood flow and shear stress. However, it is possible to obtain more complex cell co-cultures on 3D matrices that better mimic the *in vivo* milieu, for example, by utilizing biomaterials such as hydrogels.

4.3.1.1 Endothelial Cells

2D cell cultures from mouse and human cells were used in this thesis to study the *in vitro* cellular interactions of MBs or modified HSA probes. Both commercially available cells and primary cells isolated from the rat peritoneum or from human buffy coats were used in the studies. In **study I**, MyEnd$^{+/+}$ microvascular myocardial endothelial cells were used to study the interaction of MBs with endothelial cells. Human umbilical vein endothelial cells (HUVECs) are one of the most utilized cell lines to study the function and pathogenesis of endothelial cells (Cheung 2007). In **study II**, HUVECs were incubated with pro-inflammatory cytokines in order to induce the upregulation of adhesion molecules (ICAM-1, VCAM-1 and E-selectin). The adhesion of MBs to the endothelial cells was assessed during both static and flow conditions. Since HUVECs originate from venous vessels, and since atherosclerosis is a disease that affects the arterial wall, we also included mouse aortic endothelial cells in **study II**. In **study III**, HUVECs were used only as a physiological model of ECs.

4.3.1.2 Macrophages

The RAW264.7 mouse leukemic monocyte macrophage cell line is commonly used to study phagocytosis in macrophages in laboratory research. This cell line was originally established from the ascites of a tumor induced in a male mouse by intraperitoneal injection of the Abelson murine leukemia virus. RAW264.7 cells were utilized in **study I** to evaluate the non-specific adhesion or uptake of non-targeted MBs with or without SPIONs. In **study II**, peritoneal macrophages from a rat peritonitis model were isolated and cultured to evaluate macrophage interaction with anti-ICAM-1-labeled MBs. In **study III**, THP-1 cells, a human monocytic leukemia-derived cell line, were differentiated into THP-1 macrophages and also THP-1 foam cells to study the cellular interaction of modified HSA probes. Peripheral blood was obtained from healthy volunteers, with their written consent, at the Blood Center of Karolinska University Hospital, Stockholm, Sweden. The blood monocytes were induced to differentiate into macrophages *in vitro* and further polarized into M1 or M2 macrophages.

4.3.1.3 Vascular Smooth Muscle Cells

The interaction of human carotid SMCs with modified HSA probes was investigated in **study III**.

4.4 Experimental Animal Models

In vivo rodent models were used for the molecular imaging of inflammation (**study II**) and atherosclerosis (**study IV**).

4.4.1 Animal Model of Inflammation (Study II)

In study II, a rat model of peritonitis was utilized for targeting inflammation *in vivo*. Peritonitis was induced by intraperitoneal injection of Zymozan, which triggers an inflammatory response and induces expression of ICAM-1 on inflammatory cells. The targeting of ICAM-1 on peritoneal macrophages was evaluated *in vivo* with SPECT/CT after intravenous injection of ^{99m}Tc-*anti*-ICAM-1-labeled MBs. Isolated peritoneal macrophages were assessed by flow cytometry after incubation with anti-ICAM-1-labeled MBs. Ideally, *ex vivo* evaluation of peritoneal macrophages after intravenous administration of ^{99m}Tc-*anti*-ICAM-1-labeled MBs would have provided a more direct evaluation of the *in vivo* uptake of the probes by these cells.

4.4.2 Animal Model of Atherosclerosis (Study IV)

Most atherosclerotic mouse models are based on genetic modifications of the C57BL/6 mouse strain (Paigen 1985). In **study IV**, an *Apoe*$^{-/-}$ mouse model on the C57BL/6 genetic background was utilized. Female mice were used, and the mice were provided a western diet (21% fat, 0.15% cholesterol) to aggravate disease progression. Female mice are known to develop atherosclerosis at an earlier age and are less prone to fight with each other than male mice. Ideally, for the purpose of research, animals of both sexes should be included. However, examining sex-based differences in the properties and functions of the probes was not within the scope of this work.

4.5 Ethical Considerations

Experimental animals were utilized in **study II** and **IV**. We complied with the 3R principle: replace, reduce, refine. Good laboratory practices were applied, and institutional and national guidelines for the care and use of laboratory animals were followed with the approval of the Stockholm Animal Ethics Committee. No human subjects were used in the work of this thesis. The development of molecular imaging probes, which are not yet approved for clinical use, requires thorough preclinical evaluation in small animals and thereafter in larger animals for the assessment of *in vivo* stability and toxicity profiles, before clinical phase trials are permitted. To some extent, *in vitro* evaluation can be performed to study specificity and cellular uptake

routes; however, the *in vitro* conditions will not satisfactorily simulate the complexity of the *in vivo* state. Therefore, the molecular imaging probes in the present study were also investigated using non-invasive techniques in animal models for the evaluation of their biodistribution and pharmacokinetic profiles. A strict protocol that was in accordance with the legislations for animal studies was followed for determining the injection frequency, injection volume, as well as imaging time under anesthesia. The imaging techniques used in this project are non-invasive, and they are not known to cause any discomfort to the animal. Biocompatible materials were used as the basis of the molecular probes, but they are also considered as foreign material. When injected into the bloodstream, these materials may cause immunogenic responses, allergic reactions or unwanted side effects. Moreover, the size of the molecular probes would affect their biodistribution profile, so *in vivo* studies in animals are necessary to evaluate these components. Rodents are feasible as animal models, as they are easy to handle and are far less costly than larger animal models. However, imaging in small animal models may be more challenging due to the small size of organs as compared to rabbits or pigs. Especially with regard to the vascular imaging of atherosclerosis, the spatial resolution of the small-sized vessels is limited to the spatial resolution of the preclinical imaging modality (Razuvaev et al. 2008), and the specificity and sensitivity of the molecular probes.

4.6 In Vitro Fluorescence Techniques

4.6.1 Flow Cytometry (Study II, III, and IV)

Flow cytometry was used to quantify probe adhesion to cell-surface receptors by utilizing the fluorescence properties of the MBs in **study II**, and to quantify the adhesion or uptake of HSA-based probes by cells in **study III** and **IV**. Flow cytometry was also applied to correctly characterize isolated cells with specific markers, although no single marker is specific or sensitive enough for a certain polarization (Jaguin et al. 2013).

The working principle of flow cytometry is based on single-cell analysis of fluorescently labeled cells conjugated with either antibodies or beads (in our case, a fluorescent MB labeled with antibodies or fluorescent HSA-based probes). Fluorescent antibodies or molecular probes are incubated with cells in suspension and can be used to stain either surface markers or intracellular markers via cell permeabilization protocols. Thereafter, quantitative data are acquired in a flow cytometer: different lasers are used to excite the fluorescently labeled cell markers and the cells are distinguished based on their size (forward scatter), granularity (side scatter) and fluorescence intensity. To account for fluorescence spillover when

utilizing several fluorochromes in a staining panel, single staining and fluorescence minus one can be applied. To assess antibody specificity, the corresponding isotype control for the antibody of interest can be utilized (Adan et al. 2017). Post-processing analysis was performed with the FlowJo software, and different gating strategies were applied to evaluate the cell populations of interest.

4.6.2 Fluorescence Microscopy (Study I, II, and III)

Fluorescence microscopy was used to assess *in vitro* MB- or HSA-based probe–cell interactions and uptake in **study I**, **II**, and **III** respectively. Fluorescence microscopy is an essential tool for imaging cell morphology and molecule localization. In fluorescence microscopy, the whole sample is illuminated by the excitation light. Although the highest intensity of excitation light will be at the focal point of the lens, the fluorescence from out-of-focus points will cause background fluorescence and reduce the sharpness of the images. Confocal microscopy is a specialized form of standard fluorescence microscopy that has improved optical resolution in the z-axis plane as a result of a reduction in the amount of out-of-focus light reaching the detector; moreover, serial optical sections can be visualized in a thick specimen. In brief, an excitation laser is reflected off a dichroic mirror, as a result of which light of shorter wavelengths is reflected and light of longer wavelengths passes through. The reflected light hits mirrors that are mounted on motors; this allows the laser to scan across the sample and also scan in different planes in a z-stack. The emitted light from the sample (with longer wavelength) is scanned by the same mirrors and emitted through the dichroic mirror and focused onto a pinhole, and the out-of-focus light is filtered out. The emitted fluorescent light is measured by a detector and a photomultiplier tube coupled to a computer, which creates a sharp image. Factors that affect the fluorescence signal are the sample preparation method, the mounting media used, and the choice of fluorophores. For imaging fluorophores in a stained sample, the fluorophores should be excited separately, but this increases the scanning time. If possible, separate lasers should be used for exciting the fluorophores, and their emission should be evaluated for potential “bleed through” of the signal into other detection channels (Hibbs 2004).

4.7 In Vivo Molecular Imaging

4.7.1 SPECT/CT Hybrid Imaging and Quantification (Study II)

In **study II**, SPECT was performed in conjunction with CT for anatomical imaging. SPECT data were reconstructed using a 3D method (Siemens Flash 3D), and the volume was matched to the reconstructed CT volume. Data analyses were performed by an independent investigator, who drew volumes of interests around the whole body and each organ on the CT images.

4.7.2 Vascular PET/MR Fusion Imaging and Quantification (Study IV)

The acquired PET data were processed using MicroPET Manager and evaluated using the Inveon Research Workplace software (Siemens Medical Systems, Malvern, PA, USA). MR bright-blood images were used to define the anatomy of the vasculature and MR black-blood images of the aortic root were acquired to observe the vessel wall of the aortic root. Co-registration with MR images was done mainly by fitting the PET signal from the liver, vertebral column and sternum to the bright-blood MR image. After co-registration, volumes of interest were manually drawn around the aortic arch and the blood pool signal in the vena cava.

There are several methods for the quantification of PET tracer uptake in vascular imaging. The two principle quantitative measures of this variable are standardized uptake value (SUV) and target-to-background ratio (TBR). SUV is calculated with the following formula: (radioactivity in tissue/tissue volume)/(injected radioactivity/body weight). TBR is the ratio of SUV in the target tissue (atherosclerotic lesion) to SUV in the background (e.g., blood). The maximum and mean TBR and SUV values are also calculated. TBR_{max} refers to the ratio of maximum SUV in the lesion to mean SUV in blood, whereas TBR_{mean} refers to the ratio of mean SUV in the lesion to mean SUV in blood. There is some variability in the reported results in the literature, depending on the quantification method, the vessel area under analysis (whether it is the most diseased part of the vessel or the whole vessel), the timing of imaging after radiotracer injection, and the metabolic state. In **study IV**, we measured both SUV_{max} and TBR_{max}.

4.7.3 Ex Vivo Evaluation of Radioactive Uptake (Study IV)

Radiotracer uptake in excised organs after intravenous injection or by cells *in vitro* after incubation was evaluated with a gamma counter (Wallac™ Wizard 3” 1480, Perkin Elmer).

Phosphor imaging autoradiography (PI-ARG) was used for visual and quantitative measurement of radiotracer uptake in atherosclerotic plaques in **study IV**. Hand-drawn regions of interests with manually applied thresholds or a semi-automatic method for the calculation of radiotracer signal in the regions of interest, with one set threshold, were used to evaluate radiotracer accumulation in diseased areas of the mouse aorta. The methodological procedure is described in detail in **study IV**.

4.8 Statistical Analysis

All statistical analyses were conducted using GraphPad Prism (version 7 for Macintosh). Assessment of normal distribution with the Shapiro-Wilk normality test, the drawing of histograms and q-q plots, and assessment of homogeneity of variance with Levene's test were performed in SPSS (version 24 for Macintosh). If normality and equality of variance were not rejected at the significance level of 0.05, the group means were compared using parametric tests. For the comparison of two groups, Student's *t*-test was applied (**study II**, **III**, and **IV**). For the comparison of measurements within the same animal, a paired *t*-test was applied (**study II**). For comparison of more than two groups, one-way ANOVA was applied (study **III** and **IV**). In **study III**, two-way ANOVA was applied when more than two variables existed, and linear regression was applied to test relationships. A repeated-measures ANOVA was applied in the time-lapse experiments in **study III**. The post-hoc correction methods used for ANOVA were Tukey's multiple comparison test (**study III** and **IV**) or Dunnett's test (**study III**). If data did not follow a Gaussian distribution, nonparametric tests were applied: the Mann Whitney *U*-test was used for comparisons between two groups (**study II**). Two-tailed *P*-values less than 0.05 were considered to indicate significance.

5 RESULTS AND DISCUSSION

A series of probes have been evaluated in the literature with the aim of increasing the specificity of molecular multimodal imaging techniques. In an attempt to develop molecular probes with high target specificity for different markers of inflammation in atherosclerosis, we evaluated cellular interactions, cellular uptake routes as well as specificity for the *in vitro* target, and imaging feasibility and accumulation at the target site *in vivo,* within the scope of this thesis.

5.1.1 Cellular Interaction of Non-targeted Molecular Probes

In order to assess the contribution of non-specific uptake by inflammatory cells, we evaluated how cells interact with non-target contrast agents with different physical properties. In **study I**, three different types of MBs were evaluated. The cellular interaction of plain PVA MBs and two types of MBs (types A and B) with SPIONs was evaluated by light microscopy and confocal laser scanning microscopy (CLSM). Uptake or adhesion of these 3-μm MBs seemed to be driven by phagocytosis in RAW264.7 macrophages or low, non-specific weak adherence to MyEnd$^{+/+}$ endothelial cells. Particles larger than 0.5 μm have been known to enter phagocytic cells via phagocytic pathways (Champion et al. 2008; Oh et al. 2014). However, non-specific uptake via pinocytosis is also a possible route of uptake into the cells. The engulfment pattern of the RAW264.7 macrophages was different between the plain, type A and type B MBs. We found that SPION-FITC-labeled type A MBs were already localized inside RAW264.7 macrophages after 30 min, and the uptake by macrophages increased 10-fold after 2 h of incubation with the cells, **Figure 5.1**. Observational and quantitative data obtained using CLSM showed that macrophages favored uptake of type A MBs externally coated with SPIONs over uptake of type B MBs with the SPIONs embedded inside the polymer shell. These results are in line with other published data which have shown that the coating of nanoparticles, is an important strategy for increasing biocompatibility and circulation time and for minimizing rapid clearance by immune cells in the bloodstream (Shi et al. 2009; Singh et al. 2010; Sosale et al. 2015). The plain PVA MBs that were not associated with SPIONs showed the lowest uptake by the macrophages. They were first observed in the macrophages only after 6 h of incubation, but no adherence or uptake was observed in endothelial cells. Several factors are known to influence the uptake of MBs by phagocytic cells such as macrophages and other immune cells. MBs with SPIONs on their external surface might induce immunogenic responses and are therefore cleared faster (Singh et al. 2010; Sosale et al. 2015), so the presence

of the nanoparticle on the surface might be an influential factor. Other factors that influence the pattern of uptake might be the surface shape, size, and net charge of the particle (Xiao et al. 2011).

In **study II**, we used a polymeric streptavidin-coated MB with SPIONs embedded in the shell, and in accordance with the discussion above, we found a low level of engulfment or adherence of non-target multimodal MBs to macrophages or endothelial cells. The evaluation of cellular uptake was conducted with flow cytometry and CLSM under *in vitro* conditions. Molecular probes, such as MBs, are known to acquire a "protein corona" after exposure to serum, which is primarily composed of albumin (Mahmoudi et al. 2011; Wan et al. 2016), a known suppressor of phagocytic uptake; this is probably why these MBs are less prone to phagocytosis under *in vivo* conditions. However, hypothetically, this would also affect the probability of the probes reaching their target site. Targeting strategies that employ antibodies or peptides have been shown to improve the specificity of and to increase the accumulation of molecular imaging probes at the target site (Kaufmann et al. 2007a; Kaufmann et al. 2007b; Kiessling et al. 2014; Klibanov et al. 2006). Such strategies are important for signal generation in imaging applications.

In **study III** and **IV**, we evaluated a considerably smaller type of molecular probe that was in the nanosize range (4–10 nm) and consisting of modified HSA. Coupling to biomacromolecule carriers is a strategy utilized to increase the circulation half-life of molecular probes, so as to increase their chances of reaching the target site (Sleep et al. 2013; Zhang et al. 2018). Cellular adhesion or uptake of non-targeted probes by macrophages was low or absent in the *in vitro* study. These results are consistent in flow cytometry, fluorescence microscopy and CLSM (**study III**).

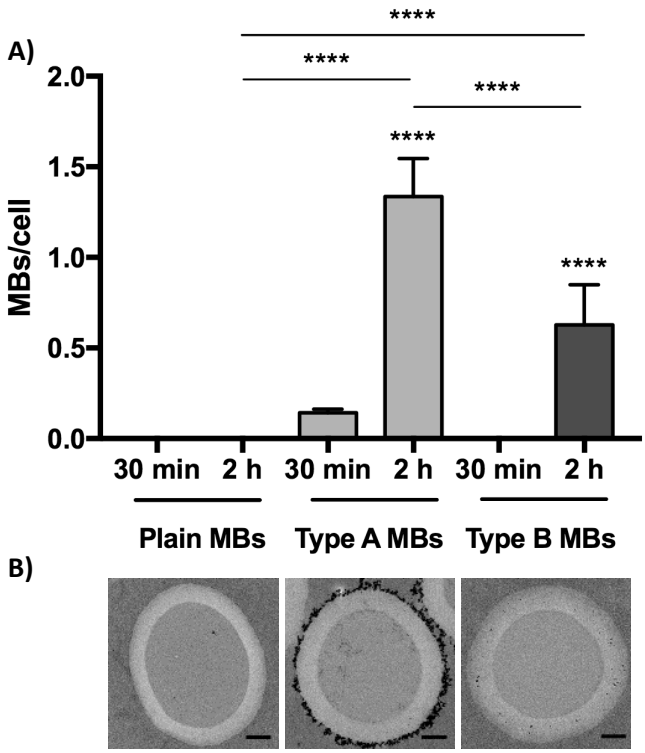

Figure 5.1: Results from study I, showing (A) Uptake counted as MBs per cell of plain, types A and B MBs by macrophages after 30 min and 2 h incubation. The uptake of MBs by macrophages was monitored in transmission mode, and the FITC-labeled MBs were visualized by laser excitation at 488 nm by confocal laser scanning microscopy (CLSM). MBs and cells were quantified by counting in five to nine random regions-of-interest (ROIs) per sample. To discriminate between internalized and extracellular MBs, the MB suspension was replaced by Trypan Blue resulting in the quenching of external MBs, but not internalized MBs. In each ROI 50–300 cells were counted. Bars represent the mean and SD. Statistical significance was determined with ANOVA and Tukey´s post hoc test, **** $P<0.0001$. (B) Transmission electron microscopy images of the three different types of MBs; plain MBs; type A MBs; and type B MBs. Scale bar represents 500 nm.

5.1.2 Cellular Interaction of the Targeted Molecular Probes

In molecular imaging, the targeting specificity can be increased by functionalizing probes with antibodies, peptides or other chemical modifications. This will result in the accumulation of the probes at the target site and improved signal for imaging. In **study II**, **III**, and **IV**, we evaluated the specificity of our probes for targeting markers upregulated in inflammation and in atherosclerotic lesions.

5.1.2.1 Microbubbles

In **study II**, the MBs were further functionalized, within the scope of the European Commission's 3MiCRON project, to improve their multimodal as well as targeting properties. The targeting properties of these novel MBs were evaluated for the first time, within the scope

of this thesis. We found that the labeling of streptavidin-coated MBs with biotinylated antibodies was feasible and resulted in high surface density (it was indicated that 47% of the MB surface area was covered by antibodies, corresponding to 4900 antibodies/μm^2). Interestingly, these MBs might be coupled to other biotinylated antibodies or peptides to target other disease-specific markers.

Antibody–antigen interactions are of a reversible non-covalent nature, as they involve electrostatic forces, van der Waals forces, hydrogen bonds, and hydrophobic interactions. Labeling with monoclonal antibodies would potentially increase target specificity and target affinity, which is considered as the strength of the interaction between an epitope and an antibody's antigen-binding site. Monoclonal antibodies were coupled to MBs in **study II** to target adhesion molecules expressed by endothelial cells and peritoneal macrophages. We found that adhesion to the activated endothelium was increased up to 6-fold in HUVECs and up to 12-fold in mouse aortic endothelial cells as compared to non-targeted MBs (Figure 2, **study II**). Further, evaluation of the MBs by flow cytometry and CLSM was facilitated by the physical properties of the shell-fluorescent layer. MBs labeled with monoclonal antibodies recognized their target antigens under both static (Figure 4, **study II**) and flow conditions (Figure 5 and 6, **study II**), with both immobilized antigens and free antigens contained in a single cell suspension (Figure 2 and 3, **study II**). Highlights from CLSM and flow cytometry results of VCAM-1 labeled MBs are shown in **Figure 5.2**. The overall strength of the antibody–antigen complex, referred to as "avidity," was improved by Ab-labeled MBs as compared to the non-targeted MBs or the isotype controls, as demonstrated by the almost complete clearance of non-specifically bound MBs after the application of high shear stress-pulse in an *in vitro* flow set up in **study II**.

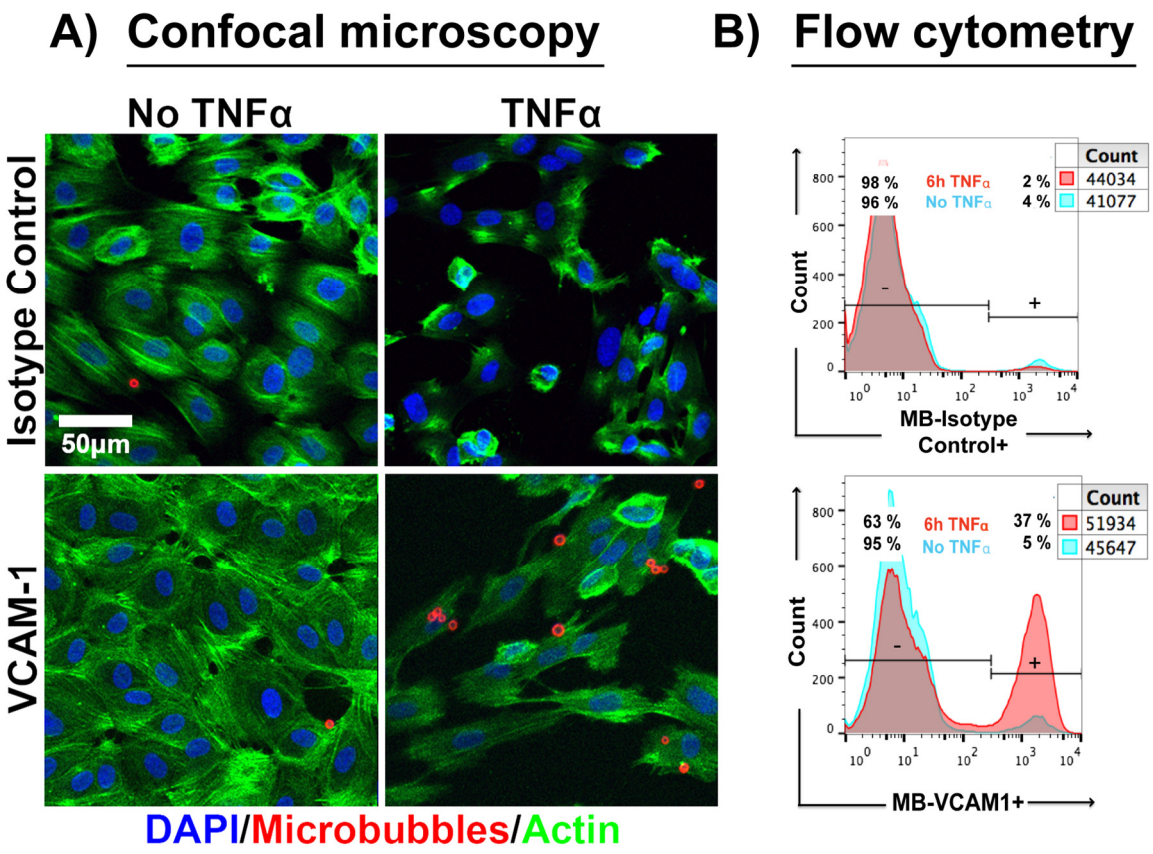

Figure 5.2: Results from study II, showing (A) Confocal laser scanning microscopy (CLSM) Z-stack images showing HUVECs with attached anti-VCAM1 MBs, and low or no adherence of isotype-control-MBs after flow. Images were acquired after 2 min continuous flow at 2 dyn cm^{-2} followed by wash and a 20 dyn cm^{-2} pulse. Blue staining represents DAPI staining of cell nuclei; red represents Cy3 antibody-labeled MBs; green represents Alexa Fluor 488-phalloidin staining of actin. (B) Flow cytometry analysis of anti-VCAM-1-MBs and isotype-control-MBs incubated with HUVECs in cell suspension under continuous agitation for 1h. Histograms showing increased binding of anti-VCAM-1-MBs to cytokine-treated cells; measured as % Cy3 positive cell.

5.1.2.2 Modified HSA Probes

In addition to the polymeric non-targeted and targeted MBs used in **study I** and **II**, chemical modification of the biomacromolecule HSA was utilized for targeting macrophages in **study III** and **IV**. We hypothesized that modified HSA can be taken up by macrophages in atherosclerotic lesions, and serve as probes for molecular imaging. Mal-BSA is a known ligand of SR-A1, and it has been extensively studied under *in vitro* and *in vivo* conditions in relation to atherosclerosis (Ben et al. 2015; Goldstein et al. 1979; Greaves et al. 2009; Haberland et al. 1986a; Haberland et al. 1986b). Recently, radiolabeled Mal-BSA has been proposed as a possible radiotracer for the imaging of vascular inflammation in atherosclerosis. However, only proof-of-concept studies have been conducted in a small number of *Apoe*$^{-/-}$ mice (n = 3) at 13 weeks of age (Jarrett et al. 2010).

Here, we hypothesized that HSA would be more suitable for human application, and investigated aconityl (Aco) as an alternative chemical modification in addition to maleyl for cellular uptake routes and evaluation of specificity *in vitro* in **study III**. The modified HSA probes Mal-HSA and Aco-HSA were successfully labeled with FITC or ^{89}Zr via a DFO chelator. The signaling agents enabled further investigation with flow cytometry, CLSM, real-time microscopy and gamma counter measurements. An increase of several folds in the cellular uptake of these probes was found in comparison to non-modified HSA. The uptake was dependent on the concentration of the probes, and the time of incubation. The uptake mechanism of these molecular probes was mediated primarily via SR-A1 receptor-mediated endocytosis, as demonstrated by silencing, blocking and competition studies as well as co-staining with lysosomal markers, **Figure 5.3** (Figures 4, 8, 5 and 2 respectively, **study III**). Our findings were in line with previously published data on maleylated probes (Gustafsson et al. 2015; Gustafsson et al. 2006; Haberland et al. 1986b; Jarrett et al. 2010; Zhang et al. 2018). The receptors CD36 and LOX-1 had no or little contribution to receptor-mediated uptake when they were silenced. Further, maleyl is covalently bound to HSA, where MalA reacts with an amine group on HSA to result in the formation of an amide bond. The interaction of Mal-HSA with SR-A1 most probably involves several types of non-covalent interactions that are similar to antibody–antigen interactions.

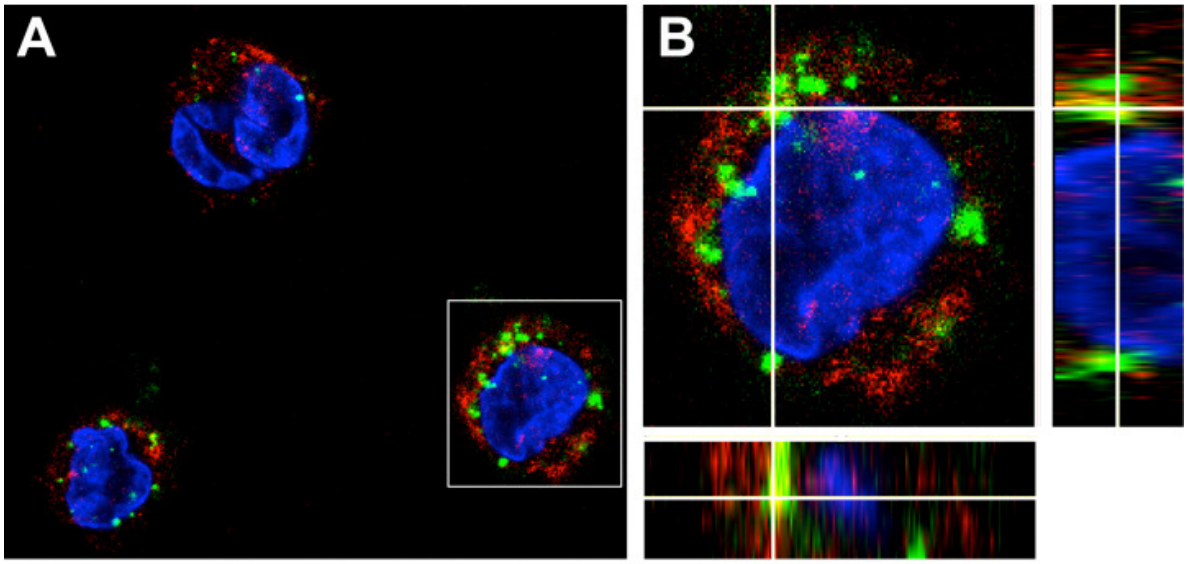

Figure 5.3: Results from study III, showing (A) Confocal laser scanning microscopy (CLSM) Z-stack image of THP-1 macrophages with internalized Mal-HSA-FITC probes (green). (B) Images of orthogonal views with white cross indicating co-localized (yellow) Mal-HSA-FITC probe (green) and LAMP2 lysosome staining (red-Alexa Fluor 568) shown in the merged image. DAPI cell nuclei staining (blue).

Mal-HSA was shown to be primarily recognized by differentiated THP-1 cells and subsets of polarized primary human macrophages, preferably M0 and M2 polarized macrophages, under *in vitro* conditions (Figure 1,3 and 7, **study III**). However, no or little uptake of Mal-HSA by HUVECs or human carotid SMCs was observed (Figure 9, **study III**). The results for FITC-labeled modified HSA probes were consistent with those of flow cytometry and CLSM. The results for ^{89}Zr-labeled probes were also in line with those for FITC-labeled probes. In summary, both types of modified HSA probes (Mal-HSA and Aco-HSA) showed specific recognition of SR-A1 primarily on macrophages. This encouraged us to investigate the imaging feasibility of our probe as a potential PET radiotracer for the targeting of macrophages and atherosclerotic plaques *in vivo.*

5.1.3 In Vivo SPECT/CT Hybrid Imaging of Inflammation with Targeted Anti-ICAM-1-labeled MBs

To evaluate the feasibility of nuclear imaging with targeted multimodal MBs, a model of rat peritonitis was utilized to increase macrophage infiltration and expression of ICAM-1. MBs were successfully labeled with ^{99m}Tc and further conjugated to anti-ICAM-1 antibodies. A detectable two-fold increase in the radiotracer signal was observed in the peritoneal cavity of rats with induced peritonitis as compared to the control rats (Figure 8 and 9, **study II**).

5.1.4 In Vivo PET/MR Fusion Imaging of Inflammation in Atherosclerosis

To our knowledge, no large-scale *in vivo* imaging studies have yet been performed with ^{89}Zr-radiolabeled Mal-HSA probes targeting macrophages in inflamed atherosclerotic lesions. Small-scale proof-of-concept studies with ^{64}Cu-radiolabeled Mal-BSA have been attempted through Jarrett et al. (Jarrett et al. 2010). In order to evaluate the feasibility of using the radiotracer ^{89}Zr-Mal-HSA for targeting atherosclerotic plaques in *Apoe*$^{-/-}$ mice, we conducted *in vivo* PET/MR imaging studies, as well as *ex vivo* studies with non-targeted ^{89}Zr-HSA and wild-type mice (C57BL/6) for comparison. In summary, *in vivo* PET/MRI of the atherosclerotic aortic arch showed a 26% increase in SUV_{max} and a 19% increase in TBR_{max} in *Apoe*$^{-/-}$ mice at 16 weeks of age as compared to age and diet-matched wild-type mice. Representative PET/MRI and MR images are shown in **Figure 5.4**. The *ex vivo* quantitative analysis corroborated the *in vivo* PET measurements, and showed significant accumulation of the specific radiotracer at target sites with the gamma counter; and similar findings were obtained with PI-ARG of excised atherosclerotic aortas in the *Apoe*$^{-/-}$ mice as compared to the control animals. An example of the PI-ARG measurements in an *Apoe*$^{-/-}$ mouse is shown in **Figure 5.5**. The ^{89}Zr-Mal-HSA radiotracer signal was found in CD68-stained aortic root

sections of *Apoe*$^{-/-}$ mice, but the signal was absent in wild-type mice without macrophage staining (indicated by CD68). In contrast, no detectable differences were found between the wild-type mice and *Apoe*$^{-/-}$ mice for the radiotracer ^{18}F-FDG in our experimental set-up. This could partly have been the result of a suboptimal imaging time point after the ^{18}F-FDG injection. Improved vascular imaging has been reported at 90–180 min after injection of ^{18}F-FDG (Bucerius et al. 2014). Further, Blomberg et al. showed that quantification was improved, as indicated by higher TBRs, when atherosclerotic plaque inflammation was imaged at 180 min as compared to 90 min after injection of ^{18}F-FDG (Blomberg et al. 2014a); however, such improvement was not observed in the quantification of vascular calcification metabolism (Blomberg et al. 2014b).

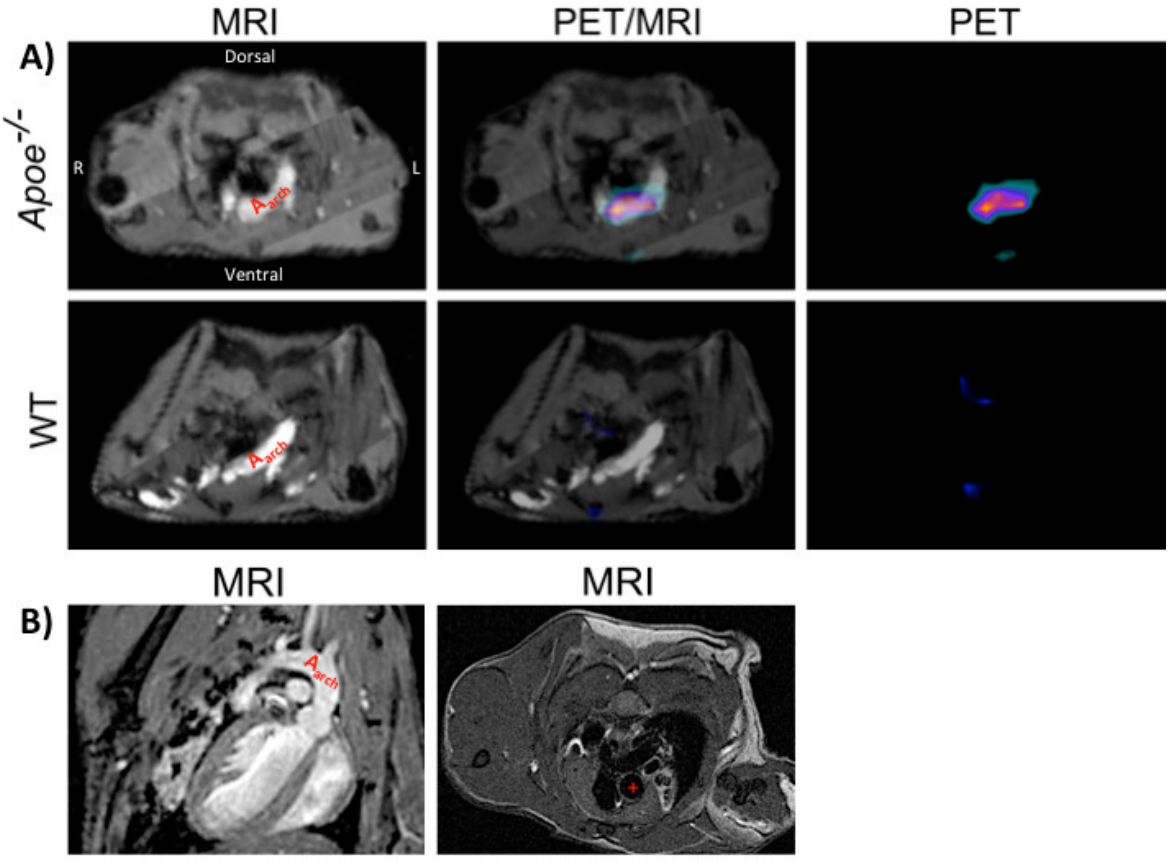

Figure 5.4: Results from study IV, showing (A) Molecular imaging of aortic arch by ^{89}Zr-Mal-HSA. Images (transverse plane) from 9.4 T MRI (left panel) and the 1 h dynamic MicroPET scan (right panel) are fused (middle panel). Images show accumulation of radiotracer signal from atherosclerotic aortic arch (A_{arch}) in the *Apoe*$^{-/-}$ mouse, and void of the signal in the wild type (WT) mouse. Image data were processed using MicroPET manager and evaluated using the Inveon Research Workplace (IRW) software (Siemens Medical Systems). (B) 9.4 T MRI in *Apoe*$^{-/-}$ mouse utilizing the phenomenon of flow to give rise to different image appearances. Bright blood image (coronal plane) of the A_{arch} and branches with gradient echo sequence (left panel), and black blood image (transverse plane) of aortic root, indicated by the red cross, with spin echo sequence (right panel).

Blomberg et al. (2014) suggested that the SUV_{max} of the carotid plaque is the most reliable surrogate for plaque vulnerability. However, in another study published by Niccoli Asabella et al., the authors argued that the maximum and mean TBR values are more reliable than SUV for identifying inflamed plaques (Niccoli Asabella et al. 2014). Hence, there is some controversy about these measures, and we have therefore reported both the SUVs and TBRs in **study IV**.

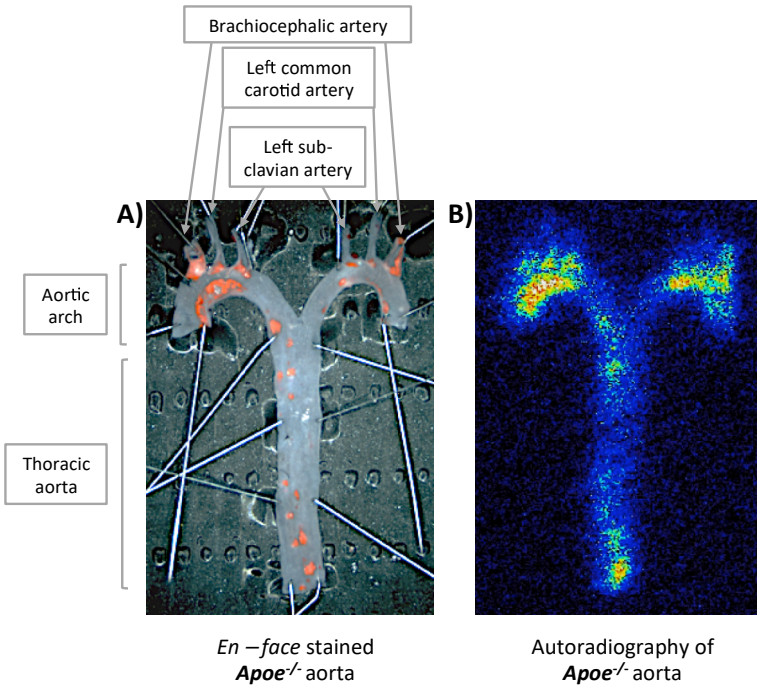

Figure 5.5: Results from study IV, showing aortic arch with branches and thoracic aorta from *Apoe*$^{-/-}$ mouse. (A) Excised aorta, cut open and *en face* stained with Sudan IV (red color). (B) Corresponding phosphor imaging autoradiography of ^{89}Zr-Mal-HSA shows radiotracer signal in plaque area identified by *en face* staining.

5.2 Strengths and Limitations

- *Nomenclature*: Specificity and sensitivity are important concepts in diagnostic measurements, but the terminology is utilized differently according to the purpose of the study in question. In the case of diagnostic tests, specificity is defined as the ability of the test to correctly exclude individuals who do not have a given disease, and it determines the rate of true negative results. Diagnostic sensitivity is the ability of a test to correctly identify people who have a given disease, and it determines the rate of true positive results. Ideally, diagnostic tests should have 100% sensitivity and 100% specificity, but this is rarely the case. In molecular imaging, the term "sensitivity" is utilized in relation to the detection limit: that is, it is the minimum amount of radiotracer

required to provide a detectable signal, which is in the picomolar range in the case of PET. Specificity is determined by factors such as probe specificity for the target and CNR, among others. An understanding of these concepts is important for the development of probes for diagnostic molecular imaging. Within the scope of this thesis, we can conclude that probes functionalized with antibodies or chemically modified probes showed specificity for the target, as well as increased adherence or uptake by cells as compared to non-targeted molecular probes. These results were consistent across several different fluorescence techniques performed *in vitro*. Further, when these molecular probes were radiolabeled, they provided detectable signals on SPECT and PET; this could mean that they have the potential to improve diagnostic accuracy and precision. However, there are some limitations that need to be addressed for the sake of future improvement.

- *Toxicity studies*: No toxicity studies, *in vitro* or *in vivo*, were performed. Cells were evaluated visually by microscopy, and the expression of classical markers as well as live/dead staining was evaluated by flow cytometry. However, a low toxicity profile was assumed in the case of the utilized HSA-modified probes, as a similar BSA-based maleylated probe showed low toxicity profiles in fibroblasts (Gustafsson et al. 2006). Nonetheless, a thorough investigation of the toxicity profiles and *in vivo* stability must be conducted before any clinical experiments can be undertaken.
- *Power calculation*: No power analysis was done to determine the minimal sample size for the animal experiments in **study II** and **IV**, although pilot studies were conducted prior to the imaging studies in **study IV**.
- *Ex vivo evaluation*: In **study II**, *ex vivo* evaluation of the injected ^{99m}Tc-labeled *anti*-ICAM-1-labeled MBs was not performed, for example, by isolating peritoneal macrophages for flow cytometry evaluation or gamma counter measurements. In addition, it would have been interesting to compare the imaging findings with non-targeted MBs for the evaluation of *in vivo* target specificity.
- *Fusion imaging*: In **study IV**, the major drawback was the non-simultaneous PET-MRI imaging. The fusion of both imaging modalities was challenging, and a mis-match in image alignment that affected the data analysis might have been possible. Moreover, misinterpretations of the signal source on account of a partial volume effect might have occurred, as a result of which the PET signal may have been under- or over-estimated. This is of crucial importance in the imaging of small structures such as atherosclerotic plaques. However, imaging with a 9.4 T MR scanner allowed us to obtain detailed

images of the aortic arch with high spatial resolution and acceptable SNR. Moreover, the *ex vivo* evaluations supported the *in vivo* PET findings and validated the *in vivo* quantifications.

- *Comparison with ^{18}F-FDG*: In **study IV**, the time protocols for FDG imaging might have contributed to low TBRs, possibly due to a high signal and spill-over effect of the surrounding myocardium, and hence, led to underestimation of the PET signal. No head-to-head comparison with the same radionuclide was performed. It might have been possible to compare Mal-HSA and FDG by coupling ^{18}F to Mal-HSA or, theoretically, ^{89}Zr to FDG, but that would not have been feasible. Not utilizing the advantage of the long half-life of ^{89}Zr would have limited the *ex vivo* evaluation due to rapid decay of ^{18}F.
- *Off-target distribution*: In biodistribution studies, high-intensity liver signals were observed. This could be partly explained by SR-A1 expression by the liver sinusoidal cells, but it might also be a result of non-specific clearing mechanisms by the liver, a common challenge for all intravenously injected compounds in the body. The blocking experiments in **study IV** showed a clear decrease in the liver uptake with a resulting increase in the aortic uptake. The challenge for the future would be to decrease the liver uptake/clearance of these probes. Unlike ^{18}F-FDG, which is known to be taken up by metabolically active cells and tissues and therefore influenced by the metabolic state, ^{89}Zr-Mal-HSA would not present this problem to the same extent.
- *Radiotracer signal and macrophage content:* The macrophage content was not determined in **study IV**, so it was not possible to correlate macrophage accumulation to the radiotracer signal. This could be performed by digital quantification of immunohistochemistry CD68-positive staining in aortic root sections and coregistration with the radiotracer signal on PI-ARG images.
- *Spatial resolution:* Spatial resolution is a limitation in studies on small structures. In our setting, spatial resolution was affected by several factors, one of which was the spatial resolution of the SPECT or PET scanner. The μPET in our setting has an inner spatial resolution of approximately 1.2 mm, and SPECT, <8 mm. When small structures such as atherosclerotic lesions in mouse aorta, 1 mm (average) in diameter, are imaged, the positron range will also determine the diagnostic precision or accuracy of the source signal. Although ^{89}Zr is classified as a short-range positron emitter, it has a longer average positron range than ^{18}F: ^{18}F = 0.6 (max, 2.4) mm, ^{89}Zr = 1.3 (max, 3.8)

mm (Conti et al. 2016). The positron range also influences the overall spatial resolution in PET imaging.

- *Choice of radioisotope:* We obtained a stable signal already at 1 h after injection of the tracer; therefore, we concluded that the long half-life of ^{89}Zr is not necessary for imaging evaluation of only the initial probe uptake. However, from a preclinical perspective, it is more feasible to use radionuclides with a longer half-life than ^{18}F to enable excessive *ex vivo* evaluation. Another more suitable radionuclide would have been ^{64}Cu, but it is difficult to obtain this radionuclide within Europe.
- *Disease model*: We tried to select optimal disease models for testing the molecular probes of this thesis project. However, no single animal model ideally reflects the complexity of the human disease condition. The pharmacokinetic data obtained from animal models cannot be directly translated into humans, but at the least, they provide valuable indications for future improvements.

5.3 Concluding Remarks on the Development of Molecular Probes for Multimodal Imaging

Polymer-based molecular probes, which were examined in **study I** and **II**, have several advantages over the commercially available lipid-shelled MBs that are currently used for CEUS imaging. The differences were recently reviewed (Hernot et al. 2008; Lentacker 2009): polymer-based MBs are more stable and have a longer shelf- and circulation half-life; however, both lipid-based and polymer-based MBs can be functionalized for targeting purposes and drug loaded for therapeutic purposes. The acoustic, magnetic and imaging properties of MBs in **study I** and **II** have been evaluated previously (Barrefelt et al. 2013a; Barrefelt et al. 2013b; Brismar et al. 2012; Cavalieri et al. 2005; Grishenkov et al. 2009; Poehlmann et al. 2014; Sciallero et al. 2016; Sciallero et al. 2013; Yang et al. 2008).

Similar approaches with dual targeting of US and MRI have been described in the literature (Park et al. 2010; Yang et al. 2008). The dual-targeting MB assessed in **study I** might be more relevant for clinical translation if targeting can be improved by further functionalization of the shell, preferably by utilizing the type B MB with SPIONs physically embedded in the shell to minimize non-specific uptake by phagocytic cells. The multimodal MB theoretically allows several imaging applications and evaluation through both *in vitro* fluorescent applications and *in vivo* imaging applications. The multimodal MBs utilized in **study II** were too stiff to have the optimal acoustic US properties due to their multi-layer

structure. However, they might still be applicable from the nuclear imaging perspective or for potential drug loading in a preclinical setting. We can conclude that the multimodal MBs utilized in **study II** serves as a prototype and is less likely to have any clinical potential; moreover, the excessive multimodal approach might be more relevant for pre-clinical evaluation of disease-specific markers.

In **study III** and **IV**, we investigated the targeting and imaging properties of modified HSA-based molecular probes. Biomacromolecule carriers such as albumin have proven to be beneficial for decreasing toxicity, increasing specificity and *in vivo* stability as well as prolonging circulation half-life, and might therefore show some promise for the development of clinical radiotracers in molecular imaging (Sleep et al. 2013; Zhang et al. 2018). However, the half-life of diagnostic molecular probes also depends on the endogenous clearance of the probe itself and the impact that the coupling of the probe has on the interaction of the albumin portion with FcRn, as this can affect the re-circulation of albumin. For instance, conformationally modified albumins are cleared more rapidly through the gp18/gp30 system than native albumin (Sleep et al. 2013).

Possible conformational changes during chemical reactions of the targeting moiety of the probe must be taken into consideration, as this might affect the targeting specificity. Another important factor is also the host system employed to study the pharmacokinetic profiles of the albumin−probe complex. In our case, we used rodent models, and therefore, cross-species binding of albumin might differ between endogenous and exogenous albumin (Cao et al. 2015; Mathias et al. 1995). Andersen et al. showed that HSA bound weakly to mouse FcRn, while mouse albumin bound with a 10-fold higher affinity, which means that human albumin is re-circulated to a lesser extent than mouse albumin in the mouse model (Andersen et al. 2010). Human FcRn is selective in that it only binds IgG from a limited number of species (human, bovine and rabbit) (Ober et al. 2001). Despite their differences, both human and bovine albumin are utilized as carriers for molecular probes.

The HSA-based imaging probes were recently reviewed (Cao et al. 2015), as were their therapeutic applications (Lee et al. 2015; Zhang et al. 2018). In the case of the HSA-based targeting probes, their clinical application is dependent on manufacturing processes for purity and the cost aspect. The modified HSA probes employed in **study III** and **IV** have potential for hybrid imaging with PET/MRI, as was previously demonstrated by Jarret et al. with Mal-BSA (Jarrett et al. 2010; Jarrett et al. 2008). With HSA as a carrier, it is possible to combine imaging techniques such as SPECT, PET and MRI. Multimodal molecular imaging in cardiovascular diseases based on nanoprobes conjugated to PET signaling agents was recently

reviewed by (Tu et al. 2018). Thus, all the studies so far indicate that HSA is an excellent platform for molecular imaging probes and multimodal strategies.

5.4 The Future of Molecular Imaging of Atherosclerosis

The molecular imaging field has evolved rapidly in the last decade. The technical challenges of vascular imaging will require further optimization to improve spatial resolution. With new improved dual-imaging approaches, such as US/MRI or PET/MRI, different components of plaques can be imaged at the molecular and cellular level. Imaging of inflammation in atherosclerosis could help monitor disease progression and shed light on the suitability of therapeutic interventions such as newly developed anti-inflammatory drugs. This can also create a need for more specific probes in clinical applications. With regard to radiotracer developments, the cornerstone of all molecular imaging probes is non-toxicity, *in vivo* stability and sufficient circulation half-life to enable accumulation at the target site. Furthermore, the major challenges in the future for the development of molecular imaging probes would be to optimize their biodistribution and pharmacokinetic profiles.

Based on all the new biomarkers identified in atherosclerotic lesions, we could optimize molecular probes so that they target clinically relevant and specific biomarkers, and thereby, improve the precision and accuracy of targeting. In combination with evolving imaging techniques that have improved spatial and temporal resolution, more detailed information about plaque vulnerability could be obtained. In the future, the development of molecular imaging probes will most probably focus on theranostics approaches and combine diagnostic imaging with direct and local treatment at the target site.

6 SUMMARY AND CONCLUSIONS

A total of seven different imaging probes were evaluated in this thesis for the targeting of inflammatory markers on endothelial cells and macrophages: four MB-based molecular probes and three HSA-based molecular probes.

The specific conclusions of the thesis are as follows:

I. SPION modifications of MBs increased cellular uptake by macrophages.

II. Monoclonal antibody labeling of our novel MBs was feasible and demonstrated improved target specificity to adhesion molecules in both static and flow set-ups *in vitro.* ^{99m}Tc-labeled *anti*-ICAM-1-MBs showed detectable signal in the inflamed peritoneal area of the rat model *in vivo.*

III. The uptake of Mal-HSA and Aco-HSA is primarily receptor-mediated through specific binding to SR-A1 on macrophages. Differentiated and polarized macrophages recognized the Mal-HSA probe.

IV. ^{89}Zr-radiolabeling of Mal-HSA probes resulted in detectable signals in atherosclerotic lesions in *Apoe*$^{-/-}$ mice, as demonstrated by PET/MRI. The findings were corroborated by *ex vivo* quantitative measurements with gamma counter and phosphor imaging autoradiography.

7 ACKNOWLEDGEMENTS

I feel truly honored and humbled by the fact that I have had the opportunity to dive into research and pursue a PhD. The studies in this thesis were conducted between the years 2012-2018 at Karolinska Institutet. During these years I got the chance to meet so many fantastic and inspiring people, and I would like to take this chance to thank them.

Thank you **Kenneth Caidahl** for giving me this opportunity and believing in me. I came to you as a medical student to pursue my dream of combining research with my clinical career, and I have learnt so much from you since then. I have never seen someone so dedicated to his work as you are, and also so willing to help people around you, this has truly inspired me to work harder. As a professor you have taught me valuable things about research that I will cherish for life.

Björn Gustafsson, if anyone deserves a medal it's you. This work wouldn't have been possible without you. Thanks for all your support and hard work together during these years. Thanks for teaching me about chemistry and always trying your best to help. We have had so much fun during these years, not only in the lab but also outside together with your beautiful family.

Ulf Hedin, you always ask the most interesting questions about science and challenge my way of thinking. The collaboratory work of both your lab and Kenneth's group established the foundation of this work, and enabled the research in this thesis to be conducted. Thanks for welcoming me into your lab, and for all the great scientific discussions.

Silvia Aldi, I have learned so much about molecular biology from you. Your research accuracy has taught me so much about reproducibility in research. You have not only been my co-supervisor, but also my friend.

Stina Salomonsson, the best mentor ever! Where do I begin. You were my supervisor during my medical degree project when I studied medicine, and some way along the road we became friends and now you are like a big sister to me. Thank you for your love and support and all the pep talks!

Thanks to all the wonderful people in **Ulf Hedin's group**. I would like to acknowledge some of the people who have had an impact on me during my PhD. Thank you **Ljubica Matic** for the vigorous discussions and fun times at conferences. A special thanks to **Anton Razuvaev** and **Joy Roy** for your inspiring ways and hospitality. The way you all welcome your students, involving them in every aspects of science, including teaching, and making them a part of your team and family is truly inspiring. **Mette**, thank you for teaching me important aspects of immunohistochemistry. **Malin** and **Siw**, thanks for all the delicious fika! I would also like to acknowledge all the former colleagues in the group.

To all my fellow PhD students; thanks for making my time worthwhile, and for all the fun experiences together, both in Sweden and abroad. I would also like to mention **Oskar Kövamees** and **Philip Tannenberg**; who both successfully have entered life post thesis defense. A special thanks to the PhD team; **Bianca Suur**, **Moritz Lindquist Liljeqvist**, **Samuel Röhl**, **Antti Siika**, **Urszula Rykaczewska**, **Till Seime**, **Marko Bogdanovic**, **Olga**

Nilsson and **Ali Mahdi**. You all made it worth to come to work every day. I am looking forward to following your future careers in research, just keep going, you guys rock!

Peter Damberg, thanks for answering all my questions about MR physics and being so helpful and solution oriented, you have been a great collaborator!

Dianna Bone, thanks for being my go-to genius and always solving complicated problems in the most creative ways. **Maria Eriksson**, thanks for your positive support of my research.

To all my fellow co-authors and collaborators, thank you for all your effort and scientific discussions. You have truly given me perspective on science and new insights. Thanks to all the collaborators within the **3MiCRON project**, and in particular **Gaio Paradossi**, **Barbara Cerroni**, **Lars Dähne** and **Gabriella Egri**, who produced the microbubbles for study I-II. I would also like to thank all the collaborators in study IV; **Staffan Holmin** and his group; **Thuy Tran**; **Tetyana Tegnebratt**, and **Li Lu**; as well as **Per Eriksson**, **Nancy Simon**, **Anton Gisterå**, and **Laura Tarnawski** for your great effort and scientific contribution. Thanks also to all the wonderful people at **KERIC**.

I want to especially acknowledge **Roland Baumgartner, Anton Gisterå** and **Philip Dusart**; thanks for being such awesome collaborators. Roland you truly inspire me to become a better researcher and challenge me in research discussions. Anton thanks for all the interesting scientific discussions about atherosclerosis. Thank you Philip for all your effort and teaching me how to improve my image analysis skills! Thank you all for being so enthusiastic about research, that really encouraged me to move forward.

To all my fellow research colleagues; **Daniel Ketelhuth**, **Hong Jin**, **Sanna Hellberg**, **and Marita Wallin**, you have been great additional support for me during these years, and I really am thankful that I got the opportunity to work with all of you!

All my wonderful colleagues at the **Department of Clinical Physiology,** the **Functional area of Emergency Care**, and the **Department of Cardiology**, for making my time spent there such a pleasure.

To all the scientists out in the world who have inspired me to become a better scientist, and to keep searching for answers to make our world a little bit better together. I would like to mention some of the people who have really contributed to the research field of molecular imaging; **Jonathan Lindner**, **Alexander Klibanov**, **Karen Briley-Saebo** and **James Rudd**. You inspire young scientists like me to keep going!

To all my fellow **union colleagues**; the Swedish Junior Doctors Association (SYLF) Stockholm, and the Swedish Medical Association; it has been a pleasure to work with you towards a common goal. I have learnt so much during these years and it has been a rewarding environment. Thanks for giving me perspective on important questions and teaching me so many important things about how to make a change and why!

I want to thank all my wonderful friends who have supported me throughout medical school, as well as during my PhD. There are so many I would like to thank personally for being so awesome and inspiring, but there are a few that I truly would like to acknowledge that have

been important throughout this journey. **Anna Gibbs**, **Katrin Habir**, **Madeleine Liljegren**, **Karin Ljung**, you guys have been such an amazing support and continuously encourage me to reach higher. Thanks for all the laughter and important lessons about life. Thanks also to my closest gems **Emma Bergner** and **Johanna Hanson**, and for your patience! You guys are truly amazing; you have given me so much love and support throughout this whole process, and also throughout the roller-coaster that we call life. I am most grateful for having you all in my life.

Benita and **Frank**; thanks for all the love and support and for being the most welcoming people, you guys are the best parents-in-law, I love you!

Samy, Samsam, I can´t describe in words what you mean to me. When did you grow up all of a sudden? Now you are teaching me lessons about life. From the bottom of my heart I love you little brother.

The reason for my existence, **Mom** and **Dad**, thank you both for your unconditional love and support, regardless of my performances. You have always been my number one go-to persons through the challenging path in life. You have made me the person I am today, thanks to you I am a strong independent woman. You never stopped believing in me, and even if I think that you sometimes are "over-believing" in my research abilities that I would someday win the Nobel Prize, but I love you for that mama and I will never stop trying to pursue my dreams thanks to you. I know baba would be proud and he certainly taught me that nothing in life comes easy and I should not be afraid to work hard to achieve my goals and to never settle for the easy way out. Life is beautiful because I got to share it with you <3

Last but absolutely not least, my soulmate, my husband, my number one critic but also my number one supporter, together you make everything feel possible. **Alexander** you've stood by me through the darkest times in my life but also through the most joyful. You inspire me with your work ethics, discipline and your humble ways. Thanks for cooking me dinner and taking care of me unconditionally. I don't think that a day has passed by since we met without you telling me how beautiful I am or making me laugh, even when I feel the worst. You truly inspire me to become a better person. With you I want to share every adventure in life, and make new memories! I love you endlessly habibi.

And finally, I dedicate this work to my beloved **mother <3** because I could not ever possibly repay all that you have done and continue to do for me and Samy, you are truly the greatest woman on this earth!

8 REFERENCES

(ESC) ESoC. Clinical Practice Guidelines 2018 [Available from: https://www.escardio.org/Guidelines/Clinical-Practice-Guidelines.

Adan A, Alizada G, Kiraz Y, Baran Y, Nalbant A. Flow cytometry: basic principles and applications. Crit Rev Biotechnol. 2017;37(2):163-76.

Ahn CH, Choi SH. New drugs for treating dyslipidemia: beyond statins. Diabetes Metab J. 2015;39(2):87-94.

Alexander MR, Owens GK. Epigenetic control of smooth muscle cell differentiation and phenotypic switching in vascular development and disease. Annu Rev Physiol. 2012;74:13-40.

Alonso A, Artemis D, Hennerici MG. Molecular imaging of carotid plaque vulnerability. Cerebrovasc Dis. 2015;39(1):5-12.

Amento EP, Ehsani N, Palmer H, Libby P. Cytokines and growth factors positively and negatively regulate interstitial collagen gene expression in human vascular smooth muscle cells. Arterioscler Thromb. 1991;11(5):1223-30.

Amirbekian V, Lipinski MJ, Briley-Saebo KC, et al. Detecting and assessing macrophages in vivo to evaluate atherosclerosis noninvasively using molecular MRI. Proc Natl Acad Sci U S A. 2007;104(3):961-6.

Andersen JT, Daba MB, Berntzen G, Michaelsen TE, Sandlie I. Cross-species binding analyses of mouse and human neonatal Fc receptor show dramatic differences in immunoglobulin G and albumin binding. J Biol Chem. 2010;285(7):4826-36.

Antonov AS, Kolodgie FD, Munn DH, Gerrity RG. Regulation of macrophage foam cell formation by alphaVbeta3 integrin: potential role in human atherosclerosis. Am J Pathol. 2004;165(1):247-58.

Ballotta E, Angelini A, Mazzalai F, Piatto G, Toniato A, Baracchini C. Carotid endarterectomy for symptomatic low-grade carotid stenosis. J Vasc Surg. 2014;59(1):25-31.

Barbier CE, Bjerner T, Johansson L, Lind L, Ahlstrom H. Myocardial scars more frequent than expected: magnetic resonance imaging detects potential risk group. J Am Coll Cardiol. 2006;48(4):765-71.

Barrefelt A, Paradossi G, Asem H, et al. Dynamic MR imaging, biodistribution and pharmacokinetics of polymer shelled microbubbles containing SPION. Nano. 2014;9(6):1-13.

Barrefelt A, Saghafian M, Kuiper R, et al. Biodistribution, kinetics, and biological fate of SPION microbubbles in the rat. Int J Nanomed. 2013a;8:3241-54.

Barrefelt AA, Brismar TB, Egri G, et al. Multimodality imaging using SPECT/CT and MRI and ligand functionalized 99mTc-labeled magnetic microbubbles. EJNMMI Res. 2013b;3(1):12.

Baynes JWD, M. H. Medical Biochemistry. 5th ed: Elsevier; 2018.

Beer AJ, Pelisek J, Heider P, et al. PET/CT imaging of integrin alphavbeta3 expression in human carotid atherosclerosis. JACC Cardiovasc Imaging. 2014;7(2):178-87.

Behm CZ, Kaufmann BA, Carr C, et al. Molecular imaging of endothelial vascular cell adhesion molecule-1 expression and inflammatory cell recruitment during vasculogenesis and ischemia-mediated arteriogenesis. Circulation. 2008;117(22):2902-11.

Ben J, Zhu X, Zhang H, Chen Q. Class A1 scavenger receptors in cardiovascular diseases. Br J Pharmacol. 2015;172(23):5523-30.

Benjamin EJ, Virani SS, Callaway CW, et al. Heart Disease and Stroke Statistics-2018 Update: A Report From the American Heart Association. Circulation. 2018;137(12):e67-e492.

Bennett MR, Sinha S, Owens GK. Vascular Smooth Muscle Cells in Atherosclerosis. Circ Res. 2016;118(4):692-702.

Bettinger T, Bussat P, Tardy I, et al. Ultrasound Molecular Imaging Contrast Agent Binding to Both E- and P-Selectin in Different Species. Investigative Radiology. 2012;47(9):516-23.

Bigalke B, Phinikaridou A, Andia ME, et al. Positron emission tomography/computed tomographic and magnetic resonance imaging in a murine model of progressive atherosclerosis using (64)Cu-labeled glycoprotein VI-Fc. Circ Cardiovasc Imaging. 2013;6(6):957-64.

Binder CJ, Papac-Milicevic N, Witztum JL. Innate sensing of oxidation-specific epitopes in health and disease. Nat Rev Immunol. 2016;16(8):485-97.

Blomberg BA, Thomassen A, Takx RA, et al. Delayed (1)(8)F-fluorodeoxyglucose PET/CT imaging improves quantitation of atherosclerotic plaque inflammation: results from the CAMONA study. J Nucl Cardiol. 2014a;21(3):588-97.

Blomberg BA, Thomassen A, Takx RA, et al. Delayed sodium 18F-fluoride PET/CT imaging does not improve quantification of vascular calcification metabolism: results from the CAMONA study. J Nucl Cardiol. 2014b;21(2):293-304.

Bobryshev YV, Ivanova EA, Chistiakov DA, Nikiforov NG, Orekhov AN. Macrophages and Their Role in Atherosclerosis: Pathophysiology and Transcriptome Analysis. Biomed Res Int. 2016;2016:9582430.

Bot I, Shi GP, Kovanen PT. Mast cells as effectors in atherosclerosis. Arterioscler Thromb Vasc Biol. 2015;35(2):265-71.

Braun A, Trigatti BL, Post MJ, et al. Loss of SR-BI expression leads to the early onset of occlusive atherosclerotic coronary artery disease, spontaneous myocardial infarctions, severe cardiac dysfunction, and premature death in apolipoprotein E-deficient mice. Circ Res. 2002;90(3):270-6.

Brinjikji W, Huston J, 3rd, Rabinstein AA, Kim GM, Lerman A, Lanzino G. Contemporary carotid imaging: from degree of stenosis to plaque vulnerability. J Neurosurg. 2016;124(1):27-42.

Brismar TB, Grishenkov D, Gustafsson B, et al. Magnetite nanoparticles can be coupled to microbubbles to support multimodal imaging. Biomacromolecules. 2012;13(5):1390-9.

Broisat A, Toczek J, Dumas LS, et al. 99mTc-cAbVCAM1-5 imaging is a sensitive and reproducible tool for the detection of inflamed atherosclerotic lesions in mice. J Nucl Med. 2014;55(10):1678-84.

Brown MS, Goldstein JL, Krieger M, Ho YK, Anderson RG. Reversible accumulation of cholesteryl esters in macrophages incubated with acetylated lipoproteins. J Cell Biol. 1979;82(3):597-613.

Bucerius J, Dijkgraaf I, Mottaghy FM, Schurgers LJ. Target identification for the diagnosis and intervention of vulnerable atherosclerotic plaques beyond (18)F-fluorodeoxyglucose positron emission tomography imaging: promising tracers on the horizon. Eur J Nucl Med Mol Imaging. 2019;46(1):251-65.

Bucerius J, Mani V, Moncrieff C, et al. Optimizing 18F-FDG PET/CT imaging

of vessel wall inflammation: the impact of 18F-FDG circulation time, injected dose, uptake parameters, and fasting blood glucose levels. Eur J Nucl Med Mol Imaging. 2014;41(2):369-83.

Bucerius J, Schmaljohann J, Bohm I, et al. Feasibility of 18F-fluoromethylcholine PET/CT for imaging of vessel wall alterations in humans--first results. Eur J Nucl Med Mol Imaging. 2008;35(4):815-20.

Buono C, Come CE, Stavrakis G, Maguire GF, Connelly PW, Lichtman AH. Influence of interferon-gamma on the extent and phenotype of diet-induced atherosclerosis in the LDLR-deficient mouse. Arterioscler Thromb Vasc Biol. 2003;23(3):454-60.

Burtea C, Laurent S, Murariu O, et al. Molecular imaging of alpha v beta3 integrin expression in atherosclerotic plaques with a mimetic of RGD peptide grafted to Gd-DTPA. Cardiovasc Res. 2008;78(1):148-57.

Byun YS, Yang X, Bao W, et al. Oxidized Phospholipids on Apolipoprotein B-100 and Recurrent Ischemic Events Following Stroke or Transient Ischemic Attack. J Am Coll Cardiol. 2017;69(2):147-58.

Byzova TV, Rabbani R, D'Souza SE, Plow EF. Role of integrin alpha(v)beta3 in vascular biology. Thromb Haemost. 1998;80(5):726-34.

Caidahl K, Kazzam E, Lidberg J, et al. New concept in echocardiography: harmonic imaging of tissue without use of contrast agent. Lancet. 1998;352(9136):1264-70.

Cao W, Lu X, Cheng Z. The advancement of human serum albumin-based molecular probes for molecular imaging. Curr Pharm Des. 2015;21(14):1908-15.

Caravan P, Cloutier NJ, Greenfield MT, et al. The interaction of MS-325 with human serum albumin and its effect on proton relaxation rates. J Am Chem Soc. 2002;124(12):3152-62.

Cassado Ados A, D'Imperio Lima MR, Bortoluci KR. Revisiting mouse peritoneal macrophages: heterogeneity, development, and function. Front Immunol. 2015;6:225.

Cavalieri F, El Hamassi A, Chiessi E, Paradossi G. Stable polymeric microballoons as multifunctional device for biomedical uses: synthesis and characterization. Langmuir. 2005;21(19):8758-64.

Cerroni B, Chiessi E, Margheritelli S, Oddo L, Paradossi G. Polymer shelled microparticles for a targeted doxorubicin delivery in cancer therapy. Biomacromolecules. 2011;12(3):593-601.

Champion JA, Walker A, Mitragotri S. Role of particle size in phagocytosis of polymeric microspheres. Pharm Res. 2008;25(8):1815-21.

Chellan B, Reardon CA, Getz GS, Hofmann Bowman MA. Enzymatically Modified Low-Density Lipoprotein Promotes Foam Cell Formation in Smooth Muscle Cells via Macropinocytosis and Enhances Receptor-Mediated Uptake of Oxidized Low-Density Lipoprotein. Arterioscler Thromb Vasc Biol. 2016;36(6):1101-13.

Chen IY, Wu JC. Cardiovascular molecular imaging: focus on clinical translation. Circulation. 2011;123(4):425-43.

Chen K, Chen X. Design and development of molecular imaging probes. Curr Top Med Chem. 2010;10(12):1227-36.

Chen Y, An H. Attenuation Correction of PET/MR Imaging. Magn Reson Imaging Clin N Am. 2017;25(2):245-55.

Cheung AL. Isolation and culture of human umbilical vein endothelial cells (HUVEC). Curr Protoc Microbiol. 2007;Appendix 4:Appendix 4B.

Chiellini E, Corti A, D'Antone S, Solaro R. Biodegradation of poly (vinyl

alcohol) based materials. Progress in Polymer Science. 2003;28

(6):963-1014.

Chiu JJ, Chien S. Effects of disturbed flow on vascular endothelium: pathophysiological basis and clinical perspectives. Physiol Rev. 2011;91(1):327-87.

Clevert DA, Sommer WH, Helck A, Saam T, Reiser M. Improved carotid atherosclerotic plaques imaging with contrast-enhanced ultrasound (CEUS). Clin Hemorheol Microcirc. 2011;48(1):141-8.

Colin S, Chinetti-Gbaguidi G, Staels B. Macrophage phenotypes in atherosclerosis. Immunol Rev. 2014;262(1):153-66.

Conti M, Eriksson L. Physics of pure and non-pure positron emitters for PET: a review and a discussion. EJNMMI Phys. 2016;3(1):8.

Cybulsky MI, Iiyama K, Li H, et al. A major role for VCAM-1, but not ICAM-1, in early atherosclerosis. J Clin Invest. 2001;107(10):1255-62.

Davies MJ, Gordon JL, Gearing AJ, et al. The expression of the adhesion molecules ICAM-1, VCAM-1, PECAM, and E-selectin in human atherosclerosis. J Pathol. 1993;171(3):223-9.

Davies MK, Eollman A. Leonardo da Vinci (1452-1519). Heart. 1996;76(6):464.

DeGrado TR, Baldwin SW, Wang S, et al. Synthesis and evaluation of (18)F-labeled choline analogs as oncologic PET tracers. J Nucl Med. 2001;42(12):1805-14.

Dilworth JR, Pascu SI. The chemistry of PET imaging with zirconium-89. Chem Soc Rev. 2018;47(8):2554-71.

Duewell P, Kono H, Rayner KJ, et al. NLRP3 inflammasomes are required for atherogenesis and activated by cholesterol crystals. Nature. 2010;464(7293):1357-61.

Ehara S, Kobayashi Y, Yoshiyama M, et al. Spotty calcification typifies the culprit plaque in patients with acute myocardial infarction: an intravascular ultrasound study. Circulation. 2004;110(22):3424-9.

Elangbam CS, Qualls CW, Jr., Dahlgren RR. Cell adhesion molecules--update. Vet Pathol. 1997;34(1):61-73.

Fairclough M, Prenant C, Ellis B, et al. A new technique for the radiolabelling of mixed leukocytes with zirconium-89 for inflammation imaging with positron emission tomography. J Labelled Comp Radiopharm. 2016;59(7):270-6.

Fan J, Kitajima S, Watanabe T, et al. Rabbit models for the study of human atherosclerosis: from pathophysiological mechanisms to translational medicine. Pharmacol Ther. 2015;146:104-19.

Fayad ZA, Mani V, Woodward M, et al. Safety and efficacy of dalcetrapib on atherosclerotic disease using novel non-invasive multimodality imaging (dal-PLAQUE): a randomised clinical trial. Lancet. 2011;378(9802):1547-59.

Feingold KRG, C. Introduction to Lipids and Lipoproteins: MDText.com, Inc.; 2018.

Fischer G, Seibold U, Schirrmacher R, Wangler B, Wangler C. (89)Zr, a radiometal nuclide with high potential for molecular imaging with PET: chemistry, applications and remaining challenges. Molecules. 2013;18(6):6469-90.

Furchgott RF, Zawadzki JV. The obligatory role of endothelial cells in the relaxation of arterial smooth muscle by acetylcholine. Nature. 1980;288(5789):373-6.

Gaemperli O, Shalhoub J, Owen DR, et al. Imaging intraplaque inflammation in carotid atherosclerosis with 11C-PK11195 positron emission

tomography/computed tomography. Eur Heart J. 2012;33(15):1902-10.

Gargiulo S, Gramanzini M, Mancini M. Molecular Imaging of Vulnerable Atherosclerotic Plaques in Animal Models. Int J Mol Sci. 2016;17(9).

Gaztanaga J, Farkouh M, Rudd JH, et al. A phase 2 randomized, double-blind, placebo-controlled study of the effect of VIA-2291, a 5-lipoxygenase inhibitor, on vascular inflammation in patients after an acute coronary syndrome. Atherosclerosis. 2015;240(1):53-60.

Geovanini GR, Libby P. Atherosclerosis and inflammation: overview and updates. Clin Sci (Lond). 2018;132(12):1243-52.

Getz GS, Reardon CA. Apoprotein E as a lipid transport and signaling protein in the blood, liver, and artery wall. J Lipid Res. 2009;50 Suppl:S156-61.

Getz GS, Reardon CA. Animal models of atherosclerosis. Arterioscler Thromb Vasc Biol. 2012;32(5):1104-15.

Gimbrone MA, Jr., Garcia-Cardena G. Endothelial Cell Dysfunction and the Pathobiology of Atherosclerosis. Circ Res. 2016;118(4):620-36.

Giovanella L, Lucignani G. Hybrid versus fusion imaging: are we moving forward judiciously? Eur J Nucl Med Mol Imaging. 2010;37(5):973-9.

Goldstein JL, Ho YK, Basu SK, Brown MS. Binding site on macrophages that mediates uptake and degradation of acetylated low density lipoprotein, producing massive cholesterol deposition. Proc Natl Acad Sci U S A. 1979;76(1):333-7.

Gotsman I, Sharpe AH, Lichtman AH. T-cell costimulation and coinhibition in atherosclerosis. Circ Res. 2008;103(11):1220-31.

Gough PJ, Greaves DR, Suzuki H, et al. Analysis of macrophage scavenger receptor (SR-A) expression in human aortic atherosclerotic lesions. Arterioscler Thromb Vasc Biol. 1999;19(3):461-71.

Greaves DR, Gordon S. The macrophage scavenger receptor at 30 years of age: current knowledge and future challenges. J Lipid Res. 2009;50 Suppl:S282-6.

Green NM. AVIDIN .3. NATURE OF BIOTIN-BINDING SITE. Biochemical Journal. 1963;89(3):599-&.

Grishenkov D, Pecorari C, Brismar TB, Paradossi G. CHARACTERIZATION OF ACOUSTIC PROPERTIES OF PVA-SHELLED ULTRASOUND CONTRAST AGENTS: LINEAR PROPERTIES (PART I). Ultrasound in Medicine and Biology. 2009;35(7):1127-38.

Gropler RJ, Glover DK, Sinusas AJ, Taegtmeyer H. Cardiovascular Molecular Imaging: Informa Healthcare USA Inc; 2007.

Guo S, Shen S, Wang J, et al. Detection of high-risk atherosclerotic plaques with ultrasound molecular imaging of glycoprotein IIb/IIIa receptor on activated platelets. Theranostics. 2015;5(4):418-30.

Gustafsson B, Hedin U, Caidahl K. Glycolaldehyde and maleyl conjugated human serum albumin as potential macrophage-targeting carriers for molecular imaging purposes. Contrast Media Mol Imaging. 2015;10(1):37-42.

Gustafsson B, Youens S, Louie AY. Development of contrast agents targeted to macrophage scavenger receptors for MRI of vascular inflammation. Bioconjug Chem. 2006;17(2):538-47.

Haberland ME, Rasmussen RR, Fogelman AM. Receptor recognition of maleyl-albumin induces chemotaxis in human monocytes. J Clin Invest. 1986a;78(3):827-31.

Haberland ME, Rasmussen RR, Olch CL, Fogelman AM. Two distinct receptors account for recognition of maleyl-albumin in human monocytes during

differentiation in vitro. J Clin Invest. 1986b;77(3):681-9.

Hansson GK. Inflammation, atherosclerosis, and coronary artery disease. N Engl J Med. 2005;352(16):1685-95.

Hansson GK, Hermansson A. The immune system in atherosclerosis. Nat Immunol. 2011;12(3):204-12.

Hansson GK, Libby P. The immune response in atherosclerosis: a double-edged sword. Nat Rev Immunol. 2006;6(7):508-19.

Hansson GK, Libby P, Schonbeck U, Yan ZQ. Innate and adaptive immunity in the pathogenesis of atherosclerosis. Circ Res. 2002;91(4):281-91.

Hansson GK, Libby P, Tabas I. Inflammation and plaque vulnerability. J Intern Med. 2015;278(5):483-93.

Hashimoto D, Chow A, Noizat C, et al. Tissue-resident macrophages self-maintain locally throughout adult life with minimal contribution from circulating monocytes. Immunity. 2013;38(4):792-804.

Hatsukami TS, Ross R, Polissar NL, Yuan C. Visualization of fibrous cap thickness and rupture in human atherosclerotic carotid plaque in vivo with high-resolution magnetic resonance imaging. Circulation. 2000;102(9):959-64.

Hellberg S, Silvola JMU, Kiugel M, et al. 18-kDa translocator protein ligand (18)F-FEMPA: Biodistribution and uptake into atherosclerotic plaques in mice. J Nucl Cardiol. 2017;24(3):862-71.

Hernot S, Klibanov AL. Microbubbles in ultrasound-triggered drug and gene delivery. Adv Drug Deliv Rev. 2008;60(10):1153-66.

Hibbs AR. Confocal Microscopy for Biologists: Kluwer Academic/Plenum Publishers; 2004.

Hoeffel G, Chen J, Lavin Y, et al. C-Myb(+) erythro-myeloid progenitor-derived fetal monocytes give rise to adult tissue-resident macrophages. Immunity. 2015;42(4):665-78.

Hricak H, Choi BI, Scott AM, et al. Global trends in hybrid imaging. Radiology. 2010;257(2):498-506.

Hsieh HJ, Liu CA, Huang B, Tseng AH, Wang DL. Shear-induced endothelial mechanotransduction: the interplay between reactive oxygen species (ROS) and nitric oxide (NO) and the pathophysiological implications. J Biomed Sci. 2014;21:3.

Huang PT, Huang FG, Zou CP, et al. Contrast-enhanced sonographic characteristics of neovascularization in carotid atherosclerotic plaques. J Clin Ultrasound. 2008;36(6):346-51.

Huet P, Burg S, Le Guludec D, Hyafil F, Buvat I. Variability and uncertainty of 18F-FDG PET imaging protocols for assessing inflammation in atherosclerosis: suggestions for improvement. J Nucl Med. 2015;56(4):552-9.

Hughes DA, Fraser IP, Gordon S. Murine macrophage scavenger receptor: in vivo expression and function as receptor for macrophage adhesion in lymphoid and non-lymphoid organs. Eur J Immunol. 1995;25(2):466-73.

Huibers A, de Borst GJ, Bulbulia R, Pan H, Halliday A, group A-c. Plaque Echolucency and the Risk of Ischaemic Stroke in Patients with Asymptomatic Carotid Stenosis Within the First Asymptomatic Carotid Surgery Trial (ACST-1). Eur J Vasc Endovasc Surg. 2016;51(5):616-21.

Hyafil F, Vigne J. Imaging inflammation in atherosclerotic plaques: Just make it easy! J Nucl Cardiol. 2018.

Jaffer FA, Libby P, Weissleder R. Molecular and cellular imaging of atherosclerosis: emerging applications. J Am Coll Cardiol. 2006;47(7):1328-38.

Jaguin M, Houlbert N, Fardel O, Lecureur V. Polarization profiles of human M-CSF-generated macrophages and comparison of M1-markers in classically activated macrophages from GM-CSF and M-CSF origin. Cell Immunol. 2013;281(1):51-61.

Jarrett BR, Correa C, Ma KL, Louie AY. In vivo mapping of vascular inflammation using multimodal imaging. PLoS One. 2010;5(10):e13254.

Jarrett BR, Gustafsson B, Kukis DL, Louie AY. Synthesis of 64Cu-labeled magnetic nanoparticles for multimodal imaging. Bioconjug Chem. 2008;19(7):1496-504.

Jauw YW, Menke-van der Houven van Oordt CW, Hoekstra OS, et al. Immuno-Positron Emission Tomography with Zirconium-89-Labeled Monoclonal Antibodies in Oncology: What Can We Learn from Initial Clinical Trials? Front Pharmacol. 2016;7:131.

Joshi NV, Vesey AT, Williams MC, et al. 18F-fluoride positron emission tomography for identification of ruptured and high-risk coronary atherosclerotic plaques: a prospective clinical trial. Lancet. 2014;383(9918):705-13.

Kapourchali FR, Surendiran G, Chen L, Uitz E, Bahadori B, Moghadasian MH. Animal models of atherosclerosis. World J Clin Cases. 2014;2(5):126-32.

Kato K, Schober O, Ikeda M, et al. Evaluation and comparison of 11C-choline uptake and calcification in aortic and common carotid arterial walls with combined PET/CT. Eur J Nucl Med Mol Imaging. 2009;36(10):1622-8.

Kaufmann BA. Ultrasound molecular imaging of atherosclerosis. Cardiovasc Res. 2009;83(4):617-25.

Kaufmann BA, Lewis C, Xie A, Mirza-Mohd A, Lindner JR. Detection of recent myocardial ischaemia by molecular imaging of P-selectin with targeted contrast echocardiography. Eur Heart J. 2007a;28(16):2011-7.

Kaufmann BA, Sanders JM, Davis C, et al. Molecular imaging of inflammation in atherosclerosis with targeted ultrasound detection of vascular cell adhesion molecule-1. Circulation. 2007b;116(3):276-84.

Ketelhuth DF, Hansson GK. Adaptive Response of T and B Cells in Atherosclerosis. Circ Res. 2016;118(4):668-78.

Kiessling F, Fokong S, Bzyl J, Lederle W, Palmowski M, Lammers T. Recent advances in molecular, multimodal and theranostic ultrasound imaging. Adv Drug Deliv Rev. 2014;72:15-27.

Kim EJ, Kim S, Seo HS, et al. Novel PET Imaging of Atherosclerosis with 68Ga-Labeled NOTA-Neomannosylated Human Serum Albumin. J Nucl Med. 2016;57(11):1792-7.

Klibanov AL. Ultrasound Contrast Materials in Cardiovascular Medicine: from Perfusion Assessment to Molecular Imaging. Journal of Cardiovascular Translational Research. 2013;6(5):729-39.

Klibanov AL, Rychak JJ, Yang WC, et al. Targeted ultrasound contrast agent for molecular imaging of inflammation in high-shear flow. Contrast Media Mol Imaging. 2006;1(6):259-66.

Koni PA, Joshi SK, Temann UA, Olson D, Burkly L, Flavell RA. Conditional vascular cell adhesion molecule 1 deletion in mice: impaired lymphocyte migration to bone marrow. J Exp Med. 2001;193(6):741-54.

Koppal S, Warntjes M, Swann J, et al. Quantitative fat and R2* mapping in vivo to measure lipid-rich necrotic core and intraplaque hemorrhage in carotid atherosclerosis. Magn Reson Med. 2017;78(1):285-96.

Kovanen PT, Kaartinen M, Paavonen T. Infiltrates of activated mast cells at the site of coronary atheromatous erosion or

rupture in myocardial infarction. Circulation. 1995;92(5):1084-8.

Kronenberg F. HDL in CKD-The Devil Is in the Detail. J Am Soc Nephrol. 2018;29(5):1356-71.

Kuchibhotla S, Vanegas D, Kennedy DJ, et al. Absence of CD36 protects against atherosclerosis in ApoE knock-out mice with no additional protection provided by absence of scavenger receptor A I/II. Cardiovasc Res. 2008;78(1):185-96.

Kume T, Akasaka T, Kawamoto T, et al. Measurement of the thickness of the fibrous cap by optical coherence tomography. Am Heart J. 2006;152(4):755 e1-4.

Kunjathoor VV, Febbraio M, Podrez EA, et al. Scavenger receptors class A-I/II and CD36 are the principal receptors responsible for the uptake of modified low density lipoprotein leading to lipid loading in macrophages. J Biol Chem. 2002;277(51):49982-8.

Laitinen I, Marjamaki P, Nagren K, et al. Uptake of inflammatory cell marker [11C]PK11195 into mouse atherosclerotic plaques. Eur J Nucl Med Mol Imaging. 2009a;36(1):73-80.

Laitinen I, Saraste A, Weidl E, et al. Evaluation of alphavbeta3 integrin-targeted positron emission tomography tracer 18F-galacto-RGD for imaging of vascular inflammation in atherosclerotic mice. Circ Cardiovasc Imaging. 2009b;2(4):331-8.

Laitinen IE, Luoto P, Nagren K, et al. Uptake of 11C-choline in mouse atherosclerotic plaques. J Nucl Med. 2010;51(5):798-802.

Laurberg JM, Olsen AK, Hansen SB, et al. Imaging of vulnerable atherosclerotic plaques with FDG-microPET: no FDG accumulation. Atherosclerosis. 2007;192(2):275-82.

Lecanu L, Yao ZX, McCourty A, et al. Control of hypercholesterolemia and atherosclerosis using the cholesterol recognition/interaction amino acid sequence of the translocator protein TSPO. Steroids. 2013;78(2):137-46.

Lee P, Wu X. Review: modifications of human serum albumin and their binding effect. Curr Pharm Des. 2015;21(14):1862-5.

Lentacker IDS, S.C.; Sanders, N.N. Drug loaded microbubble design for ultrasound triggered delivery. Soft Matter. 2009;5:2161-70.

Leon B, Ardavin C. Monocyte migration to inflamed skin and lymph nodes is differentially controlled by L-selectin and PSGL-1. Blood. 2008;111(6):3126-30.

Li D, Patel AR, Klibanov AL, et al. Molecular imaging of atherosclerotic plaques targeted to oxidized LDL receptor LOX-1 by SPECT/CT and magnetic resonance. Circ Cardiovasc Imaging. 2010;3(4):464-72.

Li X, Bauer W, Israel I, et al. Targeting P-selectin by gallium-68-labeled fucoidan positron emission tomography for noninvasive characterization of vulnerable plaques: correlation with in vivo 17.6T MRI. Arterioscler Thromb Vasc Biol. 2014;34(8):1661-7.

Li X, Bauer W, Kreissl MC, et al. Specific somatostatin receptor II expression in arterial plaque: (68)Ga-DOTATATE autoradiographic, immunohistochemical and flow cytometric studies in apoE-deficient mice. Atherosclerosis. 2013;230(1):33-9.

Libby P. Inflammation in atherosclerosis. Nature. 2002;420(6917):868-74.

Libby P, Theroux P. Pathophysiology of coronary artery disease. Circulation. 2005;111(25):3481-8.

Lindner JR, Dayton PA, Coggins MP, et al. Noninvasive imaging of inflammation by ultrasound detection of phagocytosed microbubbles. Circulation. 2000;102(5):531-8.

Lipinski MJ, Amirbekian V, Frias JC, et al. MRI to detect atherosclerosis with

gadolinium-containing immunomicelles targeting the macrophage scavenger receptor. Magn Reson Med. 2006;56(3):601-10.

Loppnow H, Libby P. Proliferating or interleukin 1-activated human vascular smooth muscle cells secrete copious interleukin 6. J Clin Invest. 1990;85(3):731-8.

Mahmood SS, Levy D, Vasan RS, Wang TJ. The Framingham Heart Study and the epidemiology of cardiovascular disease: a historical perspective. Lancet. 2014;383(9921):999-1008.

Mahmoudi M, Sant S, Wang B, Laurent S, Sen T. Superparamagnetic iron oxide nanoparticles (SPIONs): development, surface modification and applications in chemotherapy. Adv Drug Deliv Rev. 2011;63(1-2):24-46.

Majmudar MD, Yoo J, Keliher EJ, et al. Polymeric nanoparticle PET/MR imaging allows macrophage detection in atherosclerotic plaques. Circ Res. 2013;112(5):755-61.

Manning-Tobin JJ, Moore KJ, Seimon TA, et al. Loss of SR-A and CD36 activity reduces atherosclerotic lesion complexity without abrogating foam cell formation in hyperlipidemic mice. Arterioscler Thromb Vasc Biol. 2009;29(1):19-26.

Martinez FO, Gordon S. The M1 and M2 paradigm of macrophage activation: time for reassessment. F1000Prime Rep. 2014;6:13.

Masteling MG, Zeebregts CJ, Tio RA, et al. High-resolution imaging of human atherosclerotic carotid plaques with micro 18F-FDG PET scanning exploring plaque vulnerability. J Nucl Cardiol. 2011;18(6):1066-75.

Mateo J, Izquierdo-Garcia D, Badimon JJ, Fayad ZA, Fuster V. Noninvasive assessment of hypoxia in rabbit advanced atherosclerosis using (1)(8)F-fluoromisonidazole positron emission tomographic imaging. Circ Cardiovasc Imaging. 2014;7(2):312-20.

Mathias CJ, Bergmann SR, Green MA. Species-dependent binding of copper(II) bis(thiosemicarbazone) radiopharmaceuticals to serum albumin. J Nucl Med. 1995;36(8):1451-5.

Matic LP, Jesus Iglesias M, Vesterlund M, et al. Novel Multiomics Profiling of Human Carotid Atherosclerotic Plaques and Plasma Reveals Biliverdin Reductase B as a Marker of Intraplaque Hemorrhage. JACC Basic Transl Sci. 2018;3(4):464-80.

Matsumoto A, Naito M, Itakura H, et al. Human macrophage scavenger receptors: primary structure, expression, and localization in atherosclerotic lesions. Proc Natl Acad Sci U S A. 1990;87(23):9133-7.

Matter CM, Wyss MT, Meier P, et al. 18F-choline images murine atherosclerotic plaques ex vivo. Arterioscler Thromb Vasc Biol. 2006;26(3):584-9.

Mauer J, Chaurasia B, Plum L, et al. Myeloid cell-restricted insulin receptor deficiency protects against obesity-induced inflammation and systemic insulin resistance. PLoS Genet. 2010;6(5):e1000938.

McCarty OJ, Conley RB, Shentu W, et al. Molecular imaging of activated von Willebrand factor to detect high-risk atherosclerotic phenotype. JACC Cardiovasc Imaging. 2010;3(9):947-55.

McKenney-Drake ML, Moghbel MC, Paydary K, et al. (18)F-NaF and (18)F-FDG as molecular probes in the evaluation of atherosclerosis. Eur J Nucl Med Mol Imaging. 2018;45(12):2190-200.

Menezes LJ, Kotze CW, Agu O, et al. Investigating vulnerable atheroma using combined (18)F-FDG PET/CT angiography of carotid plaque with immunohistochemical validation. J Nucl Med. 2011;52(11):1698-703.

Metzger K, Vogel S, Chatterjee M, et al. High-frequency ultrasound-guided disruption of glycoprotein VI-targeted

microbubbles targets atheroprogressison in mice. Biomaterials. 2015;36:80-9.

Miller JM, Rochitte CE, Dewey M, et al. Diagnostic performance of coronary angiography by 64-row CT. N Engl J Med. 2008;359(22):2324-36.

Miller YI, Choi SH, Wiesner P, et al. Oxidation-specific epitopes are danger-associated molecular patterns recognized by pattern recognition receptors of innate immunity. Circ Res. 2011;108(2):235-48.

Moore KJ, Koplev S, Fisher EA, et al. Macrophage Trafficking, Inflammatory Resolution, and Genomics in Atherosclerosis: JACC Macrophage in CVD Series (Part 2). J Am Coll Cardiol. 2018;72(18):2181-97.

Moore KJ, Kunjathoor VV, Koehn SL, et al. Loss of receptor-mediated lipid uptake via scavenger receptor A or CD36 pathways does not ameliorate atherosclerosis in hyperlipidemic mice. J Clin Invest. 2005;115(8):2192-201.

Moore KJ, Sheedy FJ, Fisher EA. Macrophages in atherosclerosis: a dynamic balance. Nat Rev Immunol. 2013;13(10):709-21.

Moore KJ, Tabas I. Macrophages in the pathogenesis of atherosclerosis. Cell. 2011;145(3):341-55.

Myers KS, Rudd JH, Hailman EP, et al. Correlation between arterial FDG uptake and biomarkers in peripheral artery disease. JACC Cardiovasc Imaging. 2012;5(1):38-45.

Naghavi M, Libby P, Falk E, et al. From vulnerable plaque to vulnerable patient: a call for new definitions and risk assessment strategies: Part II. Circulation. 2003;108(15):1772-8.

Nahrendorf M, Keliher E, Panizzi P, et al. 18F-4V for PET-CT imaging of VCAM-1 expression in atherosclerosis. JACC Cardiovasc Imaging. 2009;2(10):1213-22.

Nahrendorf M, Zhang H, Hembrador S, et al. Nanoparticle PET-CT imaging of macrophages in inflammatory atherosclerosis. Circulation. 2008;117(3):379-87.

Nair A, Margolis MP, Kuban BD, Vince DG. Automated coronary plaque characterisation with intravascular ultrasound backscatter: ex vivo validation. EuroIntervention. 2007;3(1):113-20.

Naito M, Suzuki H, Mori T, Matsumoto A, Kodama T, Takahashi K. Coexpression of type I and type II human macrophage scavenger receptors in macrophages of various organs and foam cells in atherosclerotic lesions. Am J Pathol. 1992;141(3):591-9.

Nakamura I, Hasegawa K, Wada Y, Hirase T, Node K, Watanabe Y. Detection of early stage atherosclerotic plaques using PET and CT fusion imaging targeting P-selectin in low density lipoprotein receptor-deficient mice. Biochem Biophys Res Commun. 2013;433(1):47-51.

Nakashima Y, Raines EW, Plump AS, Breslow JL, Ross R. Upregulation of VCAM-1 and ICAM-1 at atherosclerosis-prone sites on the endothelium in the ApoE-deficient mouse. Arterioscler Thromb Vasc Biol. 1998;18(5):842-51.

Nakata A, Nakagawa Y, Nishida M, et al. CD36, a novel receptor for oxidized low-density lipoproteins, is highly expressed on lipid-laden macrophages in human atherosclerotic aorta. Arterioscler Thromb Vasc Biol. 1999;19(5):1333-9.

Naruko T, Ueda M, Haze K, et al. Neutrophil infiltration of culprit lesions in acute coronary syndromes. Circulation. 2002;106(23):2894-900.

Narula J, Garg P, Achenbach S, Motoyama S, Virmani R, Strauss HW. Arithmetic of vulnerable plaques for noninvasive imaging. Nat Clin Pract Cardiovasc Med. 2008;5 Suppl 2:S2-10.

Narula J, Nakano M, Virmani R, et al. Histopathologic characteristics of atherosclerotic coronary disease and implications of the findings for the invasive and noninvasive detection of vulnerable plaques. J Am Coll Cardiol. 2013;61(10):1041-51.

Narula J, Strauss HW. The popcorn plaques. Nat Med. 2007;13(5):532-4.

Naylor AR, Ricco JB, de Borst GJ, et al. Editor's Choice - Management of Atherosclerotic Carotid and Vertebral Artery Disease: 2017 Clinical Practice Guidelines of the European Society for Vascular Surgery (ESVS). Eur J Vasc Endovasc Surg. 2018;55(1):3-81.

Niccoli Asabella A, Ciccone MM, Cortese F, et al. Higher reliability of 18F-FDG target background ratio compared to standardized uptake value in vulnerable carotid plaque detection: a pilot study. Ann Nucl Med. 2014;28(6):571-9.

Nilsson J, Bjorkbacka H, Fredrikson GN. Apolipoprotein B100 autoimmunity and atherosclerosis - disease mechanisms and therapeutic potential. Curr Opin Lipidol. 2012;23(5):422-8.

Norlen O, Montan H, Hellman P, Stalberg P, Sundin A. Preoperative (68)Ga-DOTA-Somatostatin Analog-PET/CT Hybrid Imaging Increases Detection Rate of Intra-abdominal Small Intestinal Neuroendocrine Tumor Lesions. World J Surg. 2018;42(2):498-505.

O'Brien KD, Allen MD, McDonald TO, et al. Vascular cell adhesion molecule-1 is expressed in human coronary atherosclerotic plaques. Implications for the mode of progression of advanced coronary atherosclerosis. J Clin Invest. 1993;92(2):945-51.

Ober RJ, Radu CG, Ghetie V, Ward ES. Differences in promiscuity for antibody-FcRn interactions across species: implications for therapeutic antibodies. Int Immunol. 2001;13(12):1551-9.

Oh N, Park JH. Endocytosis and exocytosis of nanoparticles in mammalian cells. Int J Nanomed. 2014;9:51-63.

Paeng JC, Lee YS, Lee JS, et al. Feasibility and kinetic characteristics of (68)Ga-NOTA-RGD PET for in vivo atherosclerosis imaging. Ann Nucl Med. 2013;27(9):847-54.

Paigen Bea. Variation in susceptibility to atherosclerosis among inbred strains of mice. Atherosclerosis. 1985;57(1):65-73.

Palmowski M, Morgenstern B, Hauff P, et al. Pharmacodynamics of streptavidin-coated cyanoacrylate microbubbles designed for molecular ultrasound imaging. Investigative Radiology. 2008;43(3):162-9.

Paradossi GP, P.; Trucco, A. Ultrasound Contrast Agents - Targeting and Processing Methods for Theranostics: Springer-Verlag Italia; 2010. 193 p.

Park JG, Ryu SY, Jung IH, et al. Evaluation of VCAM-1 antibodies as therapeutic agent for atherosclerosis in apolipoprotein E-deficient mice. Atherosclerosis. 2013;226(2):356-63.

Park JI, Jagadeesan D, Williams R, et al. Microbubbles Loaded with Nanoparticles: A Route to Multiple Imaging Modalities. ACS Nano. 2010;4(11):6579-86.

Patel MR, Peterson ED, Dai D, et al. Low diagnostic yield of elective coronary angiography. N Engl J Med. 2010;362(10):886-95.

Peled M, Fisher EA. Dynamic Aspects of Macrophage Polarization during Atherosclerosis Progression and Regression. Front Immunol. 2014;5:579.

Phillips MC. Molecular mechanisms of cellular cholesterol efflux. J Biol Chem. 2014;289(35):24020-9.

Phinikaridou A, Andia ME, Passacquale G, Ferro A, Botnar RM. Noninvasive MRI monitoring of the effect of interventions on endothelial permeability in murine atherosclerosis using an albumin-

binding contrast agent. J Am Heart Assoc. 2013;2(5):e000402.

Platt N, Gordon S. Is the class A macrophage scavenger receptor (SR-A) multifunctional? - The mouse's tale. J Clin Invest. 2001;108(5):649-54.

Platt N, Haworth R, Darley L, Gordon S. The many roles of the class A macrophage scavenger receptor. Int Rev Cytol. 2002;212:1-40.

Poehlmann M, Grishenkov D, Kothapalli S, et al. On the interplay of shell structure with low- and high-frequency mechanics of multifunctional magnetic microbubbles. Soft Matter. 2014;10(1):214-26.

Poston RN, Haskard DO, Coucher JR, Gall NP, Johnson-Tidey RR. Expression of intercellular adhesion molecule-1 in atherosclerotic plaques. Am J Pathol. 1992;140(3):665-73.

Powers WJ, Rabinstein AA, Ackerson T, et al. 2018 Guidelines for the Early Management of Patients With Acute Ischemic Stroke: A Guideline for Healthcare Professionals From the American Heart Association/American Stroke Association. Stroke. 2018;49(3):e46-e110.

Prabhudas M, Bowdish D, Drickamer K, et al. Standardizing scavenger receptor nomenclature. J Immunol. 2014;192(5):1997-2006.

Quillard T, Libby P. Molecular imaging of atherosclerosis for improving diagnostic and therapeutic development. Circ Res. 2012;111(2):231-44.

Razuvaev A, Lund K, Roy J, Hedin U, Caidahl K. Noninvasive real-time imaging of intima thickness after rat carotid artery balloon injury using ultrasound biomicroscopy. Atherosclerosis. 2008;199(2):310-6.

Ridker PM, Danielson E, Fonseca FA, et al. Reduction in C-reactive protein and LDL cholesterol and cardiovascular event rates after initiation of rosuvastatin: a prospective study of the JUPITER trial. Lancet. 2009;373(9670):1175-82.

Ridker PM, Everett BM, Thuren T, et al. Antiinflammatory Therapy with Canakinumab for Atherosclerotic Disease. N Engl J Med. 2017;377(12):1119-31.

Ripa RS, Pedersen SF, Kjaer A. PET/MR Imaging in Vascular Disease: Atherosclerosis and Inflammation. PET Clin. 2016;11(4):479-88.

Robbins CS, Hilgendorf I, Weber GF, et al. Local proliferation dominates lesional macrophage accumulation in atherosclerosis. Nat Med. 2013;19(9):1166-72.

Rodriguez-Prados JC, Traves PG, Cuenca J, et al. Substrate fate in activated macrophages: a comparison between innate, classic, and alternative activation. J Immunol. 2010;185(1):605-14.

Rominger A, Saam T, Vogl E, et al. In vivo imaging of macrophage activity in the coronary arteries using 68Ga-DOTATATE PET/CT: correlation with coronary calcium burden and risk factors. J Nucl Med. 2010;51(2):193-7.

Ross R, Glomset JA. The pathogenesis of atherosclerosis (first of two parts). N Engl J Med. 1976a;295(7):369-77.

Ross R, Glomset JA. The pathogenesis of atherosclerosis (second of two parts). N Engl J Med. 1976b;295(8):420-5.

Rubin RP. Robert Furchgott (1916-2009): A scientist with a mission. J Med Biogr. 2019:967772018825365.

Rudd JH, Fayad ZA. Imaging atherosclerotic plaque inflammation. Nat Clin Pract Cardiovasc Med. 2008;5 Suppl 2:S11-7.

Rudd JH, Hyafil F, Fayad ZA. Inflammation imaging in atherosclerosis. Arterioscler Thromb Vasc Biol. 2009;29(7):1009-16.

Rudd JH, Myers KS, Bansilal S, et al. (18)Fluorodeoxyglucose positron

emission tomography imaging of atherosclerotic plaque inflammation is highly reproducible: implications for atherosclerosis therapy trials. J Am Coll Cardiol. 2007;50(9):892-6.

Rudd JH, Warburton EA, Fryer TD, et al. Imaging atherosclerotic plaque inflammation with [18F]-fluorodeoxyglucose positron emission tomography. Circulation. 2002;105(23):2708-11.

Ruiz JL, Hutcheson JD, Aikawa E. Cardiovascular calcification: current controversies and novel concepts. Cardiovasc Pathol. 2015;24(4):207-12.

Saba L, Mallarini G. A comparison between NASCET and ECST methods in the study of carotids: evaluation using Multi-Detector-Row CT angiography. Eur J Radiol. 2010;76(1):42-7.

Sage AP, Tintut Y, Demer LL. Regulatory mechanisms in vascular calcification. Nat Rev Cardiol. 2010;7(9):528-36.

Sanan DA, Newland DL, Tao R, et al. Low density lipoprotein receptor-negative mice expressing human apolipoprotein B-100 develop complex atherosclerotic lesions on a chow diet: no accentuation by apolipoprotein(a). Proc Natl Acad Sci U S A. 1998;95(8):4544-9.

Sasaki T, Kuzuya M, Nakamura K, et al. A simple method of plaque rupture induction in apolipoprotein E-deficient mice. Arterioscler Thromb Vasc Biol. 2006;26(6):1304-9.

Schnoor M. Endothelial actin-binding proteins and actin dynamics in leukocyte transendothelial migration. J Immunol. 2015;194(8):3535-41.

Schottelius M, Laufer B, Kessler H, Wester HJ. Ligands for mapping alphavbeta3-integrin expression in vivo. Acc Chem Res. 2009;42(7):969-80.

Sciallero C, Balbi L, Paradossi G, Trucco A. Magnetic resonance and ultrasound contrast imaging of polymer-shelled microbubbles loaded with iron oxide nanoparticles. R Soc Open Sci. 2016;3(8):14.

Sciallero C, Grishenkov D, Kothapalli S, Oddo L, Trucco A. Acoustic characterization and contrast imaging of microbubbles encapsulated by polymeric shells coated or filled with magnetic nanoparticles. J Acoust Soc Am. 2013;134(5):3918-30.

Segers FM, den Adel B, Bot I, et al. Scavenger receptor-AI-targeted iron oxide nanoparticles for in vivo MRI detection of atherosclerotic lesions. Arterioscler Thromb Vasc Biol. 2013;33(8):1812-9.

Senders ML, Que X, Cho YS, et al. PET/MR Imaging of Malondialdehyde-Acetaldehyde Epitopes With a Human Antibody Detects Clinically Relevant Atherothrombosis. J Am Coll Cardiol. 2018;71(3):321-35.

Seo HS, Choi MH. Cholesterol homeostasis in cardiovascular disease and recent advances in measuring cholesterol signatures. J Steroid Biochem Mol Biol. 2015;153:72-9.

Shaw LJ, Hausleiter J, Achenbach S, et al. Coronary computed tomographic angiography as a gatekeeper to invasive diagnostic and surgical procedures: results from the multicenter CONFIRM (Coronary CT Angiography Evaluation for Clinical Outcomes: an International Multicenter) registry. J Am Coll Cardiol. 2012;60(20):2103-14.

Shevach EM. Mechanisms of foxp3+ T regulatory cell-mediated suppression. Immunity. 2009;30(5):636-45.

Shi ZL, Neoh KG, Kang ET, et al. (Carboxymethyl)chitosan-Modified Superparamagnetic Iron Oxide Nanoparticles for Magnetic Resonance Imaging of Stem Cells. ACS Appl Mater Interfaces. 2009;1(2):328-35.

Silvera SS, Aidi HE, Rudd JH, et al. Multimodality imaging of atherosclerotic plaque activity and composition using FDG-PET/CT and

MRI in carotid and femoral arteries. Atherosclerosis. 2009;207(1):139-43.

Singh N, Jenkins GJ, Asadi R, Doak SH. Potential toxicity of superparamagnetic iron oxide nanoparticles (SPION). Nano Rev. 2010;1.

Sleep D, Cameron J, Evans LR. Albumin as a versatile platform for drug half-life extension. Biochim Biophys Acta. 2013;1830(12):5526-34.

Slijkhuis W, Mali W, Appelman Y. A historical perspective towards a non-invasive treatment for patients with atherosclerosis. Neth Heart J. 2009;17(4):140-4.

Smith BJ, Popplewell A, Athwal D, et al. Prolonged in vivo residence times of antibody fragments associated with albumin. Bioconjug Chem. 2001;12(5):750-6.

Sosale NG, Spinler KR, Alvey C, Discher DE. Macrophage engulfment of a cell or nanoparticle is regulated by unavoidable opsonization, a species-specific 'Marker of Self' CD47, and target physical properties. Curr Opin Immunol. 2015;35:107-12.

Sriranjan RS, Tarkin JM, Evans NR, Chowdhury MM, Rudd JH. Imaging unstable plaque. Q J Nucl Med Mol Imaging. 2016;60(3):205-18.

Stary HC, Chandler AB, Dinsmore RE, et al. A definition of advanced types of atherosclerotic lesions and a histological classification of atherosclerosis. A report from the Committee on Vascular Lesions of the Council on Arteriosclerosis, American Heart Association. Arterioscler Thromb Vasc Biol. 1995;15(9):1512-31.

Stary HC, Chandler AB, Glagov S, et al. A definition of initial, fatty streak, and intermediate lesions of atherosclerosis. A report from the Committee on Vascular Lesions of the Council on Arteriosclerosis, American Heart Association. Circulation. 1994;89(5):2462-78.

Stoger JL, Gijbels MJ, van der Velden S, et al. Distribution of macrophage polarization markers in human atherosclerosis. Atherosclerosis. 2012;225(2):461-8.

Sugano R, Yamamura T, Harada-Shiba M, Miyake Y, Yamamoto A. Uptake of oxidized low-density lipoprotein in a THP-1 cell line lacking scavenger receptor A. Atherosclerosis. 2001;158(2):351-7.

Sundin A. Imaging of neuroendocrine tumors. Expert Opin Med Diagn. 2012;6(5):473-83.

Suzuki H, Kurihara Y, Takeya M, et al. A role for macrophage scavenger receptors in atherosclerosis and susceptibility to infection. Nature. 1997;386(6622):292-6.

Tabas I, Garcia-Cardena G, Owens GK. Recent insights into the cellular biology of atherosclerosis. J Cell Biol. 2015;209(1):13-22.

Tahara N, Kai H, Ishibashi M, et al. Simvastatin attenuates plaque inflammation: evaluation by fluorodeoxyglucose positron emission tomography. J Am Coll Cardiol. 2006;48(9):1825-31.

Tahara N, Mukherjee J, de Haas HJ, et al. 2-deoxy-2-[18F]fluoro-D-mannose positron emission tomography imaging in atherosclerosis. Nat Med. 2014;20(2):215-9.

Tang T, Howarth SP, Miller SR, et al. Assessment of inflammatory burden contralateral to the symptomatic carotid stenosis using high-resolution ultrasmall, superparamagnetic iron oxide-enhanced MRI. Stroke. 2006;37(9):2266-70.

Tang TY, Howarth SP, Miller SR, et al. The ATHEROMA (Atorvastatin Therapy: Effects on Reduction of Macrophage Activity) Study. Evaluation using ultrasmall superparamagnetic iron oxide-enhanced magnetic resonance imaging in carotid

disease. J Am Coll Cardiol. 2009a;53(22):2039-50.

Tang TY, Muller KH, Graves MJ, et al. Iron Oxide Particles for Atheroma Imaging. Arterioscler Thromb Vasc Biol. 2009b;29(7):1001-8.

Tarkin JM, Dweck MR, Evans NR, et al. Imaging Atherosclerosis. Circ Res. 2016;118(4):750-69.

Tarkin JM, Joshi FR, Rudd JH. PET imaging of inflammation in atherosclerosis. Nat Rev Cardiol. 2014;11(8):443-57.

Tavakoli S, Zamora D, Ullevig S, Asmis R. Bioenergetic profiles diverge during macrophage polarization: implications for the interpretation of 18F-FDG PET imaging of atherosclerosis. J Nucl Med. 2013;54(9):1661-7.

Tawakol A, Fayad ZA, Mogg R, et al. Intensification of statin therapy results in a rapid reduction in atherosclerotic inflammation: results of a multicenter fluorodeoxyglucose-positron emission tomography/computed tomography feasibility study. J Am Coll Cardiol. 2013;62(10):909-17.

Tawakol A, Migrino RQ, Bashian GG, et al. In vivo 18F-fluorodeoxyglucose positron emission tomography imaging provides a noninvasive measure of carotid plaque inflammation in patients. J Am Coll Cardiol. 2006;48(9):1818-24.

Tawakol A, Migrino RQ, Hoffmann U, et al. Noninvasive in vivo measurement of vascular inflammation with F-18 fluorodeoxyglucose positron emission tomography. J Nucl Cardiol. 2005;12(3):294-301.

Taylor JM, Allen AM, Graham A. Targeting mitochondrial 18 kDa translocator protein (TSPO) regulates macrophage cholesterol efflux and lipid phenotype. Clin Sci (Lond). 2014;127(10):603-13.

Tsimikas S, Willeit P, Willeit J, et al. Oxidation-specific biomarkers, prospective 15-year cardiovascular and stroke outcomes, and net reclassification of cardiovascular events. J Am Coll Cardiol. 2012;60(21):2218-29.

Tu Y, Sun Y, Fan Y, Cheng Z, Yu B. Multimodality Molecular Imaging of Cardiovascular Disease Based on Nanoprobes. Cell Physiol Biochem. 2018;48(4):1401-15.

van der Valk FM, Bekkering S, Kroon J, et al. Oxidized Phospholipids on Lipoprotein(a) Elicit Arterial Wall Inflammation and an Inflammatory Monocyte Response in Humans. Circulation. 2016;134(8):611-24.

van Dongen GA, Visser GW, Lub-de Hooge MN, de Vries EG, Perk LR. Immuno-PET: a navigator in monoclonal antibody development and applications. Oncologist. 2007;12(12):1379-89.

Verdeguer F, Aouadi M. Macrophage heterogeneity and energy metabolism. Exp Cell Res. 2017;360(1):35-40.

Villanueva FS. Molecular imaging of cardiovascular disease using ultrasound. J Nucl Cardiol. 2008;15(4):576-86.

Villanueva FS, Jankowski RJ, Klibanov S, et al. Microbubbles targeted to intercellular adhesion molecule-1 bind to activated coronary artery endothelial cells. Circulation. 1998;98(1):1-5.

Virmani R, Burke AP, Kolodgie FD, Farb A. Vulnerable plaque: the pathology of unstable coronary lesions. J Interv Cardiol. 2002;15(6):439-46.

Virmani R, Burke, A.P., Kolodgie, F.D., Farb, A. Pathology of the Thin-Cap Fibroatheroma. Journal of Interventional Cardiology. 2003;16(3):267-72.

Virmani R, Kolodgie FD, Burke AP, Farb A, Schwartz SM. Lessons from sudden coronary death: a comprehensive morphological classification scheme for atherosclerotic lesions. Arterioscler Thromb Vasc Biol. 2000;20(5):1262-75.

Wan S, Egri G, Oddo L, et al. Biological in situ characterization of polymeric microbubble contrast agents. Int J Biochem Cell Biol. 2016;75:232-43.

Watanabe T, Hirata M, Yoshikawa Y, Nagafuchi Y, Toyoshima H, Watanabe T. Role of macrophages in atherosclerosis. Sequential observations of cholesterol-induced rabbit aortic lesion by the immunoperoxidase technique using monoclonal antimacrophage antibody. Lab Invest. 1985;53(1):80-90.

Watanabe Y. Serial inbreeding of rabbits with hereditary hyperlipidemia (WHHL-rabbit). Atherosclerosis. 1980;36(2):261-8.

Webb NR, Connell PM, Graf GA, et al. SR-BII, an isoform of the scavenger receptor BI containing an alternate cytoplasmic tail, mediates lipid transfer between high density lipoprotein and cells. J Biol Chem. 1998;273(24):15241-8.

Weber C, Zernecke A, Libby P. The multifaceted contributions of leukocyte subsets to atherosclerosis: lessons from mouse models. Nat Rev Immunol. 2008;8(10):802-15.

Wells RG, Ruddy TD. The dream of imaging coronary artery inflammation with FDG PET/CT imaging. J Nucl Cardiol. 2017;24(4):1171-4.

Wen S, Liu DF, Cui Y, et al. In vivo MRI detection of carotid atherosclerotic lesions and kidney inflammation in ApoE-deficient mice by using LOX-1 targeted iron nanoparticles. Nanomedicine. 2014;10(3):639-49.

Wenning C, Kloth C, Kuhlmann MT, et al. Serial F-18-FDG PET/CT distinguishes inflamed from stable plaque phenotypes in shear-stress induced murine atherosclerosis. Atherosclerosis. 2014;234(2):276-82.

Williams KJ, Tabas I. The response-to-retention hypothesis of early atherogenesis. Arterioscler Thromb Vasc Biol. 1995;15(5):551-61.

Wood KM, Cadogan MD, Ramshaw AL, Parums DV. The distribution of adhesion molecules in human atherosclerosis. Histopathology. 1993;22(5):437-44.

Woollard KJ, Geissmann F. Monocytes in atherosclerosis: subsets and functions. Nat Rev Cardiol. 2010;7(2):77-86.

World Health Organization W. Cardiovascular diseases (CVDs) 2017 [Available from: https://www.who.int/news-room/fact-sheets/detail/cardiovascular-diseases-(cvds).

Wu CX, Li F, Niu G, Chen XY. PET Imaging of Inflammation Biomarkers. Theranostics. 2013;3(7):448-66.

Wu J, Wu G, Wang MP, Liu DL, Hu ZJ, Xu GY. [Effect of atorvastatin on carotid intima-medial of thickness of primary hypertension patients of Han nationality in China]. Zhonghua Yi Xue Za Zhi. 2007;87(31):2215-7.

Xiao K, Li Y, Luo J, et al. The effect of surface charge on in vivo biodistribution of PEG-oligocholic acid based micellar nanoparticles. Biomaterials. 2011;32(13):3435-46.

Yang CT, Ghosh KK, Padmanabhan P, et al. PET-MR and SPECT-MR multimodality probes: Development and challenges. Theranostics. 2018;8(22):6210-32.

Yang F, Li L, Li Y, Chen Z, Wu J, Gu N. Superparamagnetic nanoparticle-inclusion microbubbles for ultrasound contrast agents. Phys Med Biol. 2008;53(21):6129-41.

Yona S, Kim KW, Wolf Y, et al. Fate mapping reveals origins and dynamics of monocytes and tissue macrophages under homeostasis. Immunity. 2013;38(1):79-91.

Yun M, Jang S, Cucchiara A, Newberg AB, Alavi A. 18F FDG uptake in the

large arteries: a correlation study with the atherogenic risk factors. Semin Nucl Med. 2002;32(1):70-6.

Zani IA, Stephen SL, Mughal NA, et al. Scavenger receptor structure and function in health and disease. Cells. 2015;4(2):178-201.

Zernecke A. Dendritic cells in atherosclerosis: evidence in mice and humans. Arterioscler Thromb Vasc Biol. 2015;35(4):763-70.

Zhang SH, Reddick RL, Piedrahita JA, Maeda N. Spontaneous hypercholesterolemia and arterial lesions in mice lacking apolipoprotein E. Science. 1992;258(5081):468-71.

Zhang Y, Hong H, Cai W. PET tracers based on Zirconium-89. Curr Radiopharm. 2011;4(2):131-9.

Zhang Y, Sun T, Jiang C. Biomacromolecules as carriers in drug delivery and tissue engineering. Acta Pharm Sin B. 2018;8(1):34-50.

Zhang Z, Machac J, Helft G, et al. Non-invasive imaging of atherosclerotic plaque macrophage in a rabbit model with F-18 FDG PET: a histopathological correlation. BMC Nucl Med. 2006;6:3.

Zhao Z, de Beer MC, Cai L, et al. Low-density lipoprotein from apolipoprotein E-deficient mice induces macrophage lipid accumulation in a CD36 and scavenger receptor class A-dependent manner. Arterioscler Thromb Vasc Biol. 2005;25(1):168-73.

Zhou G, Hamik A, Nayak L, et al. Endothelial Kruppel-like factor 4 protects against atherothrombosis in mice. J Clin Invest. 2012;122(12):4727-31.

Zhou X, Robertson AK, Hjerpe C, Hansson GK. Adoptive transfer of CD4+ T cells reactive to modified low-density lipoprotein aggravates atherosclerosis. Arterioscler Thromb Vasc Biol. 2006;26(4):864-70.

Zhou X, Stemme S, Hansson GK. Evidence for a local immune response in atherosclerosis. CD4+ T cells infiltrate lesions of apolipoprotein-E-deficient mice. Am J Pathol. 1996;149(2):359-66.

Zhu X, Zong G, Zhu L, et al. Deletion of class A scavenger receptor deteriorates obesity-induced insulin resistance in adipose tissue. Diabetes. 2014;63(2):562-77.